

2011

# Control tools for rapid broadband nanomechanical spectroscopy using scanning probe microscope

Zhonghua Xu  
*Iowa State University*

Follow this and additional works at: <http://lib.dr.iastate.edu/etd>



Part of the [Mechanical Engineering Commons](#)

---

## Recommended Citation

Xu, Zhonghua, "Control tools for rapid broadband nanomechanical spectroscopy using scanning probe microscope" (2011). *Graduate Theses and Dissertations*. 10211.  
<http://lib.dr.iastate.edu/etd/10211>

This Dissertation is brought to you for free and open access by the Graduate College at Iowa State University Digital Repository. It has been accepted for inclusion in Graduate Theses and Dissertations by an authorized administrator of Iowa State University Digital Repository. For more information, please contact [digirep@iastate.edu](mailto:digirep@iastate.edu).

**Control tools for rapid broadband nanomechanical spectroscopy using scanning probe  
microscope**

by

Zhonghua Xu

A dissertation submitted to the graduate faculty  
in partial fulfillment of the requirements for the degree of

DOCTOR OF PHILOSOPHY

Major: Mechanical Engineering

Program of Study Committee:  
Qingze Zou, Co-major Professor  
Pranav Shrotriya, Co-major Professor  
Namrata Vaswani  
LeAnn Faidley  
Justin Peters  
Baskar Ganapathysubramanian

Iowa State University

Ames, Iowa

2011

Copyright © Zhonghua Xu, 2011. All rights reserved.

## **DEDICATION**

I dedicate this dissertation to my wonderful family. Particularly to my understanding wife, Jie, who has given me her fullest support in many ways in my life, and to our precious daughter Katherine, who is the joy of our lives.

I would also like to thank my advisor Dr. Qingze Zou, who is most responsible for helping me complete the studies as well as the challenge research that lies behind it. He has been making unremitting efforts to help me build a solid foundation to extend my career in academic arena.

I also thank Dr. Shrotriya, who contributed insightful ideas, feedback and advice in the area of nanomechanics.

## TABLE OF CONTENTS

|   |     |
|---|-----|
| <b>LIST OF TABLES</b> . . . . .   | vi  |
| <b>LIST OF FIGURES</b> . . . . .  | vii |
| <b>ABSTRACT</b> . . . . .   | xi  |
| <b>CHAPTER 1. OVERVIEW</b> . . . . .  | 1   |
| 1.1 The Study of Nonparametric Estimation in Frequency-dependent Nanomechanical Property Measurement and the Compensation for the Dynamics Convolution Effect . . . . . | 2   |
| 1.2 Parameter Estimation and Optimal Excitation Force Design in Rapid Broadband Nanomechanical Measurement . . . . .  | 4   |
| 1.3 Dissertation overview . . . . .   | 6   |
| <b>CHAPTER 2. NANOSCALE BROADBAND VISCOELASTIC SPECTROSCOPY OF SOFT MATERIALS USING ITERATIVE CONTROL</b> . . . . .   | 8   |
| 2.1 Introduction . . . . .  | 9   |
| 2.2 Iterative Control Approach to Broadband Viscoelastic Spectrum on SPM . . . . .  | 12  |
| 2.2.1 Nanoscale Material Property Measurement using SPM . . . . .   | 12  |
| 2.2.2 Model-less Inversion-based Iterative Control . . . . .  | 13  |
| 2.2.3 Implementation of the MIIC Technique in NBVS . . . . .  | 14  |
| 2.2.4 Identification of the Frequency-dependent Plane-strain Modulus . . . . .  | 16  |
| 2.3 Experimental Example: Frequency-dependent Viscoelastic Measurement of PDMS . . . . .  | 21  |

|   |  |    |
|---|--|----|
| 2.3.1   | Experimental Setup . . . . .   | 21 |
| 2.3.2   | Experimental Results & Discussion . . . . .  | 21 |
| 2.4   | Conclusions . . . . .  | 34 |
| 2.5   | Acknowledgments . . . . .  | 34 |
| <b>CHAPTER 3. MODEL-BASED APPROACH TO COMPENSATE FOR THE DYNAMICS CONVOLUTION EFFECT IN NANOMECHANICAL PROPERTY MEASUREMENT . . . . .</b>                     |  |    |
|   |  | 36 |
| 3.1   | Introduction . . . . .   | 37 |
| 3.2   | Model-based Compensation for Instrument Dynamics Convolution Effect . .  | 40 |
| 3.2.1   | Nanomechanical Property Measurement Using SPM . . . . .  | 40 |
| 3.2.2   | Dynamics Convolution Effect on Indentation-based Nanomechanical Property Measurement . . . . .                 | 42 |
| 3.2.3   | Model-based Approach to Compensate for the Dynamics Convolution Effect on Nanomechanical Measurement . . . . . | 46 |
| 3.3   | Implementation Example . . . . .   | 49 |
| 3.3.1   | Dynamics Convolution Effect on Broadband Nanomechanical Property Measurement . . . . .                         | 50 |
| 3.3.2   | Model-based Compensation for the Convolutioned Dynamics Effect . . .   | 52 |
| 3.4   | Conclusions . . . . .  | 58 |
| <b>CHAPTER 4. OPTIMAL EXCITATION FORCE DESIGN IN INDENTATION-BASED RAPID BROADBAND NANOMECHANICAL SPECTROSCOPY: POLY (DIMETHYLSILOXANE) EXAMPLE . . . . .</b> |  |    |
|   |  | 61 |
| 4.1   | Introduction . . . . .   | 62 |
| 4.2   | Optimal Input Design for Rapid Nanomechanical Spectroscopy . . . . .   | 66 |
| 4.2.1   | Parameter Estimation in Nanomechanical Property Measurement . .  | 66 |
| 4.2.2   | Optimal Input Design for Nanomechanical Measurement . . . . .  | 70 |

|  |  |           |
|--|--|-----------|
| 4.2.3  | Implementation of the Optimal Excitation Force . . . . .   | 76        |
| 4.3  | Simulation and Experimental Example: Frequency-dependent Viscoelasticity<br>Measurements of PDMS . . . . . | 78        |
| 4.3.1  | Simulation Study of Input Force Design . . . . .   | 78        |
| 4.3.2  | Experimental Implementation and Discussion . . . . .   | 82        |
| 4.4  | Conclusions . . . . .  | 86        |
| <b>CHAPTER 5. CONCLUSION . . . . .</b>                       |  | <b>88</b> |
| <b>APPENDIX</b>  |  |           |
| <b>MODEL-LESS INVERSION-BASED ITERATIVE LEARNING CONTROL</b> |  |           |
|  | <b>(MIC) . . . . .</b>   | <b>90</b> |
| <b>BIBLIOGRAPHY . . . . .</b>                                |  | <b>92</b> |

## LIST OF TABLES

|           |  |    |
|-----------|--|----|
| Table 2.1 | Tracking performance of the MIIC technique to track a white-noise trajectory with the cut-off frequency of 4.5 KHz, where “Iter.No.” denotes the number of iterations used in the experiments. . . . .   | 25 |
| Table 2.2 | The parameters generated from the curve fitting of the real part and imaginary part of the complex modulus, and their average. . . . .   | 31 |
| Table 3.1 | The parameters of the 3 <sup>rd</sup> -order Prony series like model estimated from the curve fitting of the real part and imaginary part of the total convoluted dynamics ratio, $G_{cv}(j\omega)$ , and the averaged values. . . . .   | 57 |
| Table 4.1 | The list of the true values of the seven parameters of the 3 <sup>rd</sup> -order Prony series model (“Actual”), and those identified in Case 1 (“Case 1”), Case 2 (“Case 2”), and Case 3 (“Case 3”), and the corresponding estimation errors with respect to the true values. . . . . | 79 |
| Table 4.2 | The frequency components of the optimal input design obtained in the simulation study . . . . .  | 81 |
| Table 4.3 | The list of parameters identified in the first three (“Ite. 1”, “Ite. 2”, and “Ite. 3”) and the last three (“Ite. 13”, “Ite. 14”, and “It. 15”) iterations during the search of the optimal excitation force in the experiments. . . . .   | 85 |
| Table 4.4 | The optimal force design obtained in the experiment. . . . .   | 85 |

## LIST OF FIGURES

|            |   |    |
|------------|---|----|
| Figure 2.1 | The scheme of force curve measurement by SPM . . . . .  | 13 |
| Figure 2.2 | The system diagram of the MIIC algorithm. . . . .   | 14 |
| Figure 2.3 | The schematic comparison of the MIIC algorithm (the dashed box) with the multi-frequency excitation method (the dashed arrow) in nanomechanical measurements. . . . .   | 15 |
| Figure 2.4 | Schematic diagram of the experimental setup to implement MIIC algorithm in force-curve measurements. . . . .  | 21 |
| Figure 2.5 | (a) The experimental tracking result (i.e., the force applied to the PDMS sample, which was converted from the cantilever deflection) of the band-limited white-noise trajectory with a period of 6 sec., (b) the zoomed-in view of the tracking result for time $t \in [2, 2.01]$ sec., and (c) the tracking error of 6 sec. . . . . | 23 |
| Figure 2.6 | The experimentally measured frequency response of the SPM dynamics in the z-axis direction, where the red-dashed line at 4.5 kHz identifies the cut-off frequency of the band-limited white-noise used as the excitation force in the experiments. . . . .  | 24 |

|             |   |    |
|-------------|---|----|
| Figure 2.7  | (a) Comparison of the magnitude of the frequency components in the desired white-noise input force with that in the measured input force obtained by using the MIIC technique, (b) the magnitude of the frequency components in the tracking error by using the MIIC technique, and (c) the magnitude of the frequency components in the measured input force obtained by using the multi-frequency excitation method (6; 7). . . . . | 27 |
| Figure 2.8  | (a) The experimentally measured displacement of the probe on the PDMS sample, (b) the indentation of the probe into PDMS for a period of 6 sec., and (c) the zoomed-in view of plot (b) for time $t \in [2, 2.01]$ sec. . . . .   | 28 |
| Figure 2.9  | (a) The tip-sample interaction force that shows the band-limited white-noise characteristic, and (b) the indentation into the PDMS sample obtained under the force of (a). . . . .  | 29 |
| Figure 2.10 | Comparison of the raw experimentally measured complex modulus of the PDMS sample (“Experimental”) with that improved by removing the “spikes” in Matlab (“Improved”) for (a) the real part, (b) the imaginary part. . . . .   | 31 |
| Figure 2.11 | Comparison of the experimentally measured complex modulus of the PDMS sample to the results for (a) the real part and (b) the imaginary part, obtained by curve-fitting the real-part and the imaginary part separately. . . . .  | 32 |
| Figure 2.12 | The calculated modulus of PDMS sample in time domain by using the parameters obtained from the curve fitting with Eq. (2.10). . . .   | 32 |
| Figure 3.1  | (a) the force curve measurement scheme and (b) a schematic drawing of a force-distance curve. . . . .   | 41 |

|            |  |    |
|------------|--|----|
| Figure 3.2 | The scheme of the dynamics involved in nanomechanical property measurement using SPM. . . . .  | 43 |
| Figure 3.3 | The diagram of system dynamics. . . . .  | 44 |
| Figure 3.4 | (a) The magnitude of the frequency components of the excitation force applied onto the PDMS sample by using the multi-frequency method, (b) the amplitude of the frequency components in the corresponding indentation of the PDMS sample, and (c) the uncompensated complex compliance calculated using the force in (a) and the uncompensated indentation in (b) in the Hertz model. . . . .   | 53 |
| Figure 3.5 | (a) The comparison of the magnitude of the frequency components of the desired excitation force and the magnitude of the frequency components of the excitation force applied onto the PDMS sample by using the MIIC technique, (b) the amplitude of the frequency components in the corresponding indentation measured on the PDMS sample, and (c) the uncompensated complex compliance calculated by using the force data in (a) and the uncompensated indentation data in (b) in the Hertz model. . . . . | 54 |
| Figure 3.6 | The total deflection dynamics measured on the PDMS sample (blue line) and on the sapphire sample (red line), and the ratio of these two (black line), i.e., the total convoluted dynamics ratio (see Eq. (3.11)).  | 55 |
| Figure 3.7 | (a) The total deflection dynamics from the piezoactuator to the deflection on the sapphire sample measured by using the same control input at 5 different points, and (b) the maximum difference between these total deflection dynamics. . . . .  | 56 |
| Figure 3.8 | The comparison of the uncompensated indentation (blue line) of the PDMS sample using the MIIC-based method with the total convoluted dynamics ratio (black line). . . . .  | 56 |

|             |   |    |
|-------------|---|----|
| Figure 3.9  | The curve fitting result of (a) the real part and (b) the imaginary part of the total convoluted dynamics ratio $G_{cv}(j\omega)$ by a 3 <sup>rd</sup> -order Prony series like model. . . . .  | 57 |
| Figure 3.10 | (a) the compensated indentation data obtained by using the multi-frequency excitation, and (b) the comparison of the uncompensated compliance of the PDMS sample (red line) with the compensated compliance of the PDMS sample (blue line). . . . . | 59 |
| Figure 3.11 | (a) the compensated indentation result obtained by using the MIIC-based method, and (b) the comparison of the uncompensated compliance (red line) of the PDMS sample with the compensated compliance of the PDMS sample (blue line). . . . .        | 59 |
| Figure 4.1  | The scheme of force curve measurement by SPM . . . . .  | 67 |
| Figure 4.2  | Simulation result: the estimation error of 3 <sup>rd</sup> -order Prony series by using the proposed optimal input design in the presence of output noise. . . . .  | 80 |
| Figure 4.3  | (a) The comparison of the designed deflection (i.e., force) and the actual deflection on PDMS sample, and (b) the tracking error between the designed deflection and the actual one at the fifteenth iteration. . . . .                             | 82 |
| Figure 4.4  | Experimental parameter estimation result with optimal input design . . . . .  | 84 |

## **ABSTRACT**

The identification of frequency dependent material property at nanoscale has been extensively studied and played an important role in the failure analysis of materials, wound healing, and polymer formation mechanism. In this dissertation, the development of a suite of control tools to nanoscale broadband viscoelastic spectroscopy is presented. The combination of novel iterative control techniques with the integration of system identification and optimal input design techniques together can enable rapid measurement of nanomechanical properties of soft materials over a broad frequency band. SPM and nanoindenter have become enabling tools to quantitatively measure the mechanical properties of a wide variety of materials at nanoscale. Current nanomechanical measurement, however, is limited by the slow measurement speed: the nanomechanical measurement is slow and narrow-banded and thus not capable of measuring rate-dependent phenomena of materials. As a result, large measurement (temporal) errors are generated when material undergoes dynamic evolution during the measurement. The low-speed operation of SPM is due to the inability of current approaches to (1) rapidly excite the broadband nanomechanical behavior of materials, and (2) eliminate the convolution of the hardware adverse effects with the material response during high-speed measurements. These adverse effects include the hysteresis of the piezo actuator (used to position the probe relative to the sample); the vibrational dynamics of the piezo actuator and the cantilever along with the related mechanical mounting; and the dynamics uncertainties caused by the probe variation and the operation condition. Motivated by these challenges, this dissertation is focused on the development of novel control and system identification tools for rapid broadband nanomechanical measurement.

The first proposed approach utilizes the recently developed model-less inversion-based iterative control (MIIC) technique for accurate measurement of the material response to the applied excitation force over a broad frequency band. In the proposed approach, an input force signal with dynamic characteristics of band-limited white-noise is utilized to rapidly excite the nanomechanical response of materials over a broad frequency range. The MIIC technique is used to compensate for the hardware adverse effects, thereby allowing the precise application of such an excitation force and measurement of the material response (to the applied force). The proposed approach is illustrated by implementing it to measure the frequency-dependent plane-strain modulus of poly(dimethylsiloxane) (PDMS) over a broad frequency range extending over 3 orders of magnitude ( $\sim 1$  Hz to 4.5 kHz).

To further attenuate the dynamics convolution effect, a model-based approach to compensate for the dynamics convolution effect in nanomechanical property measurements is proposed in this dissertation. In the indentation-based nanomechanical property measurement of soft materials, an excitation force consisting of various frequency components needs to be accurately exerted to the sample material through the probe, and the indentation of the probe into the sample needs to be accurately measured. However, when the measurement frequency range increases close to the bandwidth of the instrument hardware, the instrument dynamics along with the probe-sample interaction dynamics can be convoluted with the mechanical behavior of the soft material, resulting in distortions in both the force applied and the indentation measured, which, in turn, directly lead to errors in the measured nanomechanical property (e.g., the creep compliance) of the material. In this dissertation, the dynamics involved in indentation-based nanomechanical property measurements is analyzed to reveal that the convoluted dynamics effect can be described as the difference between the lightly-damped probe-sample interaction dynamics and the over-damped nanomechanical behavior of soft materials. Thus, these two different dynamics effects can be decoupled via numerical fitting based on the viscoelastic model of the soft material. The proposed approach is illustrated by implementing it to compensate for the dynamics convolution effect in a broadband

viscoelasticity measurement of a Polydimethylsiloxane (PDMS) sample using scanning probe microscope.

This dissertation also presents an optimal input design approach to achieve rapid broadband nanomechanical measurements of soft materials using the indentation-based method for the investigation of fast evolving phenomenon, such as the the crystallization process of polymers, the nanomechanical measurement of live cell during cell movement, and force volume mapping of nonhomogeneous materials. The indentation-based nanomechanical measurement provides unique quantification of material properties at specified locations. The measurement, however, currently is too slow in time and too narrow in frequency (range) to characterize time-elapsing material properties during dynamic evolutions (e.g., the rapid-stage of the crystallization process of polymers). These limits exist because the excitation input force used in current methods cannot rapidly excite broadband nanomechanical properties of materials. The challenges arise as the instrumental hardware dynamics can be excited and convoluted with the material properties during the measurement when the frequencies in the excitation force increase, resulting in large measurement errors. Moreover, long measurement time is needed when the frequency range is large, which, in turn, leads to large temporal measurement errors upon dynamic evolution of the sample. In this dissertation, we develop an optimal-input design approach to tackle these challenges. Particularly, an input force profile with discrete spectrum is optimized to maximize the Fisher information matrix of the linear compliance model of the soft material. Both simulation and experiments on a Poly(dimethylsiloxane) (PDMS) sample are presented to illustrate the need for optimal input design, and the efficacy of the proposed approach in probe-based nanomechanical property measurements.

## CHAPTER 1. OVERVIEW

Identification of frequency dependent material properties is an important interdisciplinary research, which includes control theory, material science, nanomechanics and biomedical engineering, and has broad applications in the development of new composite material and the analysis of the mechanical failure of materials. In control engineering, the field of system identification uses statistical methods to build mathematical models of dynamical systems from measured data. The quality of system identification depends on the quality of the inputs. In recent decades, the theory of optimal experimental design has been increasingly used to specify inputs that yield maximally precise parameter estimation. This dissertation starts from developing a nonparametric estimation method in nanoscale broadband viscoelasticity spectroscopy (NBVS) to seeking a systematic control-integrated system identification and optimal excitation force design approach for rapid broadband nanomechanical property measurement of soft materials. The control method is tested and implemented using atomic force microscope. Then the proposed optimal excitation force design technique is applied in the material property measurement. The complexity mostly due to the dynamics convolution effect, nonlinearities and measurement noise is handled by the notion of model-less inversion-based iterative learning control and optimal input design. To reduce the measurement error in the viscoelasticity, the iterative control technique is integrated with the nonparametric estimation. However, the dynamics convolution effect due to the interaction dynamics between the probe and the sample surface is inevitable and will cause the measurement error in the measured indentation. Then, a model-based approach is introduced to compensate for the dynamic convolution effect in the nanomechanical measurement. To identify the fast evolving phenomenon

such as the polymerization process of polymers and measure the nanomechanical property of live cell during cell movement in liquid environment, the control-integrated optimal excitation force design is developed and implemented in rapid broadband nanomechanical property measurement. The proposed approach does not need any post-processing and is ready for online implementation to measure the frequency dependent material property, such as force volume mapping of nonhomogeneous materials.

### **1.1 The Study of Nonparametric Estimation in Frequency-dependent Nanomechanical Property Measurement and the Compensation for the Dynamics Convolution Effect**

Many approaches can be used to measure the material properties at nanoscale, force distance curve measurement is one of them. In usual force-curve measurements, the applied input force follows a triangle trajectory (1). Although the load rate of the excitation force can be substantially increased by using advanced control techniques to compensate for the instrument dynamics effect—as demonstrated in (2), the excitation force profile used is quasi-static and does not contain rich frequency components required to rapidly excite the broadband viscoelastic response of materials. One attempt at addressing the lack of frequency components in input force has been through the development of the force modulation technique (3; 4), where a sinusoidal force signal (i.e., ac signal) of small amplitude is superposed on the triangle input force and applied during measurements. The hardware dynamic response is coupled (convoluted) into the measured data and must be accounted-for afterwards using a dynamics model (4). As a result, the load/unload rates are limited to a small range because the oscillation amplitude (<100 nm) and the oscillation frequency (a few hundred Hz) have to be kept small (4) such that dynamics coupling can be adequately captured by using a simple spring-mass-damper model. Moreover, the force-modulation technique is slow for measuring material response over a large frequency range, because the de-modulation process must be

applied to accurately measure the amplitude and the phase shift of the oscillation, which is inherently time-consuming. To speed up the measurement of frequency dependent nanomechanical property of soft materials, the multifrequency approach (5; 6; 7) was developed in 2008. It has been demonstrated that the multi-frequency excitation approaches can improve the measurement time and the force sensitivity over the single-frequency force-modulation method. However, since the multi-frequency (or band-limited) input is applied to drive the cantilever, such an excitation mechanism requires a high-bandwidth actuator-cantilever system (i.e., the bandwidth contains all the excitation frequencies). Otherwise, the dynamics of the cantilever (and possibly the actuator along with the related mechanical mounting) may be convoluted with the material response in the measured data (5; 6), and undesirable distortions may be induced in the excitation force, making the extraction of the material properties from the measured data difficult and prone to calibration errors.

In order to address the problems discussed above, this dissertation presents a broadband characterization approach that uses advanced control techniques to adjust the control input (to the actuator) to “cancel” the coupling of the dynamics and other nonlinear and disturbance effects into the measured output, thus allowing the desired broadband excitation force to be exerted (from the cantilever) to the sample without distortions. Furthermore, this approach does not require additional hardware augmentation and can be readily applied to existing SPM hardware. Therefore, the developed approach extends and improves the multi-frequency excitation approach. To further eliminate the dynamics convolution effect on nanomechanical property measurements, a model-based approach was proposed. In the proposed approach, the cantilever deflection dynamics is analyzed and modeled as a cascaded dynamic system consisting of the piezoactuator, the cantilever along with the mechanical fixture, the probe-sample interaction dynamics, and the nanomechanical dynamics of the material. The cantilever deflection dynamics on both the soft sample and the hard reference sample are measured and compared to reveal that the convoluted part of the instrument dynamics is characterized by lightly-damped poles and zeros, whose locations coincide with those of the piezo and can-

tilever dynamics. On the contrary, the mechanical behavior of soft materials is characterized by over-damped dynamic behavior that can be described by for example, a Prony series model (8). Then, the convoluted dynamics effect, distinct from the material behavior in frequency domain, is removed numerically through fitting. The proposed approach is illustrated by implementing it to the measurement data obtained in a broadband viscoelasticity measurement of a PDMS sample using SPM. Both the multi-frequency approach (5; 6) and the iterative-control-based method (2; 9) are applied in the measurement. The results demonstrate that the dynamics convolution effect on the measurements in both cases can be effectively reduced by using the proposed method.

## **1.2 Parameter Estimation and Optimal Excitation Force Design in Rapid Broadband Nanomechanical Measurement**

For many applications such as identification of the crystallization process of polymers, measurement of nanomechanical property of live biological material, high speed force mapping of nonhomogeneous material, the high speed nanomechanical measurement is needed. In this dissertation, an optimal input design approach is proposed to achieve rapid identification of broadband nanomechanical properties of soft materials through indentation-based approach. Indentation-based approach using scanning probe microscope (SPM) or nanoindenter has become an enabling tool to quantitatively measure the nanomechanical properties of a wide variety of materials, both locally and globally (1). The current measurement methods (4; 6), however, are limited in both the frequency range that can be measured and the measurement time that is needed to measure the (frequency) rate-dependent viscoelasticity of materials. These limits of current measurement methods (4; 6), in both measurement frequency and time, arise as the excitation force from the probe to the sample surface employed cannot compensate for the convolution effect of the instrument dynamics, (10), nor rapidly excite the rate-dependent nanomechanical behavior of the material (11).

Inefficiencies exist in current nanomechanical measurement methods for characterizing the time-elapsing properties of soft materials. One of the main challenges to achieve rapid broadband nanomechanical measurement is to ensure that 1) the force applied shall accurately track the desired force profile and 2) the indentation should be accurately measured. Accurate tracking of the desired force profile is necessary to excite the material behavior in the measured frequency range, as well as to avoid issues related to low signal-to-noise ratio and input saturation (due to the force being too small or too large). Accurate indentation measurement is needed to capture the material behavior as the response to the force applied. Recently, model-based techniques (10; 12) have been developed to account for the dynamics convolution effect on the measured indentation data. These post-processing technique, however, cannot be used to achieve rapid broadband nanomechanical measurements. The other major challenge in rapid broadband nanomechanical measurements is to achieve rapid excitation of the material response by the force applied (from the probe). Rapid excitation (of the material response) is needed to capture the time-elapsing nanomechanical properties during dynamic evolution of the material, for example, during the initial rapid stage of the crystallization of polymers (11) or the healing process of live cell (13). Moreover, rapid excitation of material response is also needed when mapping the nanomechanical properties of the material over the sample surface. Although the mapping of elasticity/stiffness of materials at nanoscale can be obtained by using the force volume mapping technique, the force-curve measured at each sample point is quasi-static and the mapping procedure is time consuming, with mapping time in tens of minutes to several hours — which becomes even much longer to map rate-dependent nanomechanical properties. Such a long mapping time renders the adverse effects (14) due to disturbances (e.g., thermal drift) and variations of system dynamics pronounced. As a result, large measurement errors occur, particularly when the sample is evolving.

To achieve rapid nanomechanical spectroscopy, an approach based on the optimal input design was developed. First, the measurement of nanomechanical properties is transformed into a parameter identification problem by capturing the nanomechanical properties of the

sample to be measured in a parameterized model (e.g., a truncated-order exponential (Prony) series model of the complex compliance of the material (8)). Then, the optimal excitation force — acting as the input to the material mechanics model — is sought to minimize the covariance of the estimation error through the maximization of the Fisher information matrix (15; 16) of the parameterized mechanics model. Specifically, the designed optimal excitation force profile comprises multiple sinusoidal signals whose frequency and amplitude are optimized through an iterative experimental process. Not only can the obtained optimal force profile rapidly excite the nanomechanical properties of materials over a broadband frequency range, but also, with a discrete frequency spectrum, reduce the dynamics convolution effect by facilitating the tracking of such an excitation force. Then, the designed optimal excitation force profile (e.g., the cantilever deflection when using SPM) is tracked by using the recently-developed inversion-based iterative control technique (2) that compensates for the hardware dynamics convolution effect. The proposed approach is illustrated through both simulation and experimental implementations on the measurement of viscoelasticity of a Polydimethylsiloxane (PDMS) sample using an SPM. The simulation and experiment results demonstrate the need of optimal input design and the efficacy of the proposed approach in achieving broadband viscoelasticity spectroscopy.

### **1.3 Dissertation overview**

The rest of this dissertation is organized as follows. In chapter 2, two issues encountered in the nanomechanical measurement of soft materials were addressed. The first arising issue is the lack of rich frequency components in the excitation force, and the measurement speed is slow in order to sweep the frequency range for the measurement of frequency dependent material properties. This issue was addressed by using a white-noise excitation force profile. The second arising problem is the instrument dynamics effect coupled in the measured force and indentation data. This problem was tackled by using the model-less inversion-based iterative

learning control technique. The dynamics convolution effect in the measured viscoelasticity due to the probe-sample interaction was removed by curve-fitting an ideal parametric mechanics model—Prony series model. The measurement error can be dramatically reduced and the measurement speed was significantly increased. The measured viscoelasticity compared well with the dynamic mechanical analysis (DMA) result.

In chapter 3, to compensate for the dynamics convolution effect in the measured indentation data, a model-based approach is proposed. First, the dynamics from piezoactuator to cantilever was analyzed and modeled as a cascaded dynamic system. Then, the measurement error in the indentation data was removed by the numeric curve fitting. The proposed approach was implemented to measure the broadband viscoelasticity of a PDMS sample using SPM.

In chapter 4, to further increase the measurement speed for rapid broadband nanomechanical measurement, a control-integrated system identification and optimal excitation force design approach was developed. First, the nanomechanical measurement was converted to the parameter estimation problem. Then, the optimal excitation force design was implemented to attenuate the measurement noise, the dynamics uncertainty and the thermal drift. The proposed approach was simulated and implemented in experiments to demonstrate the need and efficacy of the optimal excitation force design in nanomechanical property measurement. The measurement result compared well with previous results and the measurement time was further decreased. The proposed approach does not need any post-processing and can be implemented online for investigation of fast evolving phenomenon.

Finally, the conclusion is given in chapter 5.

## **CHAPTER 2. NANOSCALE BROADBAND VISCOELASTIC SPECTROSCOPY OF SOFT MATERIALS USING ITERATIVE CONTROL**

### **Abstract**

In this chapter, a novel approach to nanoscale broadband viscoelastic spectroscopy is presented. The proposed approach utilizes the recently developed model-less inversion-based iterative control (MIIC) technique for accurate measurement of the material response to the applied excitation force over a broad frequency band. SPM and nanoindenter have become enabling tools to quantitatively measure the mechanical properties of a wide variety of materials at nanoscale. Current nanomechanical measurement, however, is limited by the slow measurement speed: the nanomechanical measurement is slow and narrow-banded and thus not capable of measuring rate-dependent phenomena of materials. As a result, large measurement (temporal) errors are generated when material undergoes dynamic evolution during the measurement. The low-speed operation of SPM is due to the inability of current approaches to 1) rapidly excite the broadband nanomechanical behavior of materials, and 2) eliminate the convolution of the hardware adverse effects with the material response during high-speed measurements. These adverse effects include the hysteresis of the piezo actuator (used to position the probe relative to the sample); the vibrational dynamics of the piezo actuator and the cantilever along with the related mechanical mounting; and the dynamics uncertainties caused by the probe variation and the operation condition. In the proposed approach, an input force

signal with dynamic characteristics of band-limited white-noise is utilized to rapidly excite the nanomechanical response of materials over a broad frequency range. The MIIC technique is used to compensate for the hardware adverse effects, thereby allowing the precise application of such an excitation force and measurement of the material response (to the applied force). The proposed approach is illustrated by implementing it to measure the frequency-dependent plane-strain modulus of poly(dimethylsiloxane) (PDMS) over a broad frequency range extending over 3 orders of magnitude ( $\sim 1$  Hz to 4.5 kHz).

## 2.1 Introduction

In this chapter, a novel indentation-based nanoscale broadband viscoelastic spectroscopy (NBVS) methodology for soft materials is presented. The proposed NBVS approach utilizes the recently developed model-less inversion-based iterative control (MIIC) technique (14) to allow rapid excitation and measurement of nanomechanical behavior of materials over a broad frequency band via indentation using scanning probe microscope (SPM) or nanoindenter. Compared to other methods for nanoscale mechanical property measurements (17; 18), the SPM-based force measurement has the unique advantage of applying force stimuli and then directly measuring material response (i.e., the indentation measurement) on the same platform. Current SPM-based force measurements, however, are limited by the slow operation of SPM: the force measurement in current state-of-the-art SPM is too slow to measure the rate-dependent phenomena of materials (19), and large measurement (temporal) errors can be generated when dynamic evolution of materials is involved during measurements (20). Operating speed of current SPMs is limited by two factors: 1) the excitation force applied, which is either quasi-static (1) or resonant-oscillation based (21), is either too narrow-banded in frequency (quasi-static) or too slow (resonant-oscillation based) to rapidly excite the nanomechanical behavior of materials over a broad frequency band; and 2) the hardware adverse effects can be coupled (convoluted) into the measured data if the measurement is at high-speed and over a broad frequency

range. These adverse effects include the hysteresis of the piezo actuator (used to position the probe relative to the sample) (22; 23), the vibrational dynamics of the piezo actuator and the probe along with mechanical parts (24), and the dynamics uncertainties (25; 26). The proposed approach aims at overcoming these drawbacks through a broadband characterization approach analogous to system dynamics identification (27).

Development of rapid nanoscale broadband viscoelastic spectroscopy is needed to study material properties (1) as well as physical and/or chemical interactions between different materials (28), particularly for biological samples that evolve and undergo significant changes in mechanical response during the measurement time of the current state-of-art SPM systems. For example, during the dehydration process of dentin collagen (29; 30) or the healing process of a wounded cell, material viscoelastic response can evolve within seconds and use of conventional force measurement techniques such as force volume mapping will result in large temporal errors (31), because the measurements at the first sample point and the last sample point are acquired at very different time instances. Rapid nanomechanical property measurements will also dramatically improve the measurement efficacy. There exists a need to achieve rapid measurement of nanomechanical properties of materials, but the rapid broadband measurement of viscoelastic response at nanoscale is challenging.

In usual force-curve measurements, the applied input force follows a triangle trajectory (1). Although the load rate of the excitation force can be substantially increased by using advanced control techniques to compensate for the instrument dynamics effect—as demonstrated in (2), the excitation force profile used is quasi-static and does not contain rich frequency components required to rapidly excite the broadband viscoelastic response of materials. One attempt at addressing the lack of frequency components in input force has been the development of the force modulation technique (3; 4), where a sinusoidal force signal (i.e., ac signal) of small amplitude is superposed on the triangle input force and applied during measurements. The hardware dynamic response is coupled (convoluted) into the measured data and must be accounted-for afterwards using a dynamics model (4). As a result, the load/unload

rates are limited to a small range because the oscillation amplitude ( $<100$  nm) and the oscillation frequency (a few hundred Hz) have to be kept small (4) such that dynamics coupling can be adequately captured by using a simple spring-mass-damper model. Moreover, the force-modulation technique is slow for measuring material response over a large frequency range, because the de-modulation process must be applied to accurately measure the amplitude and the phase shift of the oscillation, which is inherently time-consuming. During high-speed force measurements, the SPM dynamics consisting of the piezo actuator and the probe (32) can be excited, resulting in large vibrations of the probe relative to the sample, which in turn, leads to large errors in the obtained force measurements. Furthermore, substantial dynamics uncertainties exist in the SPM system due to the change of operation conditions (e.g., change of the cantilever), which makes the compensation of such dynamics effect challenging. When the displacement of the piezo actuator is large during the force measurement, the hysteresis effect of the piezo actuator becomes pronounced, further exacerbating large measurement errors. Therefore, a measurement technique that decouples the hardware dynamics, nonlinear hysteresis, and dynamic uncertainties from the high speed force measurements is required for accurate material characterization.

The proposed broadband excitation and measurement approach is fundamentally different from the recent development of broadband (or multi-frequency) excitation methods (5; 6; 7). It has been demonstrated recently (5; 6) that the multi-frequency excitation approaches can improve the measurement time and the force sensitivity over the single-frequency force-modulation method. However, since the multi-frequency (or band-limited) input is applied to drive the cantilever, such an excitation mechanism requires a high-bandwidth actuator-cantilever system (i.e., the bandwidth contains all the excitation frequencies). Otherwise, the dynamics of the cantilever (and possibly the actuator along with the related mechanical mounting) may be convoluted with the material response in the measured data (5; 6), and undesirable distortions may be induced in the excitation force, making the extraction of the material properties from the measured data difficult and prone to calibration errors.

In order to address the problems discussed above, this chapter presents a broadband characterization approach that uses advanced control techniques to adjust the control input (to the actuator) to “cancel” the coupling of the dynamics and other nonlinear and disturbance effects into the measured output, thus allowing the desired broadband excitation force to be exerted (from the cantilever) to the sample without distortions. Furthermore, this approach does not require additional hardware augmentation and can be readily applied to existing SPM hardware. Therefore, the developed approach extends and improves the multi-frequency excitation approach.

## **2.2 Iterative Control Approach to Broadband Viscoelastic Spectrum on SPM**

### **2.2.1 Nanoscale Material Property Measurement using SPM**

SPM is not only a unique tool to obtain nanoscale images of materials, but also becomes a powerful tool to characterize various nanoscale material properties through the measurement of tip-sample interaction force, i.e., the force curve measurement (2). To obtain the force curve, a micro-fabricated cantilever with a nano-sized tip (see Fig. 2.1(a)) is driven by a piezoelectric actuator to push against the sample surface until the cantilever deflection (i.e., the tip-sample interaction force) reaches the setpoint value. Then the cantilever will retrace from the sample surface to a pre-determined distance. The force distance curve is obtained by measuring the tip-sample interaction force versus the vertical displacement of the SPM-tip during the push-retraction process (see Fig. 2.1(b)). The force curve contains the information of tip-sample interaction force and the indentation and thereby can be used to explore various material mechanical properties such as the Young’s modulus (1).

Next, a novel feedforward control-based approach to achieve NBVS using SPM is presented. The method exploits a newly developed iterative feedforward control technique (14)

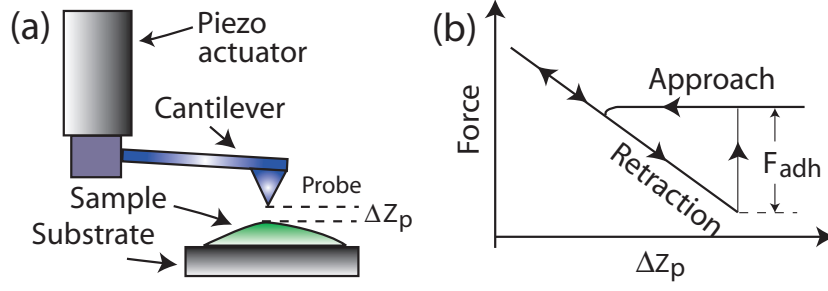


Figure 2.1 The scheme of force curve measurement by SPM

in force curve measurements—to eliminate the convolution of SPM dynamics into the measured data and enables the direct exertion of a broadband (in frequency) excitation force on the sample. Then the measured input-output data are utilized in a mechanics model to obtain the frequency-dependent (storage and loss) modulus of soft materials. The preliminary result has been reported in-brief recently in *Applied Physics Letters* (9). In this chapter, we extend the work by providing the detailed development of the proposed method, including more experimental results. We start with presenting the MIIC technique.

## 2.2.2 Model-less Inversion-based Iterative Control

The MIIC control law can be described in frequency domain as follows:

$$\begin{aligned}
 u_0(j\omega) &= \alpha z_d(j\omega), & k &= 0, \\
 u_k(j\omega) &= \begin{cases} \frac{u_{k-1}(j\omega)}{z_{k-1}(j\omega)} z_d(j\omega), & \text{when } z_{k-1}(j\omega) \neq 0, \\ 0 & \text{otherwise} \end{cases} & \text{and } k \geq 1,
 \end{aligned} \tag{2.1}$$

where ' $f(j\omega)$ ' denotes the Fourier transform of the signal ' $f(t)$ ', ' $z_d(\cdot)$ ' denotes the desired output trajectory, ' $z_k(\cdot)$ ' denotes the output obtained by applying the input ' $u_k(\cdot)$ ' to the system during the  $k^{\text{th}}$  iteration, and  $\alpha \neq 0$  is a pre-chosen constant (e.g.,  $\alpha$  can be chosen as the estimated DC-Gain of the system).

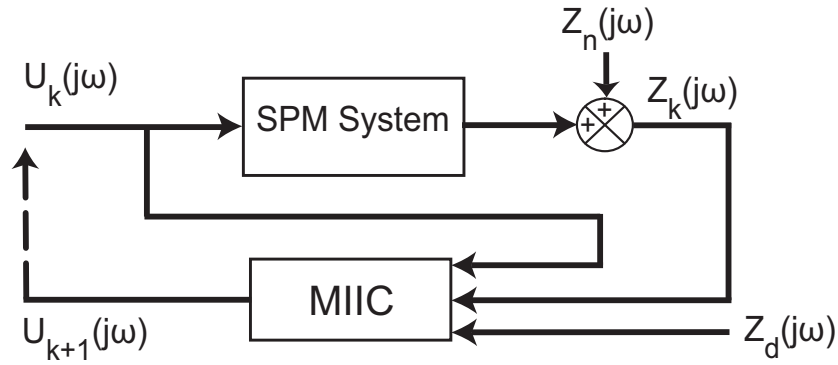


Figure 2.2 The system diagram of the MIIC algorithm.

The convergence of the MIIC algorithm has been analyzed in (14). It has been shown that the error between the desired input and the iterative control input, under effects of measurement noise and/or disturbance, is small provided that the signal to noise/disturbance ratio (SNR) is large. Furthermore, the output tracking error can be quantified in terms of the SNR. See the Appendix for details.

### 2.2.3 Implementation of the MIIC Technique in NBVS

As conceptually depicted in Fig. 2.3, the use of the MIIC technique in the proposed NBVS is to “learn” and “cancel” the dynamics of the piezo-cantilever system for the given desired force signal  $z_d(t)$ , such that the output of the piezo-cantilever system, i.e., the force exerted onto the sample,  $z_f(t)$ , will follow the desired force signal,  $z_f(t) \rightarrow z_d(t)$ . Thus this proposed approach is different from the multi-frequency excitation method (5; 6), where the desired force-signal is applied to drive the piezo-cantilever system directly (the dashed arrow path in Fig. 2.3). The MIIC technique is ideal for applications such as force-curve measurements, because in these applications, the operation is repetitive and the desired trajectory is known a priori. Therefore, the MIIC law can be *computed* offline (instead of online) directly in frequency domain—the time-domain iterative control input is obtained through the inverse Fourier transform, and then applied as a feedforward, open-loop control input to the system. In

such a frequency-domain implementation, Theorem 1 can be used to guide the use of the MIIC technique in practices—the MIIC input (Eq. (2.1)) should be applied at the frequencies where the SNR is large enough (as quantified by Eqs. (1, A.1)). At other frequencies, the control input should be set to zero. Note that in applications including nanomechanical measurements, the SNR can be experimentally estimated in practices by measuring the noise spectrum and comparing it to the pre-known desired output spectrum.

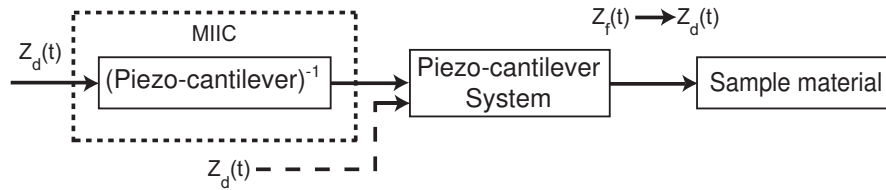


Figure 2.3 The schematic comparison of the MIIC algorithm (the dashed box) with the multi-frequency excitation method (the dashed arrow) in nanomechanical measurements.

The advantages of the MIIC technique include 1) the utilization of the noncausality of the operation (since the entire desired trajectory  $z_d(t)$  is known a priori) to improve the control performance, 2) the ease and efficacy in compensating for dynamics uncertainties through iterations, and 3) the ease of implementation with no need to acquire the frequency response (and/or dynamics model) of the system. In the proposed NBVS, the MIIC technique is used to exert a band-limited white-noise type of input force to excite the nanomechanical behavior of soft materials.

We note that the band-limited white-noise type of input (force) contains all frequency components uniformly distributed within the frequency band, thus allowing maximum excitation of the material's dynamics such as the rate-dependent mechanical behavior of the material, i.e., in the viewpoint of system identification, the white-noise input satisfies the persistent excitation condition (27). In this chapter, the obtained material response to such a band-limited white-noise input force will be used to obtain the non-parametric complex modulus (1) first, and then to identify the parametric truncated Prony series model of the storage and loss mod-

ulus (33).

## 2.2.4 Identification of the Frequency-dependent Plane-strain Modulus

As the proposed NBVS is developed for soft material characterization, the indentation (i.e., the soft material's response to the excitation force) is measured by using the MIIC technique to measure the force-deflection on the soft material and that on a reference hard material (1) (for the same driven input). The obtained input-output data are used in a mechanics model to obtain the complex modulus of the material in frequency domain. Finally, the complex modulus is modeled by a linear model (a truncated Prony series), and the parameters in the linear model are identified.

### 2.2.4.1 Obtain the Excitation Force and the Indentation Response

The force applied from the tip to the sample during the force measurements can be obtained from the measured cantilever deflection signal by using the relation (1),

$$F = K_t \times C_t \times d_S, \quad (2.2)$$

where  $K_t$  is the stiffness constant of the cantilever,  $C_t$  is the sensitivity constant of the deflection signal vs. the vertical displacement of the tip, and  $d_S$  denotes the cantilever deflection on the soft sample. Both the cantilever stiffness  $K_t$  and the deflection sensitivity  $C_t$  can be experimentally calibrated (34).

Then, the indentation of the tip into the soft sample can be obtained as (2)

$$h = C_t \times (d_H - d_S), \quad (2.3)$$

where  $d_H$  denotes the deflection on the hard material to the same control input for which the deflection on the soft material,  $d_S$ , is measured. Note that the elastic modulus of the reference hard material (e.g., sapphire) should be much higher (several orders higher) than that

of the soft material (e.g., PDMS)—thus the indentation on the reference material is negligible (compared to that on the soft material). Hence, the indentation of the tip into the soft sample can be obtained from the difference between the cantilever deflection on the soft sample and that on the reference material (1).

#### 2.2.4.2 Obtain the Complex Modulus of the Material

In the NBVS experiments, the material response is measured through superposition of two indenter loads — a constant mean load level and a vibratory load of smaller amplitude with a “white noise” like frequency spectrum. Recent work by Wahl et al. (35), Johnson et al. (36) and Barthel (37) has shown that indentation response to such a load history may be analyzed through separate analysis for static (mean) load and dynamic (vibratory) load. The material response to static load components determines the mean contact radius for the indentation. The response to oscillatory load is well approximated as indentation by a uniform cylindrical punch of radius equal to mean contact radius.

Following Wahl et al’s (35) experimental analysis and theoretical development reported by Johnson et al. (36), the frequency dependent modulus of soft materials is determined through decoupling of force-deflection response. Fast Fourier transform of the applied force and measured deflection is utilized to decouple the static and dynamic components. The static components of the force and indentation are utilized to determine the mean contact radius. Dynamic components and mean contact radius are used to determine the frequency dependent material modulus.

In the case of no adhesive interactions between the indenter and indented material, Hertz’s contact analysis (1) may be utilized to analyze the static components of load and deflections for mean contact area according to the following relation:

$$F_0 = \frac{4E_0^*a_0^3}{3R} \quad (2.4)$$

However, in the case of adhesive interactions, the static components may be analyzed using the Johnson, Kendall and Robert (JKR) theory to determine the mean contact radius. According to the JKR theory,

$$F_0 = \frac{4E_0^*a_0^3}{3R} - 2\sqrt{2\pi E_0^*wa_0^3}; \quad (2.5)$$

$$\delta_0 = \frac{a_0^2}{R} - \sqrt{\frac{2\pi a_0 w}{E_0^*}}; \quad (2.6)$$

$$F_{pullout} = -\frac{3}{2}\pi wR; \quad (2.7)$$

where  $F_0$  is the static component of the normal force between the tip and the sample surface, and  $\delta_0$  is the static component of the indentation of the tip on the sample surface. The static force  $F_0$  and the corresponding indentation  $\delta_0$  were experimentally measured at 139.3 nN and 166.7 nm, respectively.  $E_0^*$  is the combined plane-strain modulus of the sample material, which was calculated at 1.53 MPa by Eq. (2.5, 2.6), and  $w$  is the adhesion energy, which was calculated at 0.067 N/m by Eq. (2.7) ( $E_0^*$  is the geometric mean of the plane-strain moduli of the soft material and the indenter  $(1/E_0^*) = (1/E_{indenter}^*) + (1/E_{sample}^*)$ ). The plane-strain modulus of materials is a combination of its elastic modulus and Poisson's ratio. For elastic materials the plane-strain modulus is expressed as:  $E^* = E/(1 - \nu^2)$ . Since the indenter modulus (GPa) is almost three orders of magnitude greater than the soft material modulus (MPa),  $E_0^*$  is dominated by the lower of the two moduli, namely, the soft material, ( $E_0^* \sim E_{sample}^*$ ),  $a_0$  is the mean contact radius, and  $R$  is the tip radius. The pullout force  $F_{pullout}$  is measured in a separate experiment (38). Once the adhesion energy  $w$  is known, the mean contact radius,  $a_0$ , and the combined plane-strain modulus of the material,  $E_0^*$ , can be calculated from Eqs. 2.5 and 2.6. In separate experiments where AFM tip was pulled off the surface, pull-off force was measured to be 30 nN. The measured value for PDMS samples compares well with previous reports (38). It is important to note that in the NBVS experiment, the AFM tip was always

in contact with the sample and measured pull-out force is only utilized to determine the mean contact radius.

The above analysis assumes that the SPM-tip shape can be approximated as a parabolic surface. The SPM tip is used to scan a hard sample many times before using it in the force-curve experiments such that the wear during imaging results in desired tip shape (39; 40). The resulting shape is verified by measuring the tip profile through experiments (see Sec. 2.3.2.3). Also, the friction during the contact is assumed to be negligible. This is acceptable in the proposed approach because during the force measurement, the horizontal in-plane displacement of the tip relative to the sample is negligible, and the tip is in continuous contact with the sample throughout the measurement.

The oscillatory component of the load history is analyzed using the load-displacement relation for cylindrical punch with the radius equal to mean contact radius indenting the surface (35; 36). Therefore, the frequency-dependent plane-strain modulus is computed as:

$$E^*(j\omega) = \frac{\Delta P(j\omega)}{2a_0\Delta\delta(j\omega)} \quad (2.8)$$

where  $\Delta P(j\omega)$  is the amplitude of the excitation force, and  $\Delta\delta(j\omega)$  is the amplitude of the indentation of the material at frequency  $\omega$  by the SPM-tip.

Then the storage and the loss modulus of the material are obtained as the real part and the imaginary part of the complex modulus, respectively,

$$E^*(j\omega) = E'(j\omega) + jE''(j\omega). \quad (2.9)$$

We note that some small residual SPM-dynamics effect might still appear in the complex modulus at some frequencies, for example, around the resonant peaks—due to the sensitive variation of the SPM-dynamics around those frequencies, resulting in pronounced measurement error. Thus, we introduce the parameter-based approach to identify the frequency-dependent plane-strain modulus next.

### 2.2.4.3 Identification of the Frequency-dependent Plane-strain Modulus Based on a Linear Prony Series Model

A linear Prony series model is utilized to identify the combined modulus of soft materials. The use of the Prony series model allows a substantial removal of the residual SPM dynamics effect from the measured data, and thereby a more accurate combined modulus  $E(t)$  can be obtained. In this chapter, we use a truncated Prony series (i.e., a series of discrete exponential terms) to model the combined modulus (33; 41).

$$E(t) = E_{\infty} + \sum_{i=1}^n E_i \cdot e^{-t/\tau_i}, \quad (2.10)$$

where  $E_{\infty}$  is the fully relaxed modulus,  $E_i$ s are the modulus coefficients, and  $\tau_i$ s are the discrete retardation times.

The corresponding complex combined modulus  $E^*(j\omega)$ , can be obtained from the Fourier transform of Eq. (2.10), as presented below as the summation of the real part and the imaginary part,

$$E^*(j\omega) = \left( E_{\infty} + \sum_{i=1}^n \frac{E_i \cdot \tau_i^2 \cdot \omega^2}{1 + \tau_i^2 \cdot \omega^2} \right) + \left( \sum_{i=1}^n \frac{E_i \cdot \tau_i \cdot \omega}{1 + \tau_i^2 \cdot \omega^2} \right) \cdot j, \quad (2.11)$$

The parameters in the truncated Prony series model,  $E_i$ s and  $\tau_i$ s, are identified via curve-fitting the experimentally measured storage and loss modulus (i.e., the real and the imaginary part in Eq. (2.8), respectively) with respect to the counterparts in Eq. (2.11), respectively. The curve-fitting is based on the least-square minimization, thereby it is similar to the least-square algorithm for parameter estimation commonly used in standard system identification schemes (27). Also note that the modulus coefficients  $E_i$ s and the retardation constants  $\tau_i$ s for  $i=1, \dots, 3$  appear in the fitting of both the real part and the imaginary part. Thus the average value of the fitting results is used for these parameters. Once the parameters of the linear Prony series model are identified, the plane-strain modulus can be plotted according to Eq. (2.10).

## 2.3 Experimental Example: Frequency-dependent Viscoelastic Measurement of PDMS

We demonstrate the proposed technique by implementing it to measure the combined modulus of PDMS. We start with describing the experimental system.

### 2.3.1 Experimental Setup

The experimental system is schematically shown in Fig. 2.4. A commercial SPM system (Dimension 3100, Veeco Inc.) was used in the experiment, where the SPM-controller has been customized so that the PID control circuit of the SPM-controller was bypassed when the external control input was applied to drive the vertical z-axis piezoactuator. (see Fig. 2.4). The cantilever deflection sensor signal was acquired directly through a data acquisition card (DAQ) installed in the control computer. All the control input signals to the piezoelectric actuator were generated by using the MATLAB-xPC-target package (Mathworks Inc.), and sent through the DAQ card to drive the piezotube actuator via a high-voltage amplifier.

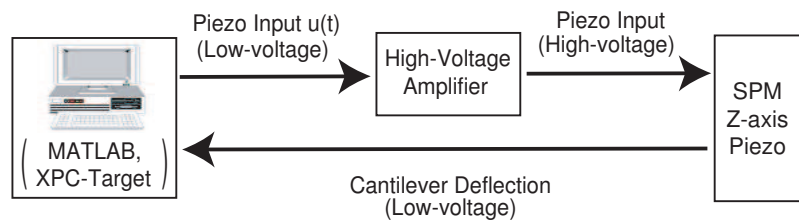


Figure 2.4 Schematic diagram of the experimental setup to implement MIIC algorithm in force-curve measurements.

### 2.3.2 Experimental Results & Discussion

#### 2.3.2.1 Tracking of the Band-limited White-noise Trajectory

First, the MIIC algorithm was applied to enable application of a band-limited white-noise type of excitation force by the cantilever on the PDMS sample (Readers are referred to Ref.

(2) for the preparation of the PDMS sample). A band-limited white-noise was generated in MATLAB for a time period of 6 seconds (In the experiment, initially a ramp signal of 0.5 sec. duration was applied to gradually increase the load force to the desired steady state load level. Then the force load was maintained at the same level for 0.5 second. Finally, two copies of the band-limited white-noise-like excitation force of 6 second duration were concatenated and then augmented to the steady-state force load and applied on the PDMS sample. Experimental results showed that the response of the initial load reached the steady-state in about 2-3 seconds, and the experimental result from the second 6-second white-noise excitation force was used in the analysis. Therefore, the effect of the starting load history was not considered in the analysis.). The cut-off frequency of the white-noise was chosen at 4.5 kHz. Note that the bandwidth of the z-axis SPM dynamics, with the voltage to the z-axis piezo actuator as the input and the cantilever deflection as the output, was at 1.27 kHz (The bandwidth was measured as usual as the frequency where the system gain drops by 3 dB from its DC-gain). Then the generated force trajectory was used as the desired trajectory in the MIIC algorithm and applied in the force measurement on the PDMS sample along with a small normal force. A mean load was used to avoid the pull-off of the tip from the sample surface during the measurements. No significant difference in the obtained data was observed when the normal force was varied a couple of times. The iteration described in Eqs. (2.1) converged in 3-5 iterations, and the converged output and the desired trajectory are compared in Fig. 2.5 (a) for the entire 6 second trajectory, and in Fig. 2.5 (b) for the zoomed-in view of the tracking in a 0.01 second period for time  $t \in [2, 2.01]$  second. The corresponding tracking error for the zoomed-in portion is also shown in Fig. 2.5 (c). In addition, the tracking performance was also quantified in terms of the relative RMS error  $e_2(\%)$  and the relative maximum error  $e_\infty(\%)$ , as shown in Table 2.1, where the relative RMS error and the relative maximum error are defined below:

$$e_2(\%) = \frac{\|z_d(\cdot) - z(\cdot)\|_2}{\|z_d(\cdot)\|_2} \times 100\%, \quad (2.12)$$

$$e_\infty(\%) = \frac{\|z_d(\cdot) - z(\cdot)\|_\infty}{\|z_d(\cdot)\|_\infty} \times 100\%. \quad (2.13)$$

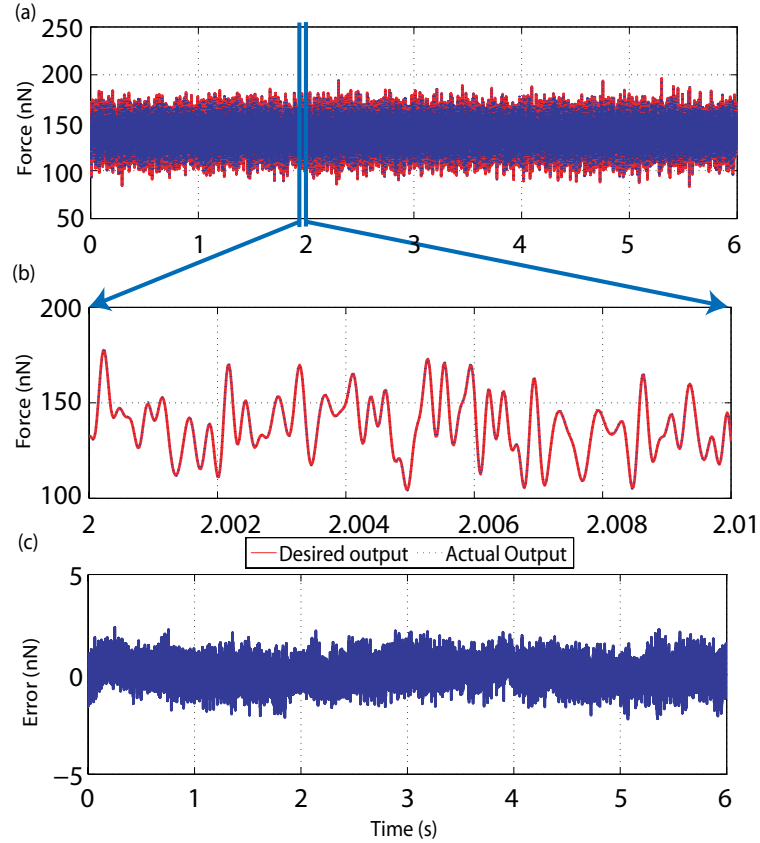


Figure 2.5 (a) The experimental tracking result (i.e., the force applied to the PDMS sample, which was converted from the cantilever deflection) of the band-limited white-noise trajectory with a period of 6 sec., (b) the zoomed-in view of the tracking result for time  $t \in [2, 2.01]$  sec., and (c) the tracking error of 6 sec.

The experimental results show that by using the MIIC technique, precise output tracking of complex desired trajectories can be achieved. For the cut-off frequency of 4.5 kHz, the output tracking trajectory converged to the desired trajectory within 4 iterations. The relative maximum-tracking error and the relative RMS-tracking error were both less than 5%. Such

a precise exertion of a complex excitation input force in the force measurement was difficult to achieve by using feedback control—if not entirely impossible, because the band-limit of the trajectory at 4.5 kHz was significantly higher than the bandwidth of the z-axis dynamics at 1.27 kHz (measured by the 3dB drop of the dynamics gain from its dc-Gain). As shown in Fig. 2.6, the z-axis SPM dynamics was quite complicated with several resonant peaks below the frequency band of the excitation force at 4.5 kHz. The z-axis SPM dynamics from the input of the piezotube actuator to the output of the cantilever deflection was measured under the condition that the SPM tip was in contact with the hard sapphire sample with a small normal load. Note since the sample was hard and the indentation was negligible, the measured z-axis frequency response should mostly represent the dynamics from the z-axis piezo actuator to the SPM-probe.

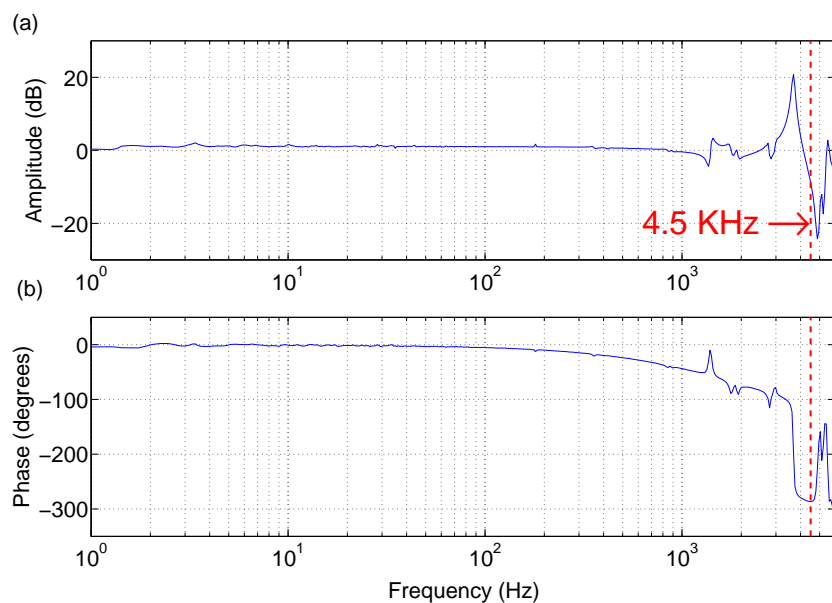


Figure 2.6 The experimentally measured frequency response of the SPM dynamics in the z-axis direction, where the red-dashed line at 4.5 kHz identifies the cut-off frequency of the band-limited white-noise used as the excitation force in the experiments.

The tracking precision of such a complex trajectory can also be evaluated by comparing

Table 2.1 Tracking performance of the MIIC technique to track a white-noise trajectory with the cut-off frequency of 4.5 KHz, where “Iter.No.” denotes the number of iterations used in the experiments.

| Iter.No.         | 1     | 2    | 3    | 4   | 5   |
|------------------|-------|------|------|-----|-----|
| $e_{\infty}$ (%) | 112.1 | 17.7 | 15.9 | 5.2 | 4.5 |
| $e_2$ (%)        | 106.1 | 14.1 | 12.5 | 4.3 | 4.1 |

the power spectrum of the tracking result with the desired one in the frequency-domain. As can be seen from Fig. 2.7, the desired trajectory has rich frequency components across the entire frequency spectrum (Fig. 2.7 (a)), and the power spectrum of the error was maintained very small with no conspicuous difference at all frequency components (Fig. 2.7 (b)). The 2-norm of the power-spectrum of the tracking error is only 2.6% of that of the desired trajectory. Therefore, the experimental results show that the MIIC technique can be used to track complex excitation force profile in force curve measurements.

For comparison, we also applied the desired band-limited white-noise input signal (after being scaled by the sensitivity of the piezo actuator to the cantilever deflection) directly to drive the piezo actuator—the same as in the multi-frequency excitation approach (5; 6; 7). The power spectrum of the obtained cantilever deflection (i.e., the desired input force) is plotted in Fig. 2.7 (c). Since the frequency band of the excitation signal at 4.5 KHz is substantially higher beyond the bandwidth of the  $z$ -axis SPM dynamics at 1.27 KHz, and significant dynamics effect exists within the 4.5 KHz frequency range (see Fig. 2.6), the power-spectrum of the excitation signal obtained in this direct implementation scheme has been dramatically distorted from being “white” (compare Fig. 2.7 (c) with (a)). Particularly, the power-spectrum of the excitation signal around the resonant peak of the  $z$ -axis SPM dynamics is over 2 orders of magnitude larger than those at other frequencies. Such an excitation force is not suitable for broadband viscoelasticity measurement as it results in poor signal to noise ratio at majority frequencies, and clearly demonstrates the limits of the multi-frequency approach (5; 6; 7)—

the frequency range of the excitation force should stay within the bandwidth of the system dynamics, whereas the use of the MIIC algorithm effectively removes such a limit.

### 2.3.2.2 The Force and the Indentation Measurements

The force applied on the PDMS sample was computed using Eq. (2.2), where the sensitivity constant of the cantilever was experimentally measured to be 65 nm/V by following the method outlined in (34), and the cantilever spring constant was determined to be 0.53 N/m by using the thermal noise method (34). Note that in nanomechanical property measurements using SPM, a cantilever with the spring constant accommodating the material to measure should be chosen, i.e., the cantilever should be soft enough with good force sensitivity to allow small probe-sample interaction force in the force-indentation measurement, whereas stiff enough to reduce the probe-sample adhesion effect. In this experiment, the cantilever with small spring constant was used. To measure the indentation, the converged iterative control input (obtained in Sec. 2.3.2.1 on the PDMS sample) was applied in the force measurement on the hard sapphire reference sample. The indentation of the SPM-tip in the PDMS sample was then calculated from the difference between the cantilever deflection on the PDMS sample and that on the sapphire sample (see Eq. (2.3)). The experimentally measured displacement of the probe on a PDMS sample is shown in Fig. 2.8(a), the indentation of the probe into the PDMS sample is plotted in Fig. 2.8(b) for a period of 6 seconds, and the zoomed-in view of Fig. 2.8(b) for time  $t \in [2, 2.01]$  sec. is shown in Fig. 2.8(c).

The experimentally measured force-indentation data reveal the frequency-dependent viscoelastic characteristics of the PDMS material. We note that compared to PDMS, sapphire sample can be practically regarded as “infinitely hard”. Therefore, under the same control input to the z-axis piezo actuator, the cantilever deflection obtained on the sapphire sample should be always larger than that on the PDMS sample. Such a prediction agreed with our experimental results: the indentation obtained in the experiments was always greater than

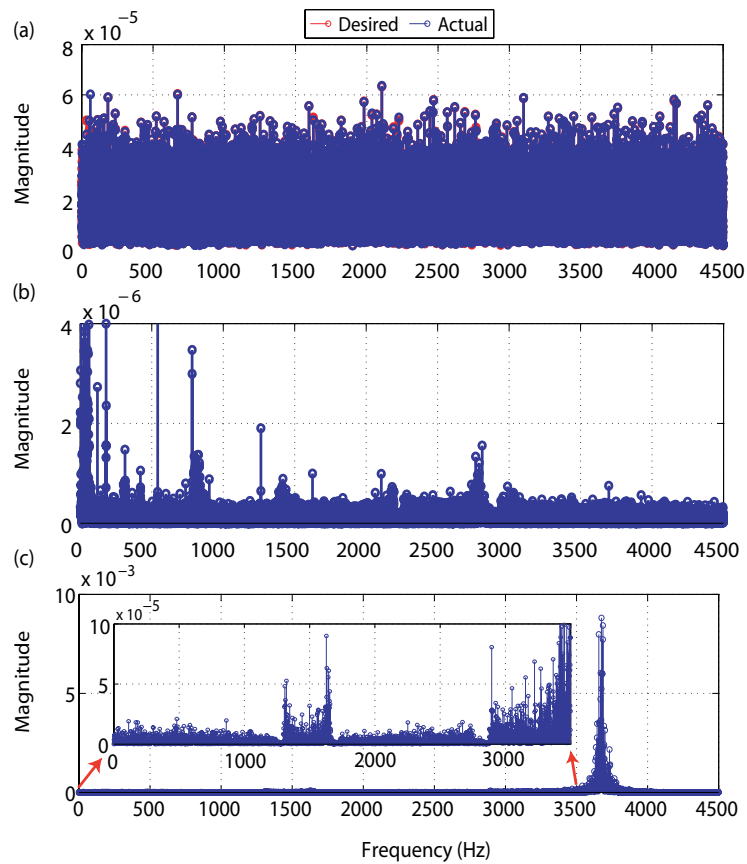


Figure 2.7 (a) Comparison of the magnitude of the frequency components in the desired white-noise input force with that in the measured input force obtained by using the MIIC technique, (b) the magnitude of the frequency components in the tracking error by using the MIIC technique, and (c) the magnitude of the frequency components in the measured input force obtained by using the multi-frequency excitation method (6; 7).

zero (see Fig. 2.8(c)). Furthermore, the experimental results also show that the indentation response of the PDMS sample was *frequency dependent*: the amplitude of the frequency components became smaller as frequency increased (see Fig. 2.9). Such a trend also agreed with the viscoelastic properties of PDMS: as the excitation frequency increased, the movements of the molecules of the PDMS sample were significantly retarded since they cannot follow the external deformation fast enough, hence, a faster external deformation rate resulted in stiffer material response. Therefore, the experiment results demonstrate that the proposed NBVS technique can be used to measure frequency-dependent viscoelastic properties of materials over a large frequency range.

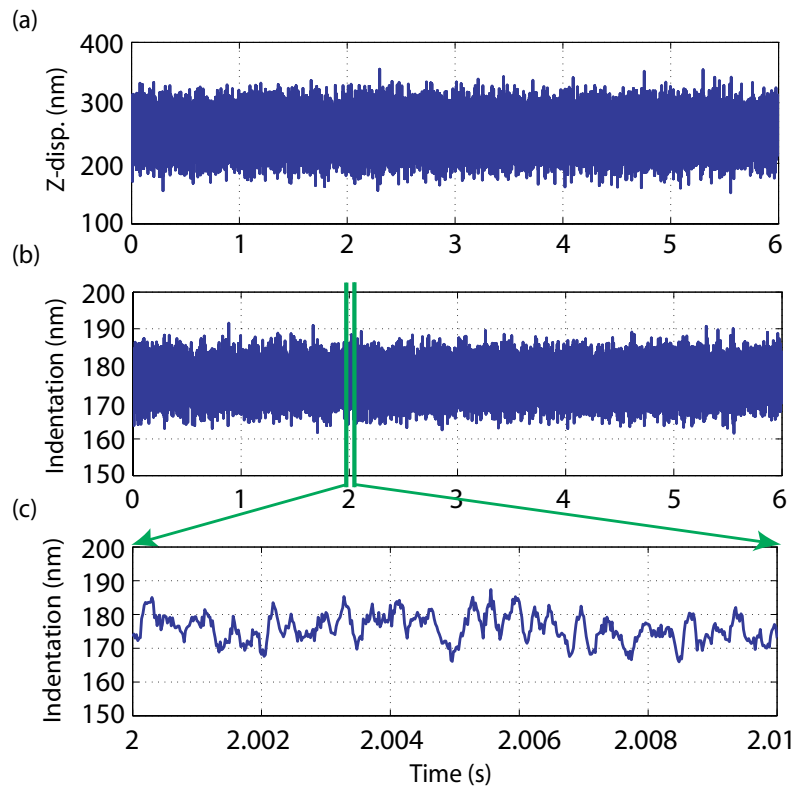


Figure 2.8 (a) The experimentally measured displacement of the probe on the PDMS sample, (b) the indentation of the probe into PDMS for a period of 6 sec., and (c) the zoomed-in view of plot (b) for time  $t \in [2, 2.01]$  sec.

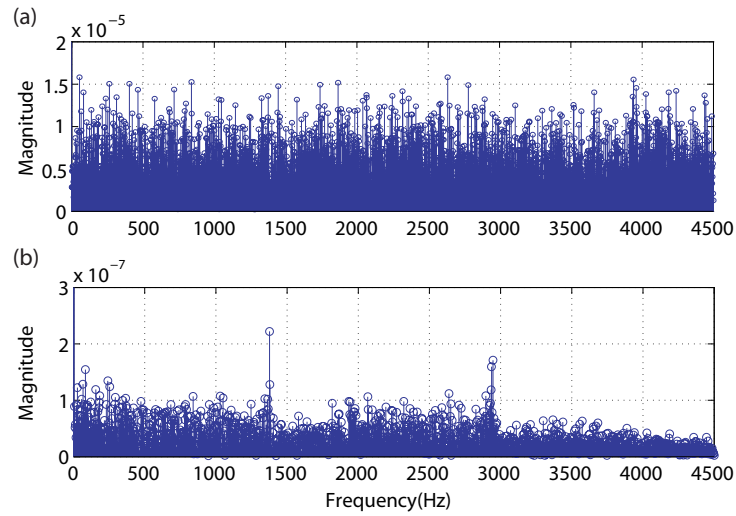


Figure 2.9 (a) The tip-sample interaction force that shows the band-limited white-noise characteristic, and (b) the indentation into the PDMS sample obtained under the force of (a).

### 2.3.2.3 Complex Modulus Identification

Load and indentation response measured on PDMS along with measured AFM tip radius and adhesive force were used in Eqs. (2.5-2.9) in order to determine the complex modulus. The PDMS sample demonstrated significant adhesive forces hence the JKR based analysis outlined in Sec. 2.2 was used to determine the material response. The AFM tip radius was experimentally characterized using a standard probe calibration sample (porous aluminum PA01) (34). The probe radius was determined to be 95 nm by fitting a parabola to the measured tip shape over a height of 150nm to 220 nm (34). Mean values of indentation and forces were used in Eqs. (2.5)-(2.7) to determine the average contact radius during the indentation. The average contact radius during the experiment was determined to be 128.9 nm. In addition, the combined plane-strain modulus of the PDMS was determined to be 1.53 MPa. The average contact radius and fourier spectrum of the measured load and indentation response were used in Eq. (2.8) to determine the complex modulus. Obtained complex modulus is plotted in Fig. 2.11 as a function of the frequencies. As commonly occurring in frequency response

measurements, “spikes” occurred in the complex modulus  $E^*(j\omega)$  plot, and MATLAB command ‘`spafdr`’ was used to remove such “spikes” (see Sec. 2.2.4.2). The improved complex modulus result was also plotted in Fig. 2.10. The obtained complex modulus result was also used to identify the parameters in the linear viscoelasticity model Eq. (2.11). Particularly, a 3<sup>rd</sup>-order Prony series model was used ( $n=3$  in Eq. (2.11)) as the fitting error became substantially larger when a lower-order model was used, whereas remained at the same level with higher order model. The real part and the imaginary part of the complex modulus,  $E^*(j\omega)$ , were fitted separately by using the MATLAB command ‘`nlinfit`’ (see Eq. (2.11)), and the averaged values from these two fittings (the real-part and the imaginary part) were used for the parameters in the linear viscoelasticity model Eq. (2.11). The fitting results (for the real-part and the imaginary-part of the complex modulus) are compared with the averaged values in Table 2.2 and in Fig. 2.11 along with the experimental data.

The results showed that the identified 3<sup>rd</sup>-order Prony series model fitted the experimental data quite well as the relative RMS errors in the curve-fitting of the real and the imaginary part were small at 4.59% and 4.96%, respectively. Note that even though the real-part and the imaginary-part were fitted independently, the real-part fitting values were quite close to those from the imaginary-part fitting (see Fig. 2.11 and Table 2.2). Table 2.2 also shows that the three fitted relaxation time constants occupied three different time orders, spanning from 0.1 ms to 10 ms. Thus, the averaged parameters were used in the linear viscoelasticity model to plot the real-part and the imaginary-part of the complex modulus, and compared to those of the experimental data, as shown in Fig. 2.11 with semi-logarithmic-scale in frequency. Moreover, we note that there exist some residual SPM z-axis dynamics effects in the modulus of the PDMS sample. However, the curve-fitting result in Fig. 2.11 captured the trend of the experimentally measured data quite well. After all the parameters  $E_i$  and  $\tau_i$  in the 3<sup>rd</sup>-order Prony series model were estimated, the modulus in time domain was calculated from Eq. (2.10), as shown in Fig. 2.12.

Table 2.2 The parameters generated from the curve fitting of the real part and imaginary part of the complex modulus, and their average.

| Param.           | Real Part | Imag. Part | Average |
|------------------|-----------|------------|---------|
| $E_\infty$ (MPa) | 3.97      | NA         | 3.97    |
| $E_1$ (MPa)      | 3.79      | 3.79       | 3.79    |
| $E_2$ (MPa)      | 3.27      | 8.26       | 5.77    |
| $E_3$ (MPa)      | 6.70      | 7.78       | 7.24    |
| $\tau_1$ (ms)    | 0.63      | 0.32       | 0.48    |
| $\tau_2$ (ms)    | 1.0       | 1.0        | 1.0     |
| $\tau_3$ (ms)    | 10.0      | 10.0       | 10.0    |

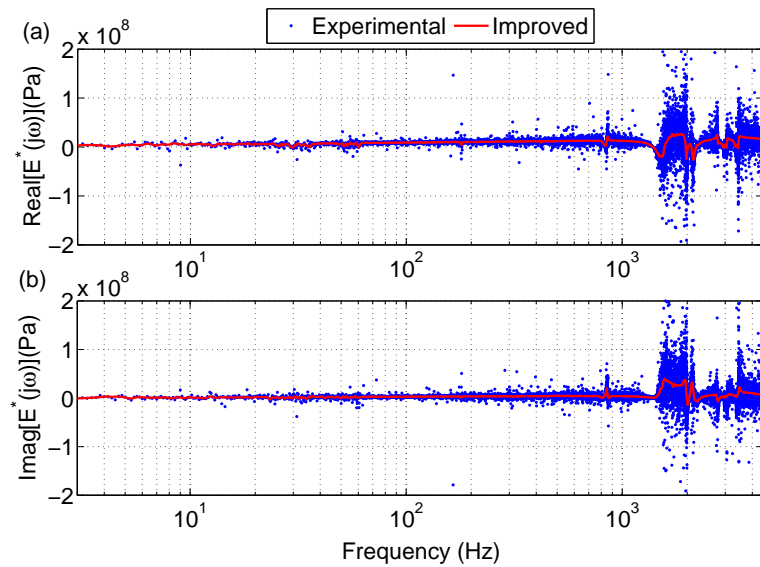


Figure 2.10 Comparison of the raw experimentally measured complex modulus of the PDMS sample (“Experimental”) with that improved by removing the “spikes” in Matlab (“Improved”) for (a) the real part, (b) the imaginary part.

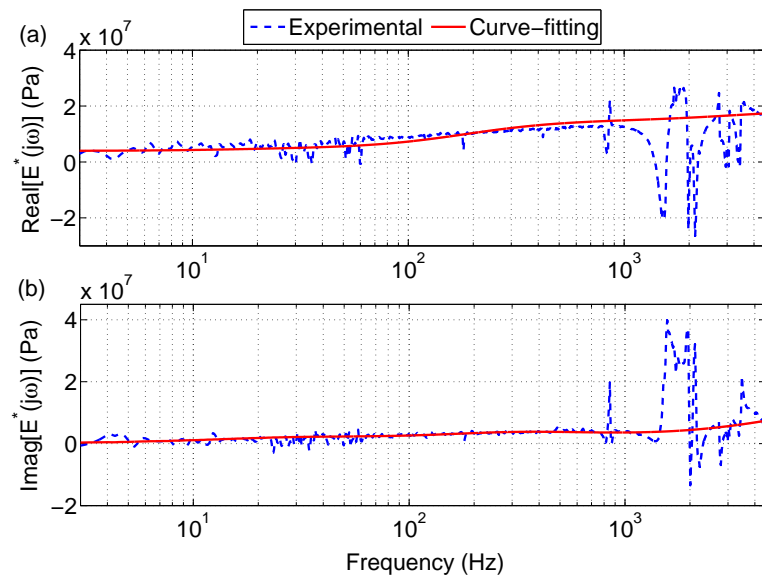


Figure 2.11 Comparison of the experimentally measured complex modulus of the PDMS sample to the results for (a) the real part and (b) the imaginary part, obtained by curve-fitting the real-part and the imaginary part separately.

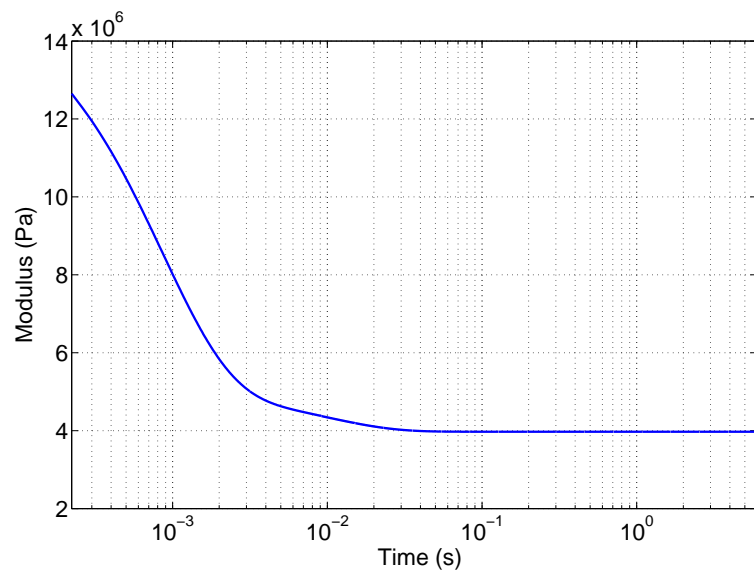


Figure 2.12 The calculated modulus of PDMS sample in time domain by using the parameters obtained from the curve fitting with Eq. (2.10).

#### 2.3.2.4 Discussion

According to the calculated complex modulus, the instantaneous modulus of PDMS is about 20.8 MPa and it quickly relaxes to 3.97 MPa. The instantaneous and the static modulus were computed by setting time  $t \rightarrow 0$  and  $t \rightarrow \infty$ , respectively, in the Prony series model Eq. (2.10). The combined plane-strain modulus determined from fitting the average indentation and load response is 1.53 MPa and compares well with the fully relaxed modulus. In addition, the magnitude of the instantaneous and the fully relaxed modulus compare well with the dynamic mechanical analysis (DMA) tests on the PDMS samples prepared with the sample procedure (2). The PDMS modulus was found to change from 6 MPa to 2 MPa as the temperature was changed from  $-30^\circ$  to room temperature. At room temperature, PDMS is above its glass temperature and displayed a clear rubbery viscoelastic response. Our proposed characterization technique clearly captures the rate dependent viscoelastic nature of PDMS polymer. These results demonstrate the efficacy of our technique for rapid broadband viscoelastic characterization. Experimental results show a larger noise for the low frequency range below 5 Hz. Since the material response is measured only over a short duration [less than 6 seconds], the low frequency response might not have been accurately captured. This source of noise and variability may be addressed through measuring material response to white noise based excitation for a longer period of time. Measured response is analyzed using contact mechanics models that account for adhesive interactions between SPM probe and sample surface. This analysis utilizes a simple model to account for this interaction that can be readily applied to other soft materials. The plane-strain modulus characterized using this approach includes the time dependence of the stress relaxation modulus and Poisson's ratio. Recently a number of reports (42; 43) have discussed the time dependence of Poisson's ratio, but there are only a few reports on its experimental characterization (44). In absence of independent experimental characterization for the Poisson's ratio, two commonly used assumptions in viscoelasticity (45) of time independent constant, Poisson's ratio or time independent constant, bulk modulus,

may be utilized to compute the other material response functions for a viscoelastic material from the experimentally measured response. More involved contact models (46) may also be used to quantify the influence of probe-surface interactions (10) on the measured response.

## 2.4 Conclusions

This chapter presented a novel nanoscale broadband viscoelastic spectroscopy (NBVS). In the proposed NBVS approach, the recently developed MIIC technique is used to: I) the exertion of excitation force with broad frequency components onto the sample, and II) the measurement of the material response for such excitation (i.e., the material indentation). The frequency-dependent viscoelasticity of the material was then obtained by using the measured excitation force and the indentation in a contact mechanics model that describes the dynamics interaction between the probe and the sample. The proposed NBVS was illustrated by implementing it to measure the rate-dependent viscoelastic response of a PDMS sample. The experimental results showed that the use of the MIIC technique enabled the cantilever deflection to precisely track a band-limited (cut-off frequency: 4.5 kHz) white-noise type of desired trajectory on the PDMS sample, thereby applying a band-limited white-noise type of excitation force on the PDMS sample. Then the indentation of the PDMS sample was obtained by applying the same control input to obtain the force measurement on a reference hard sample. The obtained excitation force and the indentation results showed that the rate-dependent modulus of soft materials like PDMS can be measured by using the proposed NBVS approach.

## 2.5 Acknowledgments

The author would like to thank Prof. Sriram Sundararajan and Prof. Zhiqun Lin, both from Iowa State University, for their help on the tip radius characterization and the PDMS sample preparation, respectively. The financial support of NSF Grants CMMI-0626417 and CAREER

award CMMI-0846350 are also gratefully acknowledged. PS and DT were supported through a NSF career development grant CAREER CMMI-0547280.

## **CHAPTER 3. MODEL-BASED APPROACH TO COMPENSATE FOR THE DYNAMICS CONVOLUTION EFFECT IN NANOMECHANICAL PROPERTY MEASUREMENT**

### **Abstract**

This chapter presents a model-based approach to compensate for the dynamics convolution effect in nanomechanical property measurements. In the indentation-based nanomechanical property measurement of soft materials, an excitation force consisting of various frequency components needs to be accurately exerted to the sample material through the probe, and the indentation of the probe into the sample needs to be accurately measured. However, when the measurement frequency range increases close to the bandwidth of the instrument hardware, the instrument dynamics along with the probe-sample interaction dynamics can be convoluted with the mechanical behavior of the soft material, resulting in distortions in both the force applied and the indentation measured, which, in turn, directly lead to errors in the measured nanomechanical property (e.g., the creep compliance) of the material. In this chapter, the dynamics involved in indentation-based nanomechanical property measurements is analyzed to reveal that the convoluted dynamics effect can be described as the difference between the lightly-damped probe-sample interaction dynamics and the over-damped nanomechanical behavior of soft materials. Thus, these two different dynamics effects can be decoupled via numerical fitting based on the viscoelastic model of the soft material. The proposed approach is illustrated by implementing it to compensate for the dynamics convolution effect in a broad-

band viscoelasticity measurement of a Polydimethylsiloxane (PDMS) sample using scanning probe microscope.

### 3.1 Introduction

In this chapter, a model-based approach to compensate for the dynamics convolution effect on indentation-based nanomechanical property measurements is proposed. Indentation-based nanomechanical property measurement of soft materials using scanning probe microscope (SPM) or nanoindenter provides unique insights into material properties at nano-scale, critical to unravel the structure-property correlation of a wide variety of materials ranging from polymers to live biological materials (1; 47; 48; 49; 50). Extraneous dynamics, however, can be convoluted with the material response during the measurement, resulting in measurement errors in the obtained material properties (e.g., the creep compliance). Such a dynamics convolution effect has limited the measurable frequency range of existing nanomechanical measurement techniques. Therefore, the goal of this chapter is to develop a systematic approach to compensate for the dynamics convolution effect on nanomechanical property measurements, thereby increasing the measurement frequency range and reducing the measurement errors.

Dynamics convolution effect exists and limits indentation-based nanomechanical property measurements. Various indentation-based techniques have been developed to measure the frequency (rate)-dependent nanomechanical properties of soft materials (2; 5; 6). For example, the rate-dependent elastic modulus of soft materials such as Polydimethylsiloxane (PDMS) can be measured by using force-curve measurements under different loading/unloading rates (2; 51). The force curve measurement, however, is quasi-static, thereby time-consuming when the frequency range to measure becomes large. Moreover, as the loading/unloading rate increases, the instrument dynamics along with the probe-sample interaction effect can be convoluted with the material response in the measured force signal (e.g., the cantilever deflection when SPM is used). As a result, the exerted force (from the probe to the sample) may fail to

follow the desired force profile. The measurement time can be reduced and the measurement frequency range can be increased by using the force modulation method (4; 5). However, the instrument dynamics along with the interaction dynamics are still convoluted into the measurement. Although in the force modulation method, the dynamics convolution effect can be accounted for by using a linear spring-damper mechanical model (52; 23), this method is still limited to relatively low frequency range because only a low-order spring-damper model is feasible in practices, which becomes inadequate to capture the dynamics convolution effect as the measurement frequency range becomes large. The frequency range as well as the sensitivity of the measurement are improved in the recently-developed multi-frequency approach (5; 6). The applicable force spectrum, however, is severely distorted by the dynamics convolution effect when the measurement frequency range becomes large, resulting in poor signal-to-noise ratio at some frequencies while input saturation at some others. Therefore, there exists a need to compensate for the dynamics convolution effect in nanomechanical property measurements.

Compensation for the dynamics convolution effect on nanomechanical property measurements using SPM is challenging. We note that only the measurement of the probe deflection—as the output of the entire deflection dynamics from the driven piezoactuator to the mechanical response of the material—is available. The convoluted dynamics effect on the excitation force can be substantially reduced by using control techniques as demonstrated recently with the use of novel iterative control techniques (2; 9). Thus, the control input obtained, when applied, allows the desired force profile to be accurately exerted onto the sample surface (2; 9). Compensation for the convoluted dynamics effect on the indentation measured, however, still remains as a challenge. This is because the indentation (of the soft material by the applied force) usually is obtained from the difference between the probe deflection on the soft sample and that on a hard reference sample. The difference in the material behaviors of these two samples (soft and hard), thereby, leads to variations in the probe-sample interaction particularly when the measurement frequency range becomes large. As a result, extraneous dynamics

effect is convoluted into the indentation measurements. Although indentation might be measured by actuating the sample and sensing the sample displacement instead of the probe (1), the measurement frequency range can be significantly lower (than actuating and sensing the probe), because the bandwidth of such an actuation system tends to be substantially smaller than that of the actuation system of the probe. Therefore, techniques need to be developed to compensate for the dynamics convolution effect on nanomechanical property measurements.

The main contribution of this chapter is the development of a model-based approach to eliminate the dynamics convolution effect on nanomechanical property measurements. In the proposed approach, the cantilever deflection dynamics is analyzed and modeled as a cascaded dynamic system consisting of the piezoactuator, the cantilever along with the mechanical fixture, the probe-sample interaction dynamics, and the nanomechanical dynamics of the material. The cantilever deflection dynamics on both the soft sample and the hard reference sample are measured and compared to reveal that the convoluted part of the instrument dynamics is characterized by lightly-damped poles and zeros, whose locations coincide with those of the piezo and cantilever dynamics. On the contrary, the mechanical behavior of soft materials is characterized by over-damped dynamic behavior that can be described by for example, a Prony series model (8). Then, the convoluted dynamics effect, distinct from the material behavior in frequency domain, is removed numerically through fitting. The proposed approach is illustrated by implementing it to the measurement data obtained in a broadband viscoelasticity measurement of a PDMS sample using SPM. Both the multi-frequency approach (5; 6) and the iterative-control-based method (2; 9) are applied in the measurement. The results demonstrate that the dynamics convolution effect on the measurements in both cases can be effectively reduced by using the proposed method.

## **3.2 Model-based Compensation for Instrument Dynamics Convolution Effect**

In this section, we start with describing nanomechanical property measurements on SPM.

### **3.2.1 Nanomechanical Property Measurement Using SPM**

SPM has become an enabling tool to image sample topography and measure material property at nanoscale (53). Specifically, the frequency-dependent mechanical properties of soft materials can be measured by exerting forces of different frequency components to the sample and measuring the indentation of the material—as the response of the material to the excitation force (1). For example, the rate-dependent elastic modulus of soft polymers such as PDMS can be measured from force-curve measurements with different loading/unloading rates (2), where the probe-sample interaction force versus the vertical displacement of the SPM-probe is measured during a push-retraction process when the SPM-probe follows a triangle-like trajectory (see Fig. 3.1). Using force-curves to measure rate-dependent mechanical properties, however, is time consuming as the experiment needs to be repeated at different rates. More efficiently, frequency-dependent nanomechanical properties can be measured by using the force-modulation method (4), where a sinusoidal excitation input is augmented to a constant (normal) force load and applied to drive the cantilever (1; 54). The indentation of the probe into the soft sample is obtained from the difference of the cantilever deflection on the soft sample and that on a hard reference sample for the same input voltage. Then, the measured excitation force and indentation data, i.e., the input and the output response, can be used in an appropriate contact mechanics model to quantify the mechanical properties (such as creep compliance, storage modulus and loss modulus) of the material (1).

The cantilever deflection signal is measured to quantify the excitation force and the indentation. The force applied is measured as (1)

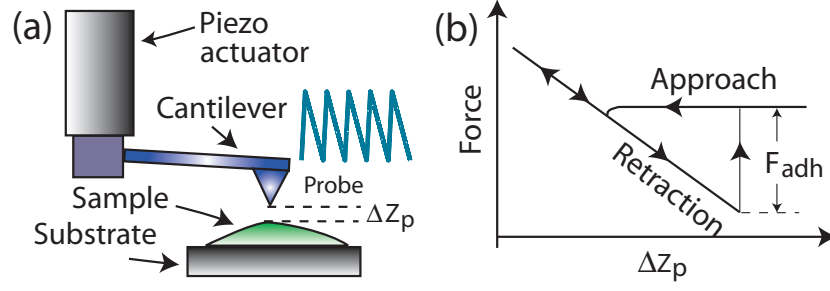


Figure 3.1 (a) the force curve measurement scheme and (b) a schematic drawing of a force-distance curve.

$$P(t) = K_t \times C_t \times d(t), \quad (3.1)$$

where  $K_t$  is the stiffness constant of the cantilever,  $C_t$  is the sensitivity constant of the deflection signal vs. the vertical displacement of the probe (both can be experimentally calibrated (34)), and  $d(t)$  denotes the cantilever deflection on the sample. Then, the indentation of the probe into the soft sample can be obtained as (1)

$$h(t) = C_t \times [d_H(t) - d_S(t)] = C_t \times \Delta D(t), \quad (3.2)$$

where  $\Delta D(t)$  denotes the difference between the cantilever deflection on the hard material,  $d_H(t)$ , and that on the soft material,  $d_S(t)$ , respectively.

Various contact mechanics models have been developed to obtain the mechanical properties of materials (e.g., the complex compliance) (55). For example, when the probe-sample interaction can be modeled as the contact of a frictionless, rigid, spherical indenter with a homogeneous, linear, and isotropic viscoelastic substrate, the complex compliance of the material in uniaxial compression,  $J^*(j\omega)$ , can be obtained from the following Hertz contact model presented in frequency-domain:

$$J^*(j\omega) = \frac{[h^{\frac{3}{2}}(\cdot)](j\omega)}{\mathcal{C}_1 \times P(j\omega)}, \quad (3.3)$$

where  $P(\cdot)$  and  $h(\cdot)$  are defined in Eqs. (3.1, 3.2), and the constant  $\mathcal{C}_1$  is given by

$$\mathcal{E}_1 = \frac{3(1 - \nu^2)}{4\sqrt{R}}, \quad (3.4)$$

where  $\nu$  is the poisson ratio of the sample, and  $R$  is the SPM-probe radius.

Note that when measuring nanomechanical properties of soft materials, usually the amplitude of the excitation force is relatively small (i.e. the mechanical behavior of the material can be adequately described by a linear viscoelasticity model), and a full probe-sample contact is maintained throughout the measurement (1; 53). Therefore in the following, we assume that the force-indentation data are measured under these two conditions.

### 3.2.2 Dynamics Convolution Effect on Indentation-based Nanomechanical Property Measurement

In indentation-based measurements of nanomechanical properties, accurately must the excitation force  $P(t)$  be applied, so must the indentation  $h(t)$  be measured. It is evident from Eqs. (3.1, 3.2, 3.3) that errors in the measured excitation force and/or the indentation directly lead to errors in the measured nanomechanical property. Particularly, the excitation force  $P(t)$ , i.e., the cantilever deflection, needs to follow the desired excitation force profile, and the difference of the cantilever deflection on the soft material and that on the hard reference material should accurately represent the indentation of the probe into the soft material. Maintaining accuracy in the force applied as well as the indentation measured, however, becomes challenging when the measurement frequency range becomes large relative to the bandwidth of the SPM instrument dynamics. The challenge arises because the excitation force is generated by applying an input voltage to drive the piezoactuator (see Fig. 3.2). Therefore, when the measurement frequency increases, the instrument dynamics (from the piezoactuator to the cantilever deflection) can be excited, and extraneous dynamic effect can be induced into the measurement. Specifically, the deflection signal on a soft sample can be represented in frequency domain as (see Fig. 3.2)

$$\begin{aligned}
D_S(j\omega) &= G_{ss}(j\omega)G_{cs}(j\omega)G_{pc}(j\omega)V(j\omega) \\
&\triangleq G_S(j\omega)V(j\omega),
\end{aligned} \tag{3.5}$$

where  $G_{ss}(j\omega)$  denotes the material dynamics of the soft sample,  $G_{cs}(j\omega)$  represents the interaction dynamics between the cantilever-probe and the soft material,  $G_{pc}(j\omega)$  models the dynamics from the piezoactuator to the cantilever along with the mechanical fixture between them, and  $V(j\omega)$  is the Fourier transform of the input voltage applied to the piezoactuator.

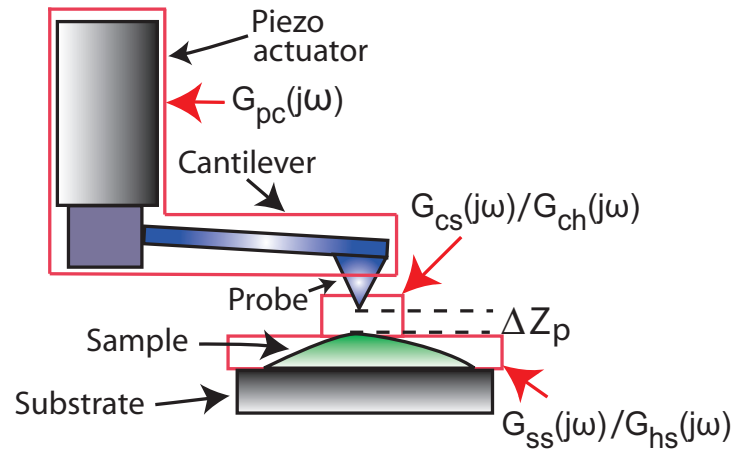


Figure 3.2 The scheme of the dynamics involved in nanomechanical property measurement using SPM.

Similarly, the measured deflection signal on a hard reference sample can be represented as

$$\begin{aligned}
D_H(j\omega) &= G_{hs}(j\omega)G_{ch}(j\omega)G_{pc}(j\omega)V(j\omega) \\
&= K_{hs}G_{ch}(j\omega)G_{pc}(j\omega)V(j\omega) \\
&\triangleq G_H(j\omega)V(j\omega),
\end{aligned} \tag{3.6}$$

where  $G_{hs}(j\omega)$  represents the dynamic behavior of the hard material,  $G_{ch}(j\omega)$  represents the interaction dynamics between the cantilever-probe and the hard sample, and  $G_{pc}(j\omega)$  and  $V(j\omega)$  are the same as defined in Eq. (3.5). Note that usually the hard reference sample,

by choice, has an elastic modulus over several orders higher than that of the soft sample, the mechanical behavior of the hard reference sample can be regarded as frequency-independent in the measured frequency range. Thus, in the following, the hard sample dynamic behavior model  $G_{hs}(j\omega)$  is replaced by a constant  $K_{hs}$ . Therefore, by Eq. (3.2, 3.5, 3.6), the dynamics involved in the indentation measurement can be depicted by the block diagram in Fig. 3.3.

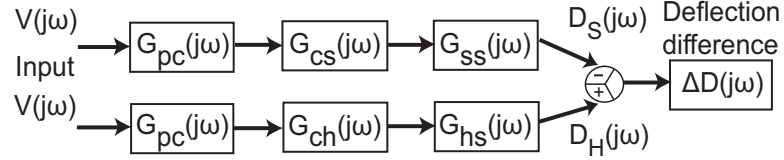


Figure 3.3 The diagram of system dynamics.

Equation (3.5) implies that the cantilever deflection  $D_S(j\omega)$  (i.e., the excitation force) follows the input voltage  $V(j\omega)$  if the total deflection dynamics involved in the measurement on the soft sample,  $G_S(j\omega)$ , can be adequately approximated as a constant. This condition can only be satisfied when the measurement frequency is relatively low (compared to the bandwidth of the total deflection dynamics  $G_S(j\omega)$ ). As the measurement frequency increases, the instrument dynamics (including the piezo-cantilever dynamics  $G_{pc}(j\omega)$  and the interaction dynamics  $G_{cs}(j\omega)$ ) is convoluted (in time-domain) with the material behavior  $G_{ss}(j\omega)$  and the desired excitation force cannot be tracked by the probe if the desired force profile (after scaling) is applied directly to drive the piezoactuator. The direct driving method is used in the multi-frequency approach (6; 56). Thus, the measurement frequency range of the multi-frequency method is limited by the dynamics convolution effect on the excitation force (i.e., cantilever deflection), which, on the contrary, can be compensated for by using control technique (9). Specifically, the desired input voltage  $V_d(j\omega)$  can be obtained by using techniques such as iterative learning control, so that the output cantilever deflection tracks the given desired excitation force profile  $D_{des}(j\omega)$ , i.e.,

$$D_s(j\omega) = G_S(j\omega)V_d(j\omega) \longrightarrow D_{des}(j\omega). \quad (3.7)$$

This approach has been demonstrated recently (2; 9).

The dynamic effect becomes more pronounced in the indentation measurement, due to the difference of the interaction dynamics on the soft sample,  $G_{cs}(j\omega)$ , and that on the hard reference sample,  $G_{ch}(j\omega)$ . By Eqs. (3.5, 3.6), the difference of the cantilever deflections (see Eq. (3.2)) is given as

$$\Delta D(j\omega) = [K_{hs}G_{ch}(j\omega) - G_{ss}(j\omega)G_{cs}(j\omega)]G_{pc}(j\omega)V(j\omega). \quad (3.8)$$

When the measurement frequency range is relatively low (compared to the bandwidth of the piezo-cantilever dynamics  $G_{pc}(j\omega)$ ), the difference of the interaction dynamics between the soft and the hard samples tends to be small also, i.e.,  $G_{cs}(j\omega) \approx G_{ch}(j\omega)$ . This is because in the relatively low frequency range, the piezo-cantilever dynamics  $G_{pc}(j\omega)$  also tends to be static, and the difference of the probe-sample interaction dynamics on the cantilever deflection also tends to be small. Thus, the measured cantilever deflection difference becomes

$$\Delta D_i(j\omega) = [K_{hs} - G_{ss}(j\omega)]G_{cs}(j\omega)G_{pc}(j\omega)V(j\omega). \quad (3.9)$$

The above Eq. (3.9) shows that in this case, the measured cantilever deflection difference is generated solely by the difference of the mechanical behavior between the soft sample and the hard reference sample,  $K_{hs} - G_{ss}(j\omega)$ , thereby representing the “true” indentation of the probe into the soft sample (after scaling, see Eq. (3.9)). When the frequency range to measure becomes large, the deflection difference becomes

$$\begin{aligned} \Delta D(j\omega) &= [K_{hs}G_{ch}(j\omega) - G_{ss}(j\omega)G_{cs}(j\omega)]G_{pc}(j\omega)V(j\omega) \\ &= [K_{hs} - G_{ss}(j\omega)]G_{cs}(j\omega)G_{pc}(j\omega)V(j\omega) \\ &\quad + [G_{ch}(j\omega) - G_{cs}(j\omega)]K_{hs}G_{pc}(j\omega)V(j\omega) \\ &\triangleq \Delta D_i(j\omega) + \Delta D_e(j\omega). \end{aligned} \quad (3.10)$$

The above Eq. (3.10) reveals that measurement error is induced into the indentation measurement due to the difference of the interaction dynamics,  $G_{ch}(j\omega) - G_{cs}(j\omega)$ , as described by the second term of the summation,  $\Delta D_e(j\omega)$ . The different interaction dynamics (soft vs. hard) is caused by issues such as different probe-sample contact area between the soft and the hard samples and different damping effect on the cantilever deflections upon the soft and the hard samples. Particularly, when the excitation frequency becomes high with respect to the dynamic behavior of the soft sample, the difference of the interaction dynamics tends to become large, resulting in large distortion in the indentation measured.

The induced interaction dynamics effect on the indentation measurement leads to large distortions (errors) in the nanomechanical measurement of soft materials. This problem might be alleviated through hardware modification, for example, by exciting the sample from below instead of the probe (1). The measurement bandwidth, however, can be substantially smaller, because the bandwidth of the actuation system for the sample is substantially lower than that for the probe due to the increase of the mass to be excited. Thus, there exists a need to compensate for the convoluted dynamics effect in the indentation measurement.

### 3.2.3 Model-based Approach to Compensate for the Dynamics Convolution Effect on Nanomechanical Measurement

Next, we present a model-based approach to compensate for the dynamics effect on nanomechanical property measurements. Since the dynamics convolution effect on the applied force can be compensated for by using control techniques as described in Sec. 3.2.2, we focus, in the following, on compensating for the convolution effect on the indentation measurement. Note that the interaction dynamics ( $G_{cs}(j\omega)$  or  $G_{ch}(j\omega)$ ) and the piezo-cantilever dynamics  $G_{pc}(j\omega)$  are convoluted together in the measurement, because only the cantilever deflection—the response of the total deflection dynamics ( $G_S(j\omega)$  or  $G_H(j\omega)$  in Eqs. (3.5) or (3.6), respectively)—can be measured. Thus, we define the total convoluted dynamics ratio,

$G_{cv}(j\omega)$ , as the ratio of the total deflection dynamics on the hard reference sample,  $G_H(j\omega)$ , to that on the soft sample,  $G_S(j\omega)$ :

$$\begin{aligned}
G_{cv}(j\omega) &\triangleq \frac{G_H(j\omega)}{G_S(j\omega)} \\
&= \frac{K_{hs}G_{ch}(j\omega)G_{pc}(j\omega)}{G_{ss}(j\omega)G_{cs}(j\omega)G_{pc}(j\omega)} \\
&= \frac{K_{hs}}{G_{ss}(j\omega)} \frac{G_{ch}(j\omega)}{G_{cs}(j\omega)} \text{ (by Eqs. (3.5, 3.6))} \\
&\triangleq \Delta G_{hs}(j\omega)\Delta G_c(j\omega).
\end{aligned} \tag{3.11}$$

The first term on the right of the above equation,  $\Delta G_{hs}(j\omega) = K_{hs}/G_{ss}(j\omega)$ , describes the dynamic behavior of the soft sample relative to the hard reference sample (called the *hard-soft material dynamics ratio thereafter*), and the second term,  $\Delta G_c(j\omega)$ , describes the ratio of the interaction dynamics between the soft and hard samples (called the *hard-soft interaction dynamics ratio thereafter*).

The total deflection dynamics,  $G_S(j\omega)$  and  $G_H(j\omega)$ , can be obtained by applying an excitation input to the piezoactuator and measuring the cantilever deflection as the output in the usual “black box” identification approach (e.g. the sweep sine method). Note that full contact of the probe with the sample is maintained by augmenting a normal load to the excitation signal, and the measured dynamics is linear by keeping a small excitation amplitude.

Combining Eqs. (3.10, 3.11), the coupling caused deflection difference error,  $\Delta D_e(j\omega)$ , can be rewritten as

$$\begin{aligned}
\Delta D_e(j\omega) &= [G_{ch}(j\omega) - G_{cs}(j\omega)] K_{hs} G_{pc}(j\omega) V(j\omega) \\
&= [\Delta G_c(j\omega) - 1] \frac{K_{hs}}{G_{ss}(j\omega)} G_{ss}(j\omega) G_{cs}(j\omega) G_{pc}(j\omega) V(j\omega) \\
&= [\Delta G_{hs}(j\omega)\Delta G_c(j\omega) - \Delta G_{hs}(j\omega)] D_S(j\omega) \\
&= [G_{cv}(j\omega) - \Delta G_{hs}(j\omega)] D_S(j\omega),
\end{aligned} \tag{3.12}$$

Thus, the above Eq.(3.12) reveals that the coupling-caused deflection difference error,  $\Delta D_e(j\omega)$ , is due to the difference between the total convoluted dynamics ratio,  $G_{cv}(j\omega)$ , and the hard-soft material dynamics ratio,  $\Delta G_{hs}(j\omega)$ . Hence, provided that these two dynamics,  $G_{cv}(j\omega)$  and  $\Delta G_{hs}(j\omega)$ , can be separated, the convolution caused indentation measurement error can be eliminated. The challenge, however, exists because although the total convoluted dynamics ratio  $G_{cv}(j\omega)$  is measurable as shown in (3.11), the hard-soft material dynamics ratio  $\Delta G_{hs}(j\omega)$  is unknown in general.

We proceed to consider the fundamental difference between the hard-soft interaction dynamics ratio,  $\Delta G_c(j\omega)$ , and the hard-soft material dynamics ratio,  $\Delta G_{hs}(j\omega)$ . Note that the hard-soft material dynamics ratio  $\Delta G_{hs}(j\omega)$  essentially represents the complex compliance of the soft material (see Eq. (3.3)), since the hard material behavior is largely frequency-independent. Moreover, as the linearity condition is satisfied during the measurement, the complex compliance of soft materials like polymers can be well described by a linear compliance model, for example, a truncated Prony series, i.e., the complex compliance of the soft sample is modeled as (8):

$$J^*(j\omega) = \frac{J_0}{j\omega} - \sum_{i=1}^n \frac{J_i}{j\omega + 1/\tau_i}, \quad (3.13)$$

where  $\tau_{i,s} > 0$  are the retardation time constants of the soft material at different time scale,  $J_0$  is the fully relaxed compliance, and  $J_i$ s are the compliance coefficients (41). Thus, in Eq. (3.13), the material compliance is modeled as a spring and  $n$  number of spring-damper pairs in parallel with each other. Thus, the hard-soft material dynamics ratio,  $\Delta G_{hs}(j\omega)$ , is overdamped in nature (8). On the contrary, the interaction dynamics difference,  $\Delta G_c(j\omega)$ , tends to be lightly-damped, i.e.,  $\Delta G_c(j\omega)$  can be represented as

$$\Delta G_c(j\omega) = \prod_{i=1}^N \frac{\omega_{n,i}^2}{s^2 + 2\zeta_i \omega_{n,i} s + \omega_{n,i}^2}, \quad (3.14)$$

where  $\omega_{n,i}$  is the undamped natural frequency and  $\zeta_i$  in  $0 < \zeta_i < 1$  is the corresponding damp-

ing ratio. The above Eq. (3.14) holds because the difference of the interaction dynamics between the soft sample and the hard one is caused by issues including the difference of the damping effect of the soft material on the piezo-cantilever dynamics and that of the hard material, and the different contact area of the probe with the soft sample and that with the hard one. The damping effect of the hard material is rate-independent (in the measurement frequency range), whereas the damping effect of the soft material is frequency-dependent (see Eq. (3.5)). Moreover, the probe-sample contact area on the soft sample tends to be larger than that on the hard sample. As a result, these effects become much more pronounced around the lightly-damped poles and zeros of the piezo-cantilever dynamics. Thus, in frequency domain, the material dynamic behavior and the difference of the interaction dynamics are distinct from each other, making it possible to eliminate the convoluted interaction dynamics effect from the indentation measurement. Particularly, numerical algorithms can be sought to decouple them. In this chapter, the hard-soft interaction dynamics ratio  $\Delta_{hs}(j\omega)$  is removed from the total convoluted dynamics ratio  $G_{cv}(j\omega)$  by fitting the latter into a Prony series like model (i.e., an over-damped linear dynamics model). Then the dynamics convolution-caused error  $\Delta_e(j\omega)$  is obtained by multiplying the fitting result with the deflection measured on the soft sample (see Eq. (3.12)), and the compensated indentation is obtained according to Eqs. (3.2, 3.10).

### 3.3 Implementation Example

The proposed model-based approach to compensate for the dynamics convolution is illustrated by implementing it to the nanomechanical property data experimentally measured on a Polydimethylsiloxane (PDMS) sample. We start with describing the dynamics convolution effect observed in the experiments.

### 3.3.1 Dynamics Convolution Effect on Broadband Nanomechanical Property Measurement

The experimental data obtained in a broadband viscoelasticity measurement of a PDMS sample were processed in this example. The dynamics convolution effects become pronounced when the measurement frequency range became large (i.e., broadband). Specifically, two different approaches to broadband nanomechanical measurements were applied. First, the multi-frequency method (6; 56) was implemented, where a desired excitation force profile with power spectrum similar to band-limited white-noise was applied to drive the piezoactuator directly, i.e., the desired force profile scaled by the DC gain of the total deflection dynamics (from the piezoactuator to the cantilever deflection) was applied as the input voltage. Secondly, the model-less inversion-based iterative learning control (MIIC)-based method was implemented (9; 14), where the input obtained by using the MIIC technique was applied to the piezoactuator so that the cantilever deflection on the PDMS sample tracked the desired force profile. The use of the MIIC technique was to demonstrate the use of control technique to compensate for the dynamics convolution effect on the excitation force (see Sec. 3.2.2). In both cases, the indentation into the PDMS sample was measured by applying the same control input to a hard reference sample—a sapphire sample whose Young’s modulus is 6 orders higher than that of PDMS. The obtained deflection signals were used to compute the force and the indentation (see Eqs. (3.1, 3.2)), where the sensitivity constant of the cantilever of 65 nm/V was experimentally measured by following the method outlined in (34), and the cantilever spring constant of 0.53 N/m was calibrated by using the thermal noise method (34). The probe radius of 95 nm was experimentally characterized by imaging a standard probe calibration sample (porous aluminum PA01) (34; 57). The frequency components of the obtained force and indentation results are presented for the amplitude part in Fig. 3.4 (a), (b) and Fig. 3.5 (a), (b) for the multi-frequency method and the MIIC-based method, respectively. The obtained force and indentation were used to obtain the complex compliance based on the Hertz

model (see Eq. (3.3)), and the corresponding amplitudes of the complex compliance obtained by using these two methods are shown in Figs. 3.4(c) and 3.5(c), respectively.

The force-indentation data measured in the experiments show that the dynamics convolution effect on both the force applied and the indentation measured is pronounced. When the multi-frequency method was used, the force applied to the PDMS sample was severely distorted from the desired force spectrum (compare Fig. 3.4 (a) with the desired force profile shown in Fig. 3.5 (a)). Particularly, the amplitude of the force components around the resonant peak at 2.85 KHz was 20 times and 25 times larger than the averaged amplitude of the force components in the low frequency range ( $< 1.2$  KHz) and that in the high frequency range (3.5 to 4.5 KHz), respectively. Such a largely uneven distribution of the excitation force spectrum can result in poor signal to noise ratio in some frequency range and signal saturation in others, both not desirable in nanomechanical property measurement. On the contrary, evenly distributed excitation force spectrum was achieved by using the MIIC excitation method. As shown in Fig. 3.5 (a), the spectrum of the force applied almost overlapped with that of the desired one. Thus, the experimental results demonstrate the efficacy of the MIIC technique in compensating for the dynamics convolution effect on excitation force.

The experimental results also demonstrated that the dynamics convolution effect on the indentation measurement was pronounced in both methods (see Fig. 3.4 (b) and Fig. 3.5 (b)). Comparing the indentation results measured in both methods, we note that by using the MIIC technique, the dominant peak of the indentation spectrum at 2.85 KHz in the multi-frequency method was eliminated (compare Fig. 3.4 (b) with Fig. 3.5 (b)), however, other convolution-caused peaks became pronounced, and distorted the indentation measured. As a result, the complex compliance results obtained were substantially distorted. As can be seen from Fig. 3.5 (c), although the value of the complex compliance in the low frequency range (around 2 Hz) at  $2.6 \times 10^{-7} Pa^{-1}$  was close to the static complex compliance of PDMS reported in the literature (2), the variation of the complex compliance with respect to the increase of frequency was severely distorted from the frequency-dependent compliance of PDMS—The complex

compliance of PDMS should monotonically decay as frequency increases, signaling the material transferred from rubbery to glassy (9; 14). Therefore, it is evident from the experiment results that the dynamics convolution effect needs to be compensated for in nanomechanical property measurements.

### 3.3.2 Model-based Compensation for the Convolutional Dynamics Effect

The proposed method was applied to compensate for the dynamics convolution effect in both methods (the multi-frequency and the MIIC-based methods). First, the total deflection dynamics on the PDMS sample  $G_S(j\omega)$  (see Eq.(3.5)) was measured as described in Sec. 3.2.3, and compared with that on the sapphire sample  $G_H(j\omega)$  (see Eq.(3.6)). Both shown in Fig. 3.6. Then, the total convolutional dynamics ratio  $G_{cv}(j\omega)$  was obtained as the ratio of these two deflection dynamics (see Eq.(3.11)), as shown in Fig. 3.6 also. To take into account of the possible variation due to the different contact points on sapphire (as the total deflection dynamics on sapphire and the reference deflection on sapphire for indentation measurement were measured at different times thereby at different sample points), the total deflection dynamics on the sapphire sample were measured five times at five different locations, respectively. As shown in Fig. 3.7, the total deflection dynamics on the sapphire sample measured at different points almost overlapped to each other (The difference is only about 1.12% of the total deflection dynamics, both measured in average sense). In addition, we compared the total convolutional dynamics ratio with the uncompensated indentation (obtained by using the MIIC-based method) in Fig. 3.8.

Next, to eliminate the coupling caused deflection error  $\Delta_e(j\omega)$  (see Eq. (3.10)), the hard-soft material dynamics ratio was modeled as a linear  $3^{rd}$  order Prony series like model, then the hard-soft material dynamics ratio  $\Delta G_{hs}(j\omega)$  (see Eq. (3.11)) was decoupled from the total convolutional dynamics ratio  $G_{cv}(j\omega)$  numerically using Matlab package (Mathworks, Inc.) according to Eq. (3.12). Specifically, the hard-soft material dynamics ratio was estimated by

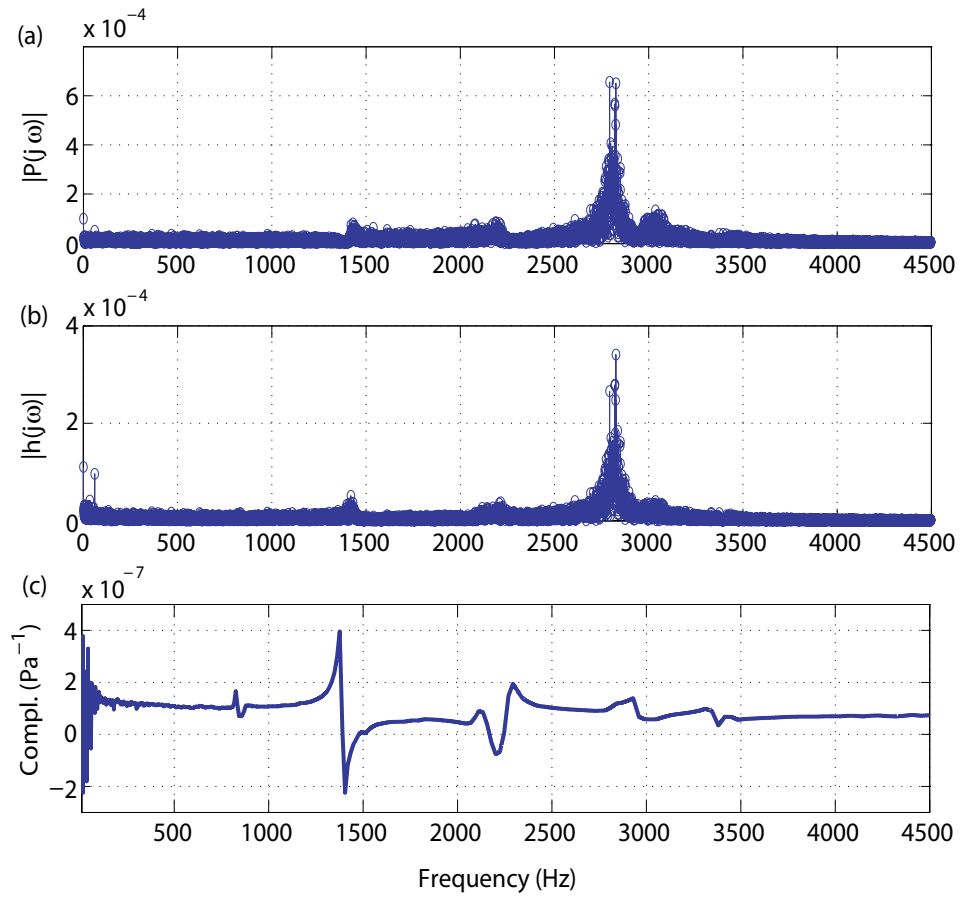


Figure 3.4 (a) The magnitude of the frequency components of the excitation force applied onto the PDMS sample by using the multi-frequency method, (b) the amplitude of the frequency components in the corresponding indentation of the PDMS sample, and (c) the uncompensated complex compliance calculated using the force in (a) and the uncompensated indentation in (b) in the Hertz model.

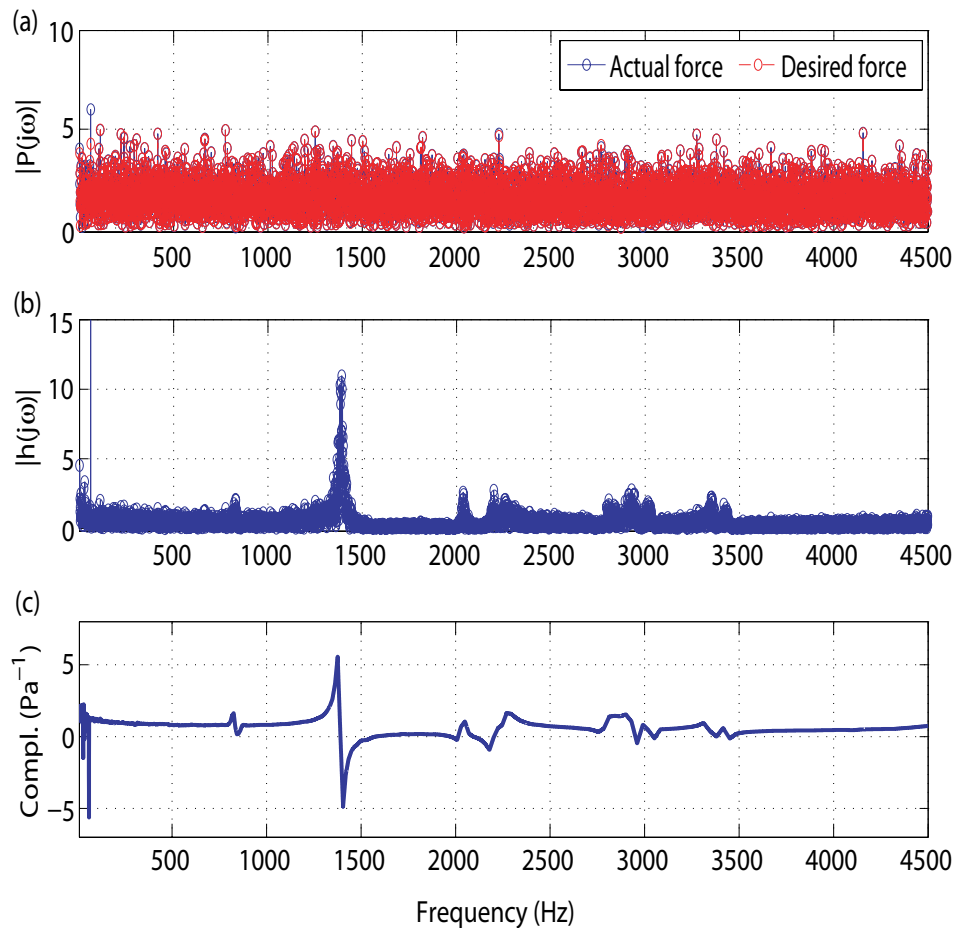


Figure 3.5 (a) The comparison of the magnitude of the frequency components of the desired excitation force and the magnitude of the frequency components of the excitation force applied onto the PDMS sample by using the MIIC technique, (b) the amplitude of the frequency components in the corresponding indentation measured on the PDMS sample, and (c) the uncompensated complex compliance calculated by using the force data in (a) and the uncompensated indentation data in (b) in the Hertz model.

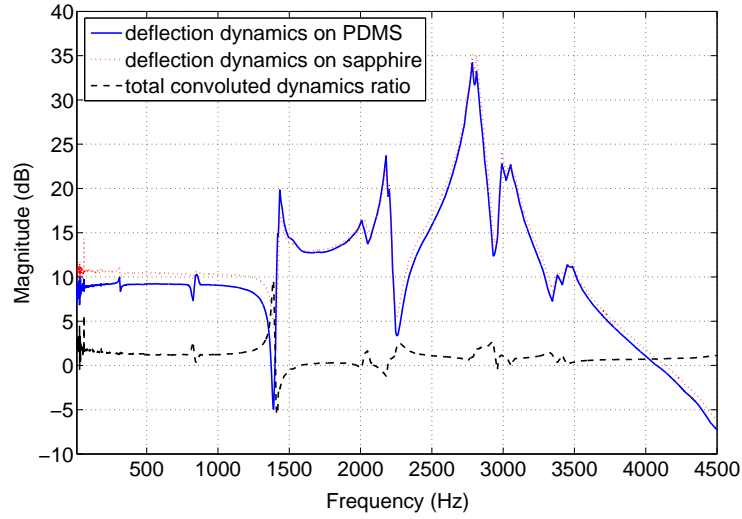


Figure 3.6 The total deflection dynamics measured on the PDMS sample (blue line) and on the sapphire sample (red line), and the ratio of these two (black line), i.e., the total convoluted dynamics ratio (see Eq. (3.11)).

curve-fitting the real part and the imaginary part of the total convoluted dynamics ratio, respectively. The obtained fitting parameters for the real-part and the imaginary-part are compared in Table 3.1). Clearly the parameters obtained from the real-part fitting were very close to those obtained from the imaginary-part fitting. Such a consistence in the fitting indicated that the material dynamics ratio  $\Delta G_{hs}(j\omega)$  can be well described by a 3<sup>rd</sup>-order Prony series like model. Then the averaged parameters were used to estimated the hard-soft material dynamics ratio and then the coupling caused deflection error  $\Delta_e(j\omega)$ . The compensated indentation results are compared with the uncompensated (raw) one in Fig. 3.10 (a), and Fig. 3.11 (a) for the multi-frequency and the MIIC-based method, respectively. Finally, the compensated indentation data were used to compute the compensated complex compliance. The uncompensated (raw) and compensated complex compliance were compared in Fig. 3.10 (b), and Fig. 3.11 (b) for the multi-frequency and the MIIC-based method, respectively.

The experimental results showed that the dynamics convolution effect on the indentation measurement was caused by the total convoluted dynamics ratio  $G_{cv}(j\omega)$ . As shown in Fig.

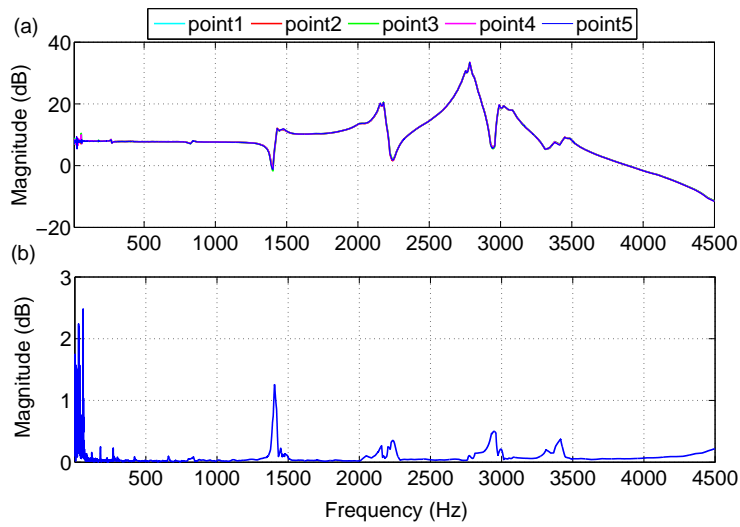


Figure 3.7 (a) The total deflection dynamics from the piezoactuator to the deflection on the sapphire sample measured by using the same control input at 5 different points, and (b) the maximum difference between these total deflection dynamics.

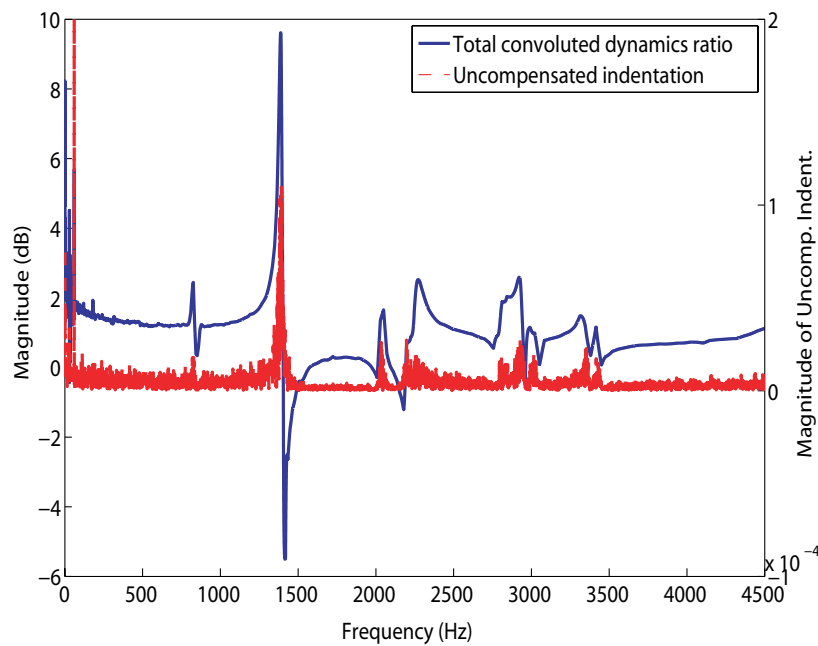


Figure 3.8 The comparison of the uncompensated indentation (blue line) of the PDMS sample using the MIIC-based method with the total convoluted dynamics ratio (black line).

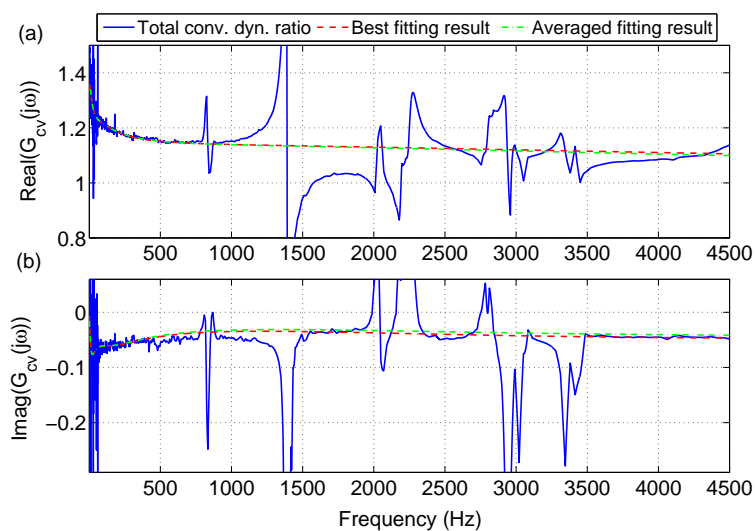


Figure 3.9 The curve fitting result of (a) the real part and (b) the imaginary part of the total convoluted dynamics ratio  $G_{cv}(j\omega)$  by a  $3^{rd}$ -order Prony series like model.

Table 3.1 The parameters of the  $3^{rd}$ -order Prony series like model estimated from the curve fitting of the real part and imaginary part of the total convoluted dynamics ratio,  $G_{cv}(j\omega)$ , and the averaged values.

| Param.          | Real Part              | Imag. Part             | Average                |
|-----------------|------------------------|------------------------|------------------------|
| $G_0$           | 1.358                  | NA                     | 1.358                  |
| $G_1$           | 0.096                  | 0.078                  | 0.0870                 |
| $G_2$           | 0.085                  | 0.086                  | 0.0855                 |
| $G_3$           | 0.135                  | 0.134                  | 0.1345                 |
| $\tau_1$ (sec.) | $2.913 \times 10^{-5}$ | $2.563 \times 10^{-5}$ | $2.738 \times 10^{-5}$ |
| $\tau_2$ (sec.) | $7.294 \times 10^{-4}$ | $7.546 \times 10^{-4}$ | $7.420 \times 10^{-4}$ |
| $\tau_3$ (sec.) | $7.583 \times 10^{-3}$ | $7.788 \times 10^{-3}$ | $7.686 \times 10^{-3}$ |

3.8, the dynamics-convolution-caused “peaks” in the uncompensated indentation coincided with those “peaks” of the total convoluted dynamics ratio. By using the proposed compensation method, such a dynamics convolution effect was substantially reduced. As can be seen from Fig. 3.10 (a), the compensated indentation obtained by using the multi-frequency method better synchronized with the excitation force than the uncompensated one (compare Fig. 3.10 (a) with Fig. 3.4 (a) and (b), particularly around frequencies near 2 KHz to 2.5 KHz, and around 3 KHz). As a result, after compensation, the complex compliance obtained by using the multi-frequency method monotonically decreased as the frequency increased, which agreed with the viscoelastic behavior of PDMS. However, when using the multi-frequency method, such a viscoelastic behavior of PDMS cannot be seen from the compensated indentation result—due to the convoluted dynamics in the excitation force applied (compare Fig. 3.4 (b) with Fig. 3.10 (a)). On the contrary, by applying the proposed method to the indentation data obtained by using the MIIC-based method, the compensated indentation monotonically decreased as the frequency increased (see Fig. 3.11). As a result, the convoluted dynamics effect was removed from the compensated complex compliance result. As shown in Fig. 3.11, the PDMS is above its glass temperature and displays a clear viscoelastic solid response at room temperature. Therefore, the proposed approach can be used to effectively eliminate the convoluted instrument dynamics effect and improve the bandwidth and/or the accuracy of the measurement of frequency-dependent broadband nanomechanical property of soft materials.

### 3.4 Conclusions

In this chapter, a model-based approach to compensate for the dynamics convolution effect in the nanomechanical property measurement of soft materials is proposed. The dynamics involved in indentation-based nanomechanical property measurements was analyzed to reveal that the convoluted dynamics effect can be described as the difference between the lightly-damped probe-sample interaction dynamics and the over-damped nanomechanical behavior

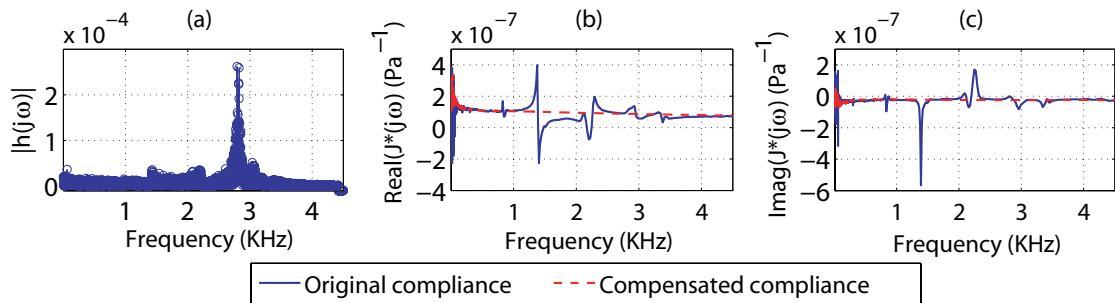


Figure 3.10 (a) the compensated indentation data obtained by using the multi-frequency excitation, and (b) the comparison of the uncompensated compliance of the PDMS sample (red line) with the compensated compliance of the PDMS sample (blue line).

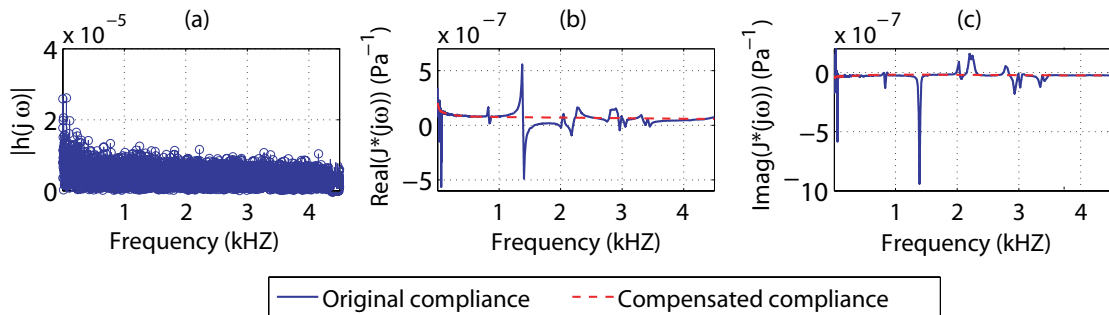


Figure 3.11 (a) the compensated indentation result obtained by using the MIC-based method, and (b) the comparison of the uncompensated compliance (red line) of the PDMS sample with the compensated compliance of the PDMS sample (blue line).

of soft materials. Then, these two different dynamics effects were decoupled via numerical fitting based on the Prony series model of the viscoelasticity of the soft material. The proposed approach was illustrated by implementing it to compensate for the dynamics convolution effect in a broadband viscoelasticity measurement of a Polydimethylsiloxane (PDMS) sample using scanning probe microscope, and the experimental results showed that the dynamics convolution effect can be effectively compensated for by using the proposed approach.

## **CHAPTER 4. OPTIMAL EXCITATION FORCE DESIGN IN INDENTATION-BASED RAPID BROADBAND NANOMECHANICAL SPECTROSCOPY: POLY (DIMETHYLSILOXANE) EXAMPLE**

### **Abstract**

This chapter presents an optimal input design approach to achieve rapid broadband nanomechanical measurements of soft materials using the indentation-based method. The indentation-based nanomechanical measurement provides unique quantification of material properties at specified locations. The measurement, however, currently is too slow in time and too narrow in frequency (range) to characterize time-elapsing material properties during dynamic evolutions (e.g., the rapid-stage of the crystallization process of polymers). These limits exist because the excitation input force used in current methods cannot rapidly excite broadband nanomechanical properties of materials. The challenges arise as the instrumental hardware dynamics can be excited and convoluted with the material properties during the measurement when the frequencies in the excitation force increase, resulting in large measurement errors. Moreover, long measurement time is needed when the frequency range is large, which, in turn, leads to large temporal measurement errors upon dynamic evolution of the sample. In this chapter, we develop an optimal-input design approach to tackle these challenges. Particularly, an input force profile with discrete spectrum is optimized to maximize the Fisher information matrix of the linear compliance model of the soft material. Both simulation and experiments on a Poly(dimethylsiloxane) (PDMS) sample are presented to illustrate the need for optimal input

design, and the efficacy of the proposed approach in probe-based nanomechanical property measurements.

## 4.1 Introduction

In this chapter, an optimal input design approach is proposed to achieve rapid identification of broadband nanomechanical properties of soft materials through indentation-based approach. Indentation-based approach using scanning probe microscope (SPM) or nanoindenter has become an enabling tool to quantitatively measure the nanomechanical properties of a wide variety of materials, both locally and globally (1). The current measurement methods (4; 6), however, are limited in both the frequency range that can be measured and the measurement time that is needed to measure the (frequency) rate-dependent viscoelasticity of materials (19). These limits of current measurement methods (4; 6), in both measurement frequency and time, arise as the excitation force from the probe to the sample surface employed cannot compensate for the convolution effect of the instrument dynamics (10; 51), nor rapidly excite the rate-dependent nanomechanical behavior of the material (11; 58). Thus, the proposed approach is developed to tackle the challenges in emerging nanomechanics studies.

Inefficiencies exist in current nanomechanical measurement methods for characterizing the time-elapsing properties of soft materials. For example, although nanomechanical properties such as elasticity can be measured by using the force-curve measurements (1), the excitation input force used is quasi-static and thereby, does not contain rich frequency components to rapidly excite viscoelastic response of materials. One attempt to address the lack of frequency components in the excitation force has been the force modulation technique (4), where a sinusoidal driven signal (i.e., the input voltage) is applied to the actuator of the cantilever — piezoelectric actuator — with the aim to generating a sinusoidal excitation force profile. Then the frequency-dependent material properties can be acquired by sweeping the frequency over the measurement frequency range, and measuring the vibration of the probe (the amplitude

and the phase) relative to the driving input. During the measurement, however, the instrument hardware dynamics effect is coupled into the measured data. Although such a coupling effect can be accounted-for by modeling the probe-sample interaction dynamics as a spring-mass-damper system, the model is adequate only for the low frequency range (4), whereas large measurement errors occur as the dynamics model becomes more complicated and erroneous when the measurement frequency becomes high (relative to the hardware bandwidth). Moreover, the force-modulation technique is slow to sweep a large frequency range as the de-modulation process involved is inherently time-consuming. The measurement time can be reduced by using the recently-developed multi-frequency method (5; 6). However, the frequency components used are not optimized, and the measurement frequency range is still limited by the instrument dynamics convolution effect. Evidently, there is a need to improve the current indentation-based nanomechanical property measurement methods.

One of the main challenges to achieve rapid broadband nanomechanical measurement is to ensure that 1) the force applied shall accurately track the desired force profile and 2) the indentation should be accurately measured. Accurate tracking of the desired force profile is necessary to excite the material behavior in the measured frequency range, as well as to avoid issues related to low signal-to-noise ratio and input saturation (due to the force being too small or too large). Accurate indentation measurement is needed to capture (and only capture) the material behavior as the response to the force applied. When the measurement frequency range becomes large (i.e., broadband), however, the dynamics of the system consisting of the piezoactuator and the probe can be excited (65), resulting in large vibrations of the probe relative to the sample. Furthermore, substantial dynamics uncertainties exist in the SPM system due to the thermal drift (66) and the change of operation condition (e.g., change of the probe). Additional force tracking errors can also be generated when the displacement of the piezoactuator is large and as a result, the hysteresis effect of the piezoactuator becomes pronounced (22; 23). These adverse effects on the excitation force can be mitigated by using control techniques so that the excitation force can be accurately exerted onto the sample

surface, as demonstrated recently by using the iterative learning control methods (2; 9; 10). Residual instrument dynamics effect, however, still exists in the indentation measured (as the indentation is measured indirectly from the difference between the probe response on the soft sample to be measured and that on a hard reference sample). Recently, model-based techniques (10; 12) have been developed to account for the dynamics convolution effect on the measured indentation data. These post-processing technique, however, cannot be used to achieve rapid broadband nanomechanical measurements, as discussed next.

The other major challenge in rapid broadband nanomechanical measurements is to achieve rapid excitation of the material response by the force applied (from the probe). Rapid excitation (of the material response) is needed to capture the time-elapsing nanomechanical properties during dynamic evolution of the material, for example, during the initial rapid stage of the crystallization of polymers (11) or the healing process of live cell (13). Moreover, rapid excitation of material response is also needed when mapping the nanomechanical properties of the material over the sample surface. Although the mapping of elasticity/stiffness of materials at nanoscale can be obtained by using the force volume mapping technique (67; 68), the force-curve measured at each sample point is quasi-static and the mapping procedure is time consuming, with mapping time in tens of minutes to several hours — which becomes even much longer to map rate-dependent nanomechanical properties. Such a long mapping time renders the adverse effects (14) due to disturbances (e.g., thermal drift) and variations of system dynamics pronounced. As a result, large measurement errors occur, particularly when the sample is evolving. Recently, a frequency-rich excitation force with power spectrum similar to band-limited white noise has been utilized for broadband nanomechanical measurement (9). Although the iterative learning control (ILC) technique has been applied for the tracking of such a complicated desired trajectory, dynamics convolution effect discussed above still exists. Thus, both the above two major challenges in rapid broadband nanomechanical measurements are closely related to the excitation force applied.

The main contribution of this chapter is the development of an approach based on the op-

timal input design to achieve rapid nanomechanical spectroscopy. First, the measurement of nanomechanical properties is transformed into a parameter identification problem by capturing the nanomechanical properties of the sample to be measured in a parameterized model (e.g., a truncated-order exponential (Prony) series model of the complex compliance of the material (8; 33)). Then, the optimal excitation force — acting as the input to the material mechanics model — is sought to minimize the covariance of the estimation error through the maximization of the Fisher information matrix (15; 16) of the parameterized mechanics model. Specifically, the designed optimal excitation force profile comprises multiple sinusoidal signals whose frequency and amplitude are optimized through an iterative experimental process. Not only can the obtained optimal force profile rapidly excite the nanomechanical properties of materials over a broadband frequency range, but also, with a discrete frequency spectrum, reduce the dynamics convolution effect by facilitating the tracking of such an excitation force. Then, the designed optimal excitation force profile (e.g., the cantilever deflection when using SPM) is tracked by using the recently-developed inversion-based iterative control technique (2) that compensates for the hardware dynamics convolution effect. The proposed approach is illustrated through both simulation and experimental implementations on the measurement of viscoelasticity of a Polydimethylsiloxane (PDMS) sample using an SPM. The simulation and experiment results demonstrate the need of optimal input design and the efficacy of the proposed approach in achieving broadband viscoelasticity spectroscopy.

The proposed approach based on optimal input design is fundamentally different from existing works. We note that recently experiment design based on the notion of system identification has been introduced to the characterization of viscoelasticity of polymers at bulk scale (59; 60). However, the experiment design in (59; 60) was focused on the optimization of sensor distribution in multi-sensor measurements, and instrument hardware dynamics convolution effect was not addressed. The design of experiment was also explored in (61; 62; 69; 70) for parameter estimation precision. However, only numerical simulations are conducted to verify the proposed methods. Moreover, although recent decade has witnessed significant develop-

ment of control techniques for nanopositioning control centering around SPM applications (see (71; 72; 73; 74)), the majority of the efforts are focused on the scanning operations and SPM imaging. Therefore, the work presented in this chapter represents one of the first attempts to the development of system identification tools for probe-based nanomechanics applications.

## 4.2 Optimal Input Design for Rapid Nanomechanical Spectroscopy

In this section, we present the proposed optimal input design approach for rapid broadband nanomechanical measurements. We start by transforming the nanomechanical property measurement, from the system identification viewpoint, into a parameter estimation problem.

### 4.2.1 Parameter Estimation in Nanomechanical Property Measurement

SPM has become a powerful tool to characterize various material properties at nanoscale (e.g., (75; 76; 77)), through the measurement of the tip-sample interaction force and the tip indentation on the sample surface, i.e., the force curve measurement (2). More specifically, the force-distance curve is obtained by measuring the tip-sample interaction force and the vertical displacement of the SPM-tip during the process when a micro-fabricated cantilever with a nanometer-radius tip is driven by a piezoelectric actuator to push against and then retrace from the sample surface (see Fig. 4.1(a)). The indentation is obtained from the difference between the cantilever deflection on the soft sample and that on a reference hard sample when the same control input voltage is applied to the piezoactuator during both force curve measurements. Such an indentation-based approach allows the material properties to be quantitatively measured at desired locations with desired force amplitude with nanoscale spatial resolutions (1; 78).

To identify material properties, the measured force and indentation results are utilized as the input and output data in an appropriate mechanics model (1; 79). For example, when the Hertz contact mechanics model (80) is employed, the creep compliance of the material,  $J(\cdot)$ ,

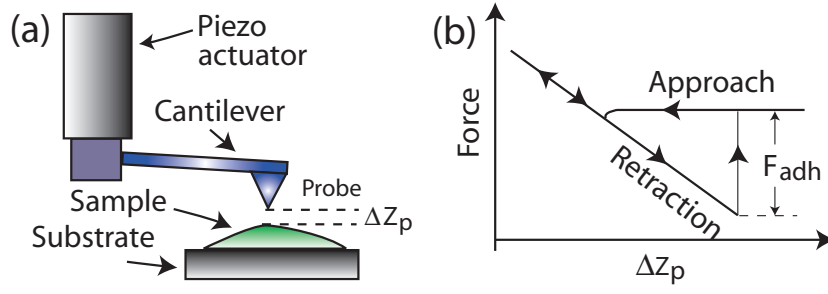


Figure 4.1 The scheme of force curve measurement by SPM

can be quantified by using the measured tip-sample interaction force,  $P(\cdot)$ , and the indentation in the material,  $h(\cdot)$ , by

$$h^{\frac{3}{2}}(t) = \frac{9}{16\sqrt{R}} \int_0^t J(t-\tau) \frac{dP(\tau)}{d\tau} d\tau, \quad (4.1)$$

where  $R$  is the tip radius. Although, the Hertz contact mechanics model captures the frequency dependent nanomechanical property of the material (8), the response speed of viscoelastic materials to the external excitation cannot be intuitively quantified by the Hertz model. To further characterize the nanomechanical properties and different response speed of materials to the excitation force, the parameterized model of the material complex compliance  $J(\cdot)$  has been proposed (8). In this chapter, we use a truncated Prony series to model the creep compliance (33; 41),

$$J(t) = J_0 - \sum_{i=1}^n J_i \cdot e^{-t/\tau_i}, \quad (4.2)$$

where  $J_0$  is the fully relaxed compliance,  $J_i$ s are the compliance coefficients, and  $\tau_i$ s are the discrete retardation times.

Combining Eq.(4.1) with Eq.(4.2) implies that the creep compliance  $J(t)$  can be viewed as a linear time-invariant mapping between the applied force  $P(t)$  and the effective indentation,  $h(t)$ , both shaped by the tip-sample interaction geometry,

$$J(t) : u(t) \triangleq \frac{9P(t)}{16\sqrt{R}} \longrightarrow h^{\frac{3}{2}}(t) \triangleq y(t). \quad (4.3)$$

Thus, the compliance model Eq.(4.2) can be converted into the following discrete autoregressive exogenous model (ARX) (27)

$$y(\ell) + \sum_{i=1}^{n_a} a_i y(\ell - i) = \sum_{i=1}^{n_b} b_i u(\ell - i), \quad (4.4)$$

where  $n_a$  is the number of poles,  $n_b$  is the number of zeros plus 1,  $\ell$  is the  $\ell^{th}$  sampling instance, and the unknown parameters  $a_i$ s and  $b_i$ s are related to the original retardation time constants  $\tau_i$ s and compliance coefficients  $J_i$ s through

$$J_0 = k - \sum_{i=1}^n \frac{r_i}{p_i}; \quad J_i = \frac{r_i}{p_i}; \quad \tau_i = -\frac{1}{p_i}, \quad (4.5)$$

where  $r_i$ s,  $p_i$ s, and  $k$ s are the coefficients of the partial fraction expansion of the continuous model obtained by converting the identified discrete ARX model Eq.(4.4) back to the continuous time domain.

As in the standard parameter identification (27), the above discrete model Eq.(4.4) is then rewritten as an affine function of the unknown parameters  $\theta$ ,

$$y(\ell) = \boldsymbol{\varphi}^T(\ell)\boldsymbol{\theta}, \quad (4.6)$$

with  $\boldsymbol{\theta} \in \mathfrak{R}^{m \times 1}$  the vector of unknown parameters

$$\boldsymbol{\theta} = [a_1, \dots, a_{n_a}, b_1, \dots, b_{n_b}]^T, \quad n_a + n_b = m, \quad (4.7)$$

and  $\boldsymbol{\varphi}(\ell)$  the sequence of measured input and output data

$$\boldsymbol{\varphi}(\ell) = [-y(\ell - 1), \dots, -y(\ell - n_a), u(\ell - 1), \dots, u(\ell - n_b)]^T. \quad (4.8)$$

Thus, the least-square estimation of the linear compliance model parameter,  $\hat{\theta}_N$ , can be obtained by minimizing the following estimation error in 2-norm,

$$\begin{aligned} \min_{\theta} V_N(\theta, Z^N) &= \min_{\theta} \frac{1}{N} \sum_{\ell=1}^N [y(\ell) - \hat{y}(\ell|\theta)]^2 \\ &= \min_{\theta} \frac{1}{N} \sum_{\ell=1}^N [y(\ell) - \boldsymbol{\varphi}^T(\ell)\theta]^2, \end{aligned} \quad (4.9)$$

where  $Z^N$  denotes the set of past inputs and outputs over the time interval  $1 \leq \ell \leq N$ , and  $\hat{y}(\ell|\theta)$  denotes the output computed by using the estimated parameters  $\theta$ ,

$$\hat{y}(\ell|\theta) = \boldsymbol{\varphi}^T(\ell)\theta. \quad (4.10)$$

The obtained optimal parameter estimation is given by

$$\hat{\theta}_N = \left[ \sum_{\ell=1}^N \boldsymbol{\varphi}(\ell)\boldsymbol{\varphi}^T(\ell) \right]^{-1} \sum_{\ell=1}^N \boldsymbol{\varphi}(\ell)y(\ell). \quad (4.11)$$

After the discrete *ARX* model is identified, the unknown parameters in the linear compliance model Eq.(4.2) can be obtained from the mapping Eq.(4.5).

To utilize the above parameter estimation approach in nanomechanical property measurements, the excitation input needs to be carefully designed. Note that the applied force is generated by the driven voltage sent to the piezoactuator (see Fig. 4.1(a)), the convolution of the input voltage with the SPM dynamics (from the piezoactuator to the cantilever) can thereby, lead to distortions in the excitation force. As a result, the distorted force may fail to excite the nanomechanical properties of interests — even if the original input force meets the persistent excitation condition (27; 81). Particularly, when the frequency spectrum of the input voltage overlaps with the locations of the poles and zeros of the piezo-cantilever dynamics (10), the dynamics convolution can result in input saturation at some frequencies (e.g., around frequencies where the poles of the piezo-cantilever dynamics locate) and/or low signal to noise ratio

at others (e.g., around the frequencies where the zeros of the piezo-cantilever dynamics locate). As discussed in the introduction, limits exist in current approaches to account for such a convolution effect on both the excitation force and the indentation measured. Therefore, optimal input design is proposed to avoid the instrument dynamics effect, and achieve rapid and accurate parameter estimations in nanomechanical property measurements.

#### 4.2.2 Optimal Input Design for Nanomechanical Measurement

Consider the following linear representation of a contact-mechanics model of the tip-sample interaction dynamics (e.g., the Hertz contact model),

$$\bar{y}(\ell) = J^*(z_\ell, \theta)\bar{u}(\ell) + \bar{v}(\ell), \quad (4.12)$$

where  $\bar{u}(\ell)$  and  $\bar{y}(\ell)$  are the equivalent input and the output in nanomechanical measurements, respectively (see Eq. (4.3)),  $\bar{v}(\ell)$  is the measurement noise of a normal distribution with mean value of  $\mu_v$  and variance of  $\sigma^2$ , i.e.,

$$\bar{v} \sim N(\mu_v, \sigma^2)$$

and  $J^*(z_\ell, \theta)$  is the discretized linear compliance model. For example, when the truncated Prony series Eq. (4.2) is used, the input-output mapping  $J^*(z_\ell, \theta)$  takes the form

$$J^*(z_\ell, \theta) = J_0 - \sum_{i=1}^n \frac{J_i(z_\ell - 1)}{(1 + \frac{T}{2\tau_i})z_\ell + (\frac{T}{2\tau_i} - 1)}, \quad (4.13)$$

where  $\theta$  is the vector of unknown parameters (see Eq. (4.2)), and the measurement frequency  $\omega$  is related to the z-transform variable  $z_\ell$  through Tustin transformation

$$j\omega = \frac{2}{T} \frac{(z_\ell - 1)}{(z_\ell + 1)}, \quad (4.14)$$

In the following, the optimal input is obtained through an iterative process: In each iteration, the designed excitation force is applied in the nanomechanical experiment, and the

measured force and indentation data are used to estimate the parameters of the compliance model, which, in turn, is utilized to seek the input design for the next iteration. Thus, for any given  $k^{\text{th}}$  iteration, the following linear mapping from the parameters to the estimation-caused error in output is obtained from the first-order Taylor series expansion of the linear compliance model,  $J^*(\cdot)$ , around the estimated parameters obtained in the previous iteration,  $\theta_{k-1}$ ,

$$\begin{aligned}\Delta\bar{y}_k(\ell) &\triangleq \bar{y}(\ell) - J^*(z_\ell, \theta_k)\bar{u}(\ell) \\ &= f(\ell)(\theta_k - \theta_{k-1}) + \bar{v}(\ell) \\ &\triangleq f(\ell)\Delta\theta_k + \bar{v}(\ell),\end{aligned}\tag{4.15}$$

where  $f(\ell) \in \mathbb{C}^{1 \times m}$  is given by

$$f(\ell) = \bar{u}(\ell) [f_1(\ell), \dots, f_m(\ell)],\tag{4.16}$$

with

$$f_i(\ell) = \frac{\partial J^*(z_\ell, \theta_k)}{\partial \theta_{k,i}},\tag{4.17}$$

and  $\Delta\theta_k$  is the difference of the estimated parameters between the  $k^{\text{th}}$  and the  $(k-1)^{\text{th}}$  iterations,

$$\Delta\theta_k = \theta_k - \theta_{k-1} = \begin{pmatrix} \Delta\theta_{k,1} \\ \vdots \\ \Delta\theta_{k,m} \end{pmatrix}.\tag{4.18}$$

Thus, the vector  $f(\ell)$  in Eq. (4.16) quantifies the relative importance of each parameter  $\theta_{k,i}$  in the compliance model  $J^*(z_\ell, \theta)$ .

Similar to the least-square-based parameter estimation of the ARX model in Sec. 4.2.1, the best linear unbiased estimate (BLUE) of  $\Delta\theta_k$  can be obtained as (15)

$$\widehat{\Delta\theta}_k = \begin{bmatrix} \text{Re} \sum_{\ell=-N/2}^{N/2-1} f^*(\ell) S_{vv}^{-1}(\ell) f(\ell) \\ \text{Re} \sum_{\ell=-N/2}^{N/2-1} f^*(\ell) S_{vv}^{-1}(\ell) \Delta\bar{y}_k(\ell) \end{bmatrix}^{-1} \quad (4.19)$$

where  $\text{Re}(\mathbb{C})$  denotes the real part of complex number  $\mathbb{C}$ , and

$$S_{vv}(\ell) = E[v^*(\ell)v(\ell)] \quad (4.20)$$

is the autocorrelation function of the measurement noise. Thus, by combining Eqs. (4.12, 4.15) with the above Eq. (4.19), an optimal input force can be sought to minimize the covariance of the parameter estimation error,  $\text{Cov}[\widehat{\Delta\theta}_k]$ , which, can be shown (15; 16), is equivalent to the inverse of the Fisher information matrix  $M$  (15), i.e.,

$$\min_{\bar{u}(\cdot)} \text{Cov}[\widehat{\Delta\theta}_k] = \min_{\bar{u}(\cdot)} E[(\widehat{\Delta\theta}_k - \mu_{\widehat{\Delta\theta}_k})^2] = \min_{\bar{u}(\cdot)} M^{-1}, \quad (4.21)$$

where  $\mu_{\widehat{\Delta\theta}_k}$  is the expectation of  $\widehat{\Delta\theta}_k$ . Note that for a nondegenerate input design (i.e., an input with the minimum required number of different frequency components for the transfer function model with given order (63)), the Fisher information matrix is nonsingular and thereby invertible (63). Thus, the optimal input can be obtained by maximizing the Fisher information matrix, which is equivalent to the minimization of the Cramer-Rao Lower Bound (CRLB), i.e., the lower bound of the variance of the estimation error  $\widehat{\Delta\theta}_k$  (16).

In Eq. (4.21), the Fisher information matrix ( $m \times m$ ),  $M$ , is given by (15; 82)

$$M = N \text{Re} \sum_{n=-N/2}^{N/2-1} E[f^*(n) S_{vv}^{-1}(n) f(n)]. \quad (4.22)$$

From Eq. (4.22), the Fisher information matrix can be derived as (see (15) for details)

$$M(\omega) = \sum_{\omega=-\pi}^{\pi} \frac{1}{2\pi} \begin{pmatrix} \frac{\partial J^*}{\partial \theta_1} \\ \vdots \\ \frac{\partial J^*}{\partial \theta_m} \end{pmatrix} S_{vv}^{-1}(\omega) \left[ \frac{\partial J}{\partial \theta_1}, \dots, \frac{\partial J}{\partial \theta_m} \right]. \quad (4.23)$$

Next, we consider multi-sinusoidal signals for the maximization of the Fisher information matrix,

$$u(\ell) = \sum_{i=1}^q A_i \sin(\omega_i \ell). \quad (4.24)$$

Such a choice of input is general because for any amplitude-normalized input with a mixed (continuous and discrete) spectrum, an equivalent input with purely discrete spectrum can be found. Moreover, the required number of distinct points in the input frequency spectrum is no more than  $[m(m+1)/2 + 1]$  (15), where  $m$  is the number of unknown parameters. Therefore, one can confine the search of the optimal input to the search of optimal frequency components in the sinusoidal input Eq.(4.24).

Next, we define the input design for the discrete input spectrum case:

**Definition 1** For the multi-sinusoidal input  $u(\ell)$  Eq.(4.24), an input design is to determine a finite set  $F$  consisting of pairs of the input frequency  $\omega_i$  and its associated power spectral density function  $p(\omega_i)$ ,

$$F(\Omega, p) = \{(\omega_1, p(\omega_1)), (\omega_2, p(\omega_2)), \dots, (\omega_q, p(\omega_q))\}, \quad (4.25)$$

such that each power spectral density  $p(\omega_i)$  equals to the amplitude  $A_i$  of that frequency  $\omega_i$  over the mean square power  $\sigma_u^2$  of the input  $u(\ell)$ , i.e.,

$$p(\omega_i) = A_i / (2\pi\sigma_u^2), \quad (4.26)$$

where  $\sigma_u^2$  is the mean square power of the input  $u(\ell)$

$$\sigma_u^2 = \frac{1}{2\pi} \sum_{i=1}^q A_i. \quad (4.27)$$

With the above definition, the optimal input design  $F^*$  amounts to the search of the optimal frequency component  $\omega_i$  through the iteration process. Specifically, after each iteration  $k$ , one candidate optimal frequency  $\omega_k$  will be obtained that maximizes the following cost function,

$$\max_{\omega} d_k(\omega, F) = \frac{\partial J(z_\ell, \theta_k)}{\partial \theta} M^{-1}(\Omega) \frac{\partial J^*(z_\ell, \theta_k)}{\partial \theta} \longrightarrow \omega_k. \quad (4.28)$$

where ‘\*’ denotes the optimal solution when maximizing the cost function, and  $M(\Omega)$  is the Fisher information matrix evaluated at the input frequencies  $\omega_i$  selected in each iteration,

$$M(\Omega) = \sum_{i=1}^q M(\omega_i), \quad (4.29)$$

where  $\omega_i$ s are the input frequencies in the current input design  $F(\Omega, p)$ .

Comparison of the above cost function Eq.(4.28) with Eq. (4.23) implies that the maximization of the cost function  $d_k(\omega, F)$  is equivalent to the maximization of the Fisher information matrix  $M(\omega)$  (63). Various criteria have been proposed to maximize the Fisher information matrix, including the A-optimality (minimize the trace of the inverse of the information matrix,  $M^{-1}$ ), the G-optimality (minimize the maximum variance of the predicted values), the E-optimality (maximize the minimum eigenvalue of the information matrix), and the D-optimality (maximize the determinant of the information matrix) (83; 84; 85). In the proposed optimal input design approach, D-optimal criterion is chosen for the property of D-optimality being invariant to the parameter scale and linear transformations of the output (64).

The D-optimality can be obtained through numerical search by using methods such as the one dimensional search, the bi-section search, or the Newton gradient search algorithms. In this chapter, the one dimensional search algorithm (86; 87) is used, where the new candidate

optimal frequency  $\omega_k$  is obtained by computing and then comparing the cost function  $d_k(\omega, F)$  at every sampling frequency within the measured frequency range.

The corresponding power spectral density function for the optimal candidate frequency  $\omega_k$ ,  $p(\omega_k)$ , is selected by choosing the corresponding spectral  $\alpha_k$  (see Eq. (4.30)) from a pre-specified sequence  $\{\alpha_1, \alpha_2, \dots\}$  satisfying

$$0 \leq \alpha_k \leq 1, \quad \sum_{k=1}^{\infty} \alpha_k = \infty, \quad \text{and} \quad \lim_{k \rightarrow \infty} \alpha_k = 0, \quad (4.30)$$

and the power spectral density of other frequency components already-existing in the input design  $F(\omega, p)$  are updated by adjusting the corresponding amplitude accordingly by

$$p(\omega_j) = (1 - \alpha_k)p(\omega_j), \quad \text{for } j = 1, 2, \dots, k-1. \quad (4.31)$$

The above iteration process to optimize the input is conducted until the variation of the identified parameters of the compliance model is within the chosen threshold.

**Remark 1** *As described above, the optimal frequency components of the input (i.e., the power spectral of the optimal frequencies) are strengthened while the non-optimal ones are diminished through the iteration process, i.e., as the optimal frequency component will be repetitively picked up, whereas the non-optimal ones won't, the adjustment through the  $\alpha$ -sequence (given by Eq. (4.30)) will continuously increase the relative power spectral of those optimal frequencies as well as decrease that of those non-optimal ones (i.e., the frequencies that occur sparsely during the iterative search process).*

The above discussion is summarized in the following algorithm to implement the proposed optimal input design in nanomechanical property measurements.

[Step 1] Choose a nondegenerate design  $F_0(\omega)$  consisting of more than  $\lceil m/2 \rceil$  points. For example,  $F_0$  may consist of  $q$  equally spaced frequencies where

$$\left\lceil \frac{m}{2} \right\rceil \leq q \leq \frac{m(m+1)}{2}, \quad (4.32)$$

[Step 2] Compute the function  $S_{vv}^{-1}(\omega)d(\omega, F_0)$  and find its maximum by D-optimality, say at  $\omega_o$ , i.e.,

$$\begin{aligned} S_{vv}^{-1}(\omega_o)d(\omega_o, F_0) &= \max_{\omega \in \Omega} \{S_{vv}^{-1}(\omega)d(\omega, F_0)\} \\ &= \max_{\omega \in \Omega} \left\{ S_{vv}^{-1}(\omega) \frac{\partial J^*}{\partial \theta} \bar{M}^{-1} \frac{\partial J}{\partial \theta} \right\}, \end{aligned} \quad (4.33)$$

[Step 3] Once a new frequency is found, update the input design by Eqs. (4.30, 4.31).

[Step 4] Repeat the above steps (2)-(4) until the change in difference of unknown parameters between successive iterations is below a threshold value.

### 4.2.3 Implementation of the Optimal Excitation Force

To implement the above optimal input force design, control input to the vertical-axis piezoactuator of the AFM needs to be obtained so that the applied excitation force (i.e., the cantilever deflection) will accurately track the desired force profile (See Fig. 4.3(a)). Note that the spectrum of the optimal excitation force contains components in the relatively high frequency range with respect to the bandwidth of the instrument dynamics (e.g., the vertical dynamics of the SPM from the  $z$ -axis piezoactuator to the cantilever). Therefore, the control input must be able to account for the instrument dynamics effects. Or, due to the convolution effect of the input with the instrument dynamics, large distortions in the excitation force occur (10).

Iterative learning control (ILC) is ideal to achieve precision tracking of the desired optimal excitation force. As the desired trajectory is known a priori, and the measurement environment usually is well controlled (i.e., random disturbances and/or dynamics variations are small during each measurement), ILC approach can fully exploit the knowledge of the system dynamics and the operation. Moreover, ILC is particularly attractive in practical implementations, as the dynamics changes of the system due to, for example, the replacement of the probe and/or the slight but inevitable variation in the probe-sample contact condition, can be easily compensated for through a few iterations without compromise of the tracking performance. Whereas when feedback control is used, the robustness to account for such dynamics uncertainties needs to be traded-off with the tracking precision. In this chapter, we utilized the modeling-free inversion-based iterative control (MIIC) (14) to track the desired force profile. Particularly, the MIIC algorithm is given in the frequency domain by

$$\begin{aligned}
 u_0(j\omega) &= \alpha z_d(j\omega), & k = 0, \\
 u_k(j\omega) &= \begin{cases} \frac{u_{k-1}(j\omega)}{z_{k-1}(j\omega)} z_d(j\omega), & \text{when } z_{k-1}(j\omega) \neq 0, \\ & \text{and } k \geq 1, \\ 0 & \text{otherwise} \end{cases} & (4.34)
 \end{aligned}$$

where ‘ $f(j\omega)$ ’ denotes the Fourier transform of the signal ‘ $f(t)$ ’, ‘ $z_d(\cdot)$ ’ denotes the desired output trajectory, ‘ $z_k(\cdot)$ ’ denotes the output obtained by applying the input ‘ $u_k(\cdot)$ ’ to the system during the  $k^{th}$  iteration, and  $\alpha \neq 0$  is a pre-chosen constant (e.g.,  $\alpha$  can be chosen as the estimated DC-Gain of the system). It has been shown (14) that the error between the desired input and the iterative control input, under effects of measurement noise and/or disturbance, is small provided that the signal to noise/disturbance ratio (SNR) is large. Furthermore, the output tracking error can be quantified in terms of the SNR. The MIIC algorithm has been implemented previously to nanomechanical measurements (9) where the spectrum of the excitation force is similar to a band-limited white noise. As discussed in the introduction, the

implementation of the proposed optimal input design will avoid the challenges in tracking such a rather complicated desired force profile, thereby facilitate broadband nanomechanical measurements.

### 4.3 Simulation and Experimental Example: Frequency-dependent Viscoelasticity Measurements of PDMS

The proposed optimal input design approach is illustrated through the nanomechanical property measurement of a PDMS sample using SPM. Both simulation and experiment were conducted to demonstrate the need and the efficacy of the proposed method.

#### 4.3.1 Simulation Study of Input Force Design

The goal of the simulation studies was two folds: 1) To evaluate parameter estimations in nanomechanical measurements; and 2) to evaluate and demonstrate the need and efficacy of optimal input design in the identification through the comparison of with and without noise presenting in the output data. Specifically, a 3<sup>rd</sup> order Prony series model of a PDMS sample was used as the target system to be identified. The parameters of the model, as listed in the second column of Table 4.1, were chosen as those obtained recently in experiments using SPM (9) (also see Eq. (4.2) for the expression of the Prony series model). Since there were 7 unknown parameters in this model, a multi-sinusoidal signal with four frequency components was used as the effective input force (Unit: nano Newton)

$$u(\ell) = A \sum_{i=1}^4 \alpha_i \sin(2\pi f_i \ell), \quad (4.35)$$

where the amplitude of each frequency component was chosen to be the same at A.

Three different scenarios were considered in the simulation. Case 1: The input design based on the a priori knowledge of PDMS viscoelasticity (2; 9) was used in the identifica-

Table 4.1 The list of the true values of the seven parameters of the 3<sup>rd</sup>-order Prony series model (“Actual”), and those identified in Case 1 (“Case 1”), Case 2 (“Case 2”), and Case 3 (“Case 3”), and the corresponding estimation errors with respect to the true values.

| Param.                  | Actual | Case 1  | Error  | Case 2 | Error | Case 3 | Error  |
|-------------------------|--------|---------|--------|--------|-------|--------|--------|
| $J_0$ ( $\mu Pa^{-1}$ ) | 9.11   | 9.11    | 0%     | 7.73   | 15.1% | 9.13   | -0.25% |
| $J_1$ ( $\mu Pa^{-1}$ ) | 2.08   | 2.08    | 0%     | -1.03  | 150%  | 2.10   | -1.14% |
| $J_2$ ( $\mu Pa^{-1}$ ) | 1.53   | 1.53    | 0%     | 3.87   | -147% | 1.68   | -10.1% |
| $J_3$ ( $\mu Pa^{-1}$ ) | 1.51   | 1.50    | 0.66%  | 2.07   | -37%  | 5.51   | 265%   |
| $\tau_1$ (ms)           | 25.28  | 25.2801 | 0.12%  | -34.79 | 238%  | 26.25  | -3.85% |
| $\tau_2$ (ms)           | 2.9    | 2.9004  | 0.01%  | 3.71   | -28%  | 2.71   | 6.7%   |
| $\tau_3$ (ms)           | 0.474  | 0.4767  | -0.57% | -0.05  | 110%  | 0.944  | -99.1% |

tion, and no noise was augmented to the effective output of the “true” compliance model when the output was used in the identification; Case 2: the input design was the same as in Case 1), but a band-limited white noise was added to the output (i.e., to mimic the measurement noise effect); and Case 3: the optimal input design by the proposed approach was used and the output noise as in Case 2) was added. In the first case, the input design  $F_0 = \{(1, 0.25), (10, 0.25), (100, 0.25), (1000, 0.25)\}$  was chosen based on the knowledge that each retardation time constant of the complex compliance of polymers tends to be separated by one decade apart from each other, and based on our previous work (9), the retardation time constants of the PDMS sample used later in the experiment spanned between 0.01 ms and 10 ms. For Cases 2) and 3), a band-limited white noise with signal to noise ratio of 134.3 and 146.7 (with respect to the desired force profile), respectively, was added to the output. In Case 3), the initial choice to search the optimal input design was set as that used in Case 1) originally, and then changed to  $F_0 = \{(1, 0.25), (10, 0.25), (30, 0.25), (60, 0.25)\}$  for faster convergence when there existed output noise. The frequency range to search was thereby limited to [1, 100] Hz, and the coefficient  $\{\alpha_k\}$  for updating the input design was chosen to be  $1/(k+3)$  (where k is the number of iteration). In the simulation, the sampling frequency was

chosen as 8 KHz.

The output of the  $3^{rd}$ -order compliance model to be identified was used along with the input to identify the parameters of the discretized linear compliance mapping by using the ARX least-square method (Eq. (4.11), see Sec. 4.2.1). The parameters of the Prony series model were then obtained from Eq. (4.5) after discrete-to-continuous conversion. The estimated parameters are presented in the third and fourth columns for Case 1), the fifth and sixth columns column for Case 2), and the seventh and eighth columns for Case 3) in Table 4.1, respectively. The obtained optimal input design is specified in Table 4.2. Notice that the amplitude at 1 and 10 Hz was kept fixed to avoid the large decreases of SNR upon the addition of high frequency components. The estimation error of the parameters along the iteration process in Case 3) (i.e., the proposed optimal input design) is shown in Fig. 4.2 also.

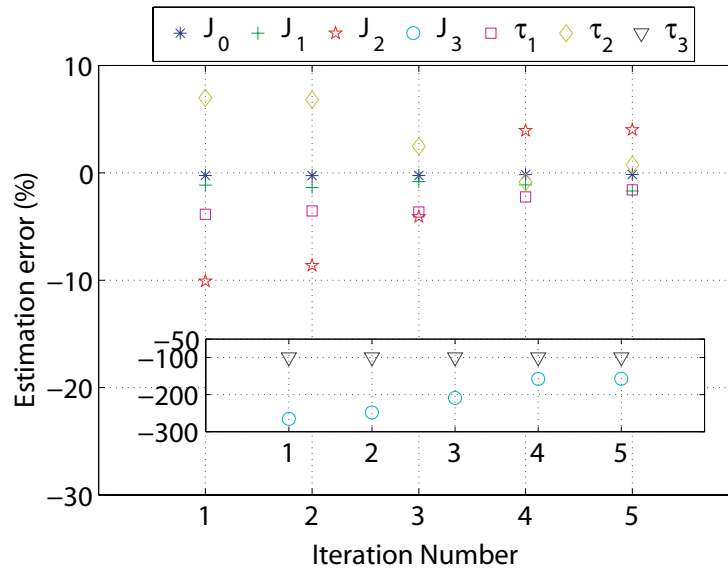


Figure 4.2 Simulation result: the estimation error of  $3^{rd}$ -order Prony series by using the proposed optimal input design in the presence of output noise.

The simulation results demonstrate that optimal input design is needed in nanomechanical measurements. As shown in Table 4.1, when there was no measurement noise, the parameters of the  $3^{rd}$ -order Prony series model can be accurately estimated by using the input design

Table 4.2 The frequency components of the optimal input design obtained in the simulation study

|           |    |    |      |      |      |      |      |      |
|-----------|----|----|------|------|------|------|------|------|
| Fre. (Hz) | 1  | 10 | 30   | 60   | 83   | 92   | 79   | 93   |
| Amp. (%)  | 25 | 25 | 10.7 | 10.7 | 7.15 | 7.15 | 7.15 | 7.15 |

based on the priori-knowledge of the material — Case 1 (where the estimation error was less than 1%, see the third and fourth columns of Table 4.1). Such a highly accurate estimation, however, was lost when noise was augmented to the output — As shown in the fifth and sixth columns of Table 4.1 for Case 2), the estimation error became substantially large (the estimation error was as large as 238%). Particularly, we note that the estimation error of small time constant was significantly larger than that of large ones. Such an increase of estimation error — when the part of the dynamics to be identified became faster — was due to the decrease of the SNR when frequency increased (since the Prony series model to be identified essentially was a low-pass filter). As noise is inevitable in real experimental measurements, the simulation results showed that the input force profile must be carefully designed in nanomechanical measurements.

The simulation results also demonstrated that the proposed optimal input design approach was very effective for nanomechanical property measurements. By using the proposed optimal input design (Case 3), the estimated parameters converged in five iterations (see Fig. 4.2). Particularly, the estimation errors of all parameters except the two related to the fastest time constant ( $J_3$  and  $\tau_3$ , see Table 4.1) were small. We note that although the estimation error of the fast part of the compliance model was relatively large, the estimated value was still within the same decade as the true value. We also note that the span of the three retardation time constants over three decades (in the given 3<sup>rd</sup>-order compliance model) rendered identifying all parameters accurately very challenging. Thus, the simulation results served well as a reference to the following experiments.

### 4.3.2 Experimental Implementation and Discussion

The simulation results were utilized to guide the implementation of the proposed approach to the nanomechanical measurement on a PDMS sample in experiments. The initial choice of the input design used in Case 3) of the simulation was used as the initial input design in the experiments. The sampling frequency was further reduced to 2 kHz in the experiments to reduce the measurement noise effect. An analog filter was also added to attenuate the output noise. The desired cantilever deflection (specified by the input design), i.e., the desired probe force applied to the sample, was tracked accurately by using the MIIC technique (2). The 2-norm and the infinity-norm of the tracking error were maintained below 2% and 5%, respectively. As a representative tracking result, the tracking result of the desired cantilever deflection obtained in the fifteenth iteration of the search for the optimal deflection (i.e., the optimal desired excitation force) is shown in Fig. 4.3.

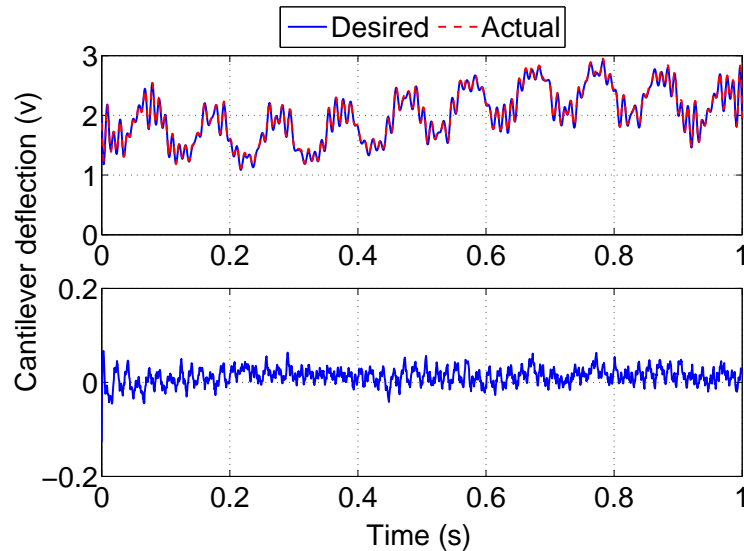


Figure 4.3 (a) The comparison of the designed deflection (i.e., force) and the actual deflection on PDMS sample, and (b) the tracking error between the designed deflection and the actual one at the fifteenth iteration.

During each iteration of the search for the optimal input design, the indentation in the PDMS (produced by the excitation force applied) was needed to identify the parameters of

the 3<sup>rd</sup>-order Prony series model. The indentation was obtained from the difference of the deflection measured on the PDMS sample and that on a hard reference sample (e.g., a sapphire sample in this experiment) when the same input voltage (to drive the piezoactuator) was applied in both force-curve measurements. To avoid the switching back and forth between the hard and the soft (PDMS) samples during the iterations of the optimal input design process, thereby reduce the measurement errors, the deflection on the hard reference sample was estimated by applying the same control input to the model of the dynamics from the piezoactuator to the cantilever deflection on the hard sample. Such a model was measured through experiments by using, for example, the sweep sine method, under the condition that continuous probe-sample contact was maintained with a given pre-load during the modeling process (No significant dynamics variation was observed when different pre-loads were applied (10; 2)).

The force applied from the tip to the sample during the force measurements can be obtained from the measured cantilever deflection signal as (1),

$$P = K_t \times C_t \times d_S, \quad (4.36)$$

where  $K_t$  is the stiffness constant of the cantilever,  $C_t$  is the sensitivity constant of the deflection signal vs. the vertical displacement of the tip (both can be experimentally calibrated (34)), and  $d_S$  denotes the cantilever deflection on the soft sample. The cantilever stiffness of  $K_t = 0.065$  N/m was experimentally calibrated by thermal noise method (34), and the deflection-to-displacement sensitivity of  $C_t = 85$  nm/V was also calibrated experimentally.

Then, the indentation of the tip in the PDMS sample was obtained as (2)

$$h = C_t \times (d_H - d_S), \quad (4.37)$$

where  $d_H$  and  $d_S$  denote the deflection on the sapphire sample and that on the PDMS sample, respectively, when the same control input was applied in both force-curve measurements.

In this experiment, the Hertz contact mechanics model was used to obtain the complex

compliance of the PDMS sample. By taking the Fourier transform in Eq. (4.1) (1; 79), the complex compliance of the PDMS was obtained from the measured force  $P$  and indentation  $h$  as

$$J^*(j\omega) = \frac{16 \left[ h^{\frac{3}{2}}(\cdot) \right] (j\omega) \sqrt{R}}{9P(j\omega)} \quad (4.38)$$

The above procedure to seek the optimal excitation force was implemented in experiments until the convergence of the parameters of the viscoelasticity model of the PDMS was observed. The evolutions of the seven parameters of the 3<sup>rd</sup>-order Prony series model along the iterations are plotted in Fig. 4.4 for the total of 15 iterations conducted in the experiment. In the first iteration, the parameters were identified by using the excitation force initially chosen based on the simulation results (see Sec. 4.3.1). The parameter estimation results are also listed in Table 4.3 for the first three and the last three iterations, respectively.

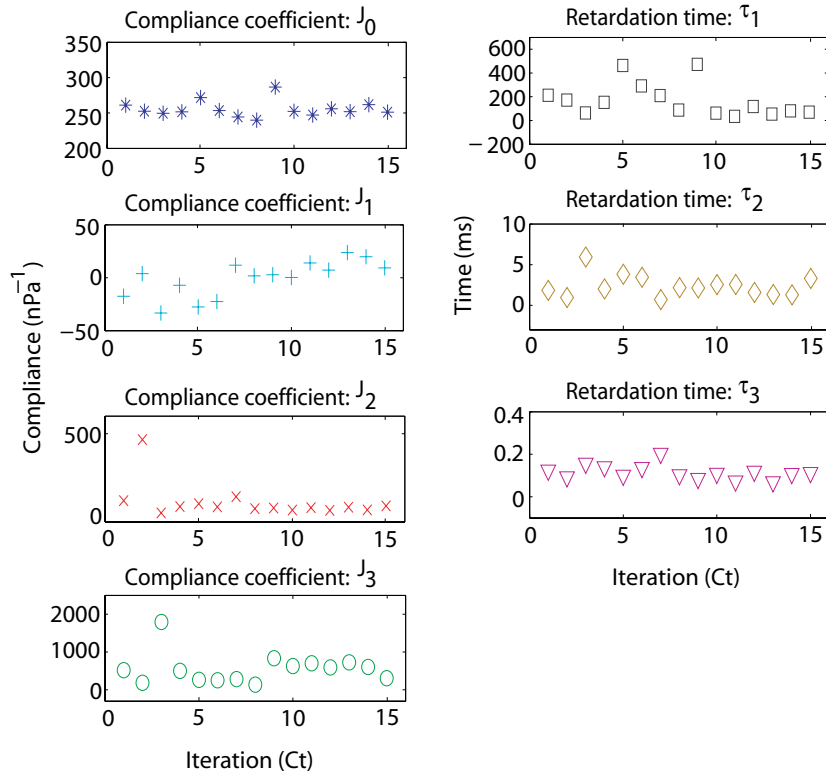


Figure 4.4 Experimental parameter estimation result with optimal input design

Table 4.3 The list of parameters identified in the first three (“Ite. 1”, “Ite. 2”, and “Ite. 3”) and the last three (“Ite. 13”, “Ite. 14”, and “It. 15”) iterations during the search of the optimal excitation force in the experiments.

| Param.               | Ite.1 | Ite.2 | Ite.3 | Ite.13 | Ite.14 | Ite.15 |
|----------------------|-------|-------|-------|--------|--------|--------|
| $J_0$ ( $nPa^{-1}$ ) | 261   | 252   | 250   | 252    | 262    | 251    |
| $J_1$ ( $nPa^{-1}$ ) | -18   | 4     | -33   | 24     | 20     | 9      |
| $J_2$ ( $nPa^{-1}$ ) | 121   | 467   | 51    | 83     | 68     | 90     |
| $J_3$ ( $nPa^{-1}$ ) | 517   | 185   | 1800  | 725    | 608    | 310    |
| $\tau_1$ (ms)        | 212.3 | 171.5 | 63.9  | 54.4   | 81.2   | 71.0   |
| $\tau_2$ (ms)        | 1.85  | 0.97  | 5.93  | 1.33   | 1.30   | 3.32   |
| $\tau_3$ (ms)        | 0.12  | 0.093 | 0.16  | 0.069  | 0.11   | 0.11   |

Table 4.4 The optimal force design obtained in the experiment.

| Fre. (Hz) | 1  | 10 | 30  | 60  | 56  | 61  | 67  | 71  | 73  | 84  | 87  | 89  | 95  | 97  | 98  | 99  |
|-----------|----|----|-----|-----|-----|-----|-----|-----|-----|-----|-----|-----|-----|-----|-----|-----|
| Amp.(%)   | 25 | 25 | 5.5 | 5.5 | 2.8 | 2.8 | 2.8 | 2.8 | 2.8 | 2.8 | 5.6 | 2.8 | 2.8 | 2.8 | 5.6 | 2.8 |

The experimental results demonstrated the efficacy of the proposed optimal excitation force design in broadband nanomechanical property measurements. As shown in Fig. 4.4, the trend of the identified parameters towards convergence was evident. Further iterations were not pursued as after the fifteen iterations, the values of the identified parameters were close to those obtained in our previous work (9). Particularly, the three identified retardation time constants evenly spanned three orders (at 71 ms, 3.32 ms, and 0.11 ms, respectively). Such an evenly distributed retardation time constants demonstrated that the nanomechanical property of the PDMS material was well captured in the experiment by using the proposed method (the retardation time constants within the same decade can be combined into one time constant at that decade). Specifically, the identified value of the static compliance  $J_0$  at 251  $nPa^{-1}$  and the instantaneous compliance  $J_\infty$  (i.e.,  $J_\infty = \sum_{i=0}^4 J_i$ ) at 660  $nPa^{-1}$  were close to those obtained in our previous work (9), respectively (where a much more complicated band-

limited white-noise type of excitation force was used). On the contrary, when the non-optimal excitation force was used — the excitation force used in the first iteration of the optimal force searching process, much larger identification error occurred: As shown in Table 4.3, the three retardation time constants were not spaced by one order from each other, and the identified value of  $J_1$  was negative, which contradicted to the physical meaning of the compliance coefficient. Moreover, compared to the much more complicated band-limited white-noise type of excitation force used in previous work (9), the number of frequency components in the obtained optimal excitation force was much smaller (see Table 4.4), and the optimal frequency components were mainly located in the relatively lower frequency region. Such an excitation force — with less number of frequency components in the lower frequency region — substantially reduced not only the convolution effect of hardware dynamics with the nanomechanical response of soft sample, thereby improving the identification accuracy, but also the measurement time needed in the experiment. The reduction of the measurement time is particularly crucial to quantitatively capture the time-elapsing nanomechanical property evolution during nanoscale dynamic phenomena, for example, during the early initial stage of polymer crystallization process (11), or the cell fusion process (13). Therefore, the experimental implementation illustrated that the proposed approach is very promising to achieve rapid broadband nanomechanical spectroscopy.

## 4.4 Conclusions

In this chapter, an optimal excitation force design was proposed for indentation-based rapid broadband nanomechanical measurement of soft materials. First, the nanomechanical property measurement was formulated, from the system identification viewpoint, as a parameter identification problem. Then the optimal excitation force was obtained through the maximization of the Fisher information matrix of the linear compliance model of the viscoelasticity of the soft material. Finally, precision tracking of the optimal excitation force was achieved by using the

MIIC technique to compensate for the instrument hardware dynamics and hysteresis effects. Simulation studies were conducted to evaluate the parameter identification in nanomechanical measurements and the need for optimal excitation force design. The proposed approach was illustrated by implementing it to identify a  $3^{rd}$  – order linear compliance model of a PDMS sample.

## CHAPTER 5. CONCLUSION

This dissertation first presented a novel nanoscale broadband viscoelastic spectroscopy (NBVS). In the proposed NBVS approach, the recently developed MIIC technique is used to: I) the exertion of excitation force with broad frequency components onto the sample, and II) the measurement of the material response for such excitation (i.e., the material indentation). The frequency-dependent viscoelasticity of the material was then obtained by using the measured excitation force and the indentation in a contact mechanics model that describes the dynamics interaction between the probe and the sample. The proposed NBVS was illustrated by implementing it to measure the rate-dependent viscoelastic response of a PDMS sample. The experimental results showed that the use of the MIIC technique enabled the cantilever deflection to precisely track a band-limited (cut-off frequency: 4.5 kHz) white-noise type of desired trajectory on the PDMS sample, thereby applying a band-limited white-noise type of excitation force on the PDMS sample. Then the indentation of the PDMS sample was obtained by applying the same control input to obtain the force measurement on a reference hard sample. The obtained excitation force and the indentation results showed that the rate-dependent modulus of soft materials like PDMS can be measured by using the proposed NBVS approach.

In NBVS approach, large measurement error in indentation is caused by different contact between the probe and the material or the reference sample. Therefore, a model-based approach to compensate for the dynamics convolution effect in the nanomechanical property measurement of soft materials is proposed. The dynamics involved in indentation-based nanomechanical property measurements was analyzed to reveal that the convoluted dynamics effect can be described as the difference between the lightly-damped probe-sample interac-

tion dynamics and the over-damped nanomechanical behavior of soft materials. Then, these two different dynamics effects were decoupled via numerical fitting based on the Prony series model of the viscoelasticity of the soft material. The proposed approach was illustrated by implementing it to compensate for the dynamics convolution effect in a broadband viscoelasticity measurement of a Polydimethylsiloxane (PDMS) sample using scanning probe microscope, and the experimental results showed that the dynamics convolution effect can be effectively compensated for by using the proposed approach.

The offline post-processing in the above approach limits its application. To accelerate the measurement process for fast applications, such as the polymerization process of polymer and the cell healing, an optimal excitation force design was proposed for indentation-based rapid broadband nanomechanical measurement of soft materials. First, the nanomechanical property measurement was formulated, from the system identification viewpoint, as a parameter identification problem. Then the optimal excitation force was obtained through the maximization of the Fisher information matrix of the linear compliance model of the viscoelasticity of the soft material. Finally, precision tracking of the optimal excitation force was achieved by using the MIIC technique to compensate for the instrument hardware dynamics and hysteresis effects. Simulation studies were conducted to evaluate the parameter identification in nanomechanical measurements and the need for optimal excitation force design. The proposed approach was illustrated by implementing it to identify a  $3^{rd}$  – order linear compliance model of a PDMS sample.

**APPENDIX**

**MODEL-LESS INVERSION-BASED ITERATIVE LEARNING**

**CONTROL (MIIC)**

We present the convergence analysis result of the MIIC algorithm in the presence of random noise/disturbance as follows.

**Theorem 1** (14)

*Let  $G(j\omega)$  be a stable single-input-single-output (SISO), linear time invariant (LTI) system, and at each frequency  $\omega$ , consider the system output  $z(t)$  to be affected by the disturbance and/or the measurement noise  $z_n(t)$  as (see Fig. 1 in (9))*

$$z(j\omega) = z_l(j\omega) + z_n(j\omega), \quad (\text{A.0})$$

where  $z_l(j\omega)$  denotes the linear part of the system response to the input  $u(j\omega)$ , i.e.  $z_l(j\omega) = G(j\omega)u(j\omega)$ , and  $z_n(j\omega)$  denotes the output component caused by the disturbances and/or the measurement noise. Then,

1. the ratio of the iterative input  $u_k(j\omega)$  to the desired input  $u_d(j\omega)$  is bounded in magnitude and phase, respectively, as

$$1 - \varepsilon(\omega) \leq \lim_{k \rightarrow \infty} \left| \frac{u_k(j\omega)}{u_d(j\omega)} \right| \leq \frac{1 - \varepsilon(\omega)}{1 - 2\varepsilon(\omega)}, \quad (\text{A.0})$$

$$\lim_{k \rightarrow \infty} \left| \angle \left( \frac{u_k(j\omega)}{u_d(j\omega)} \right) \right| \leq \sin^{-1} \left( \frac{\varepsilon(\omega)}{1 - \varepsilon(\omega)} \right), \quad (\text{A.0})$$

provided that the noise to signal ratio (NSR) as defined below, is upper-bounded by a less-than-half constant,  $\varepsilon(\omega)$ ,

$$\left| \frac{z_{k,n}(j\omega)}{z_d(j\omega)} \right| \leq \varepsilon(\omega) < 1/2, \quad \forall k, \quad (\text{A.0})$$

where the desired input  $u_d(j\omega)$  enables the linear part of the system output to exactly track the desired output, i.e.,  $z_d(j\omega) = G(j\omega)u_d(j\omega)$ , and  $z_{k,n}(j\omega)$  denotes the part of the output caused by disturbances and/or measurement noise in the  $k^{\text{th}}$  iteration. Moreover, the relative tracking error is bounded as

$$\lim_{k \rightarrow \infty} \left| \frac{z_k(j\omega) - z_d(j\omega)}{z_d(j\omega)} \right| \leq \frac{2\varepsilon(\omega)(1 - \varepsilon(\omega))}{1 - 2\varepsilon(\omega)}; \quad (\text{A.0})$$

2. The use of the MIIC algorithm will improve the output tracking at frequency  $\omega$ , i.e.,

$$\lim_{k \rightarrow \infty} \left| \frac{z_k(j\omega) - z_d(j\omega)}{z_d(j\omega)} \right| < 1, \quad (\text{A.0})$$

provided that the upper bound of the NSR is less than  $1 - \frac{\sqrt{2}}{2} \approx 0.3$ , i.e.,

$$\left| \frac{z_{k,n}(j\omega)}{z_d(j\omega)} \right| \leq \varepsilon(\omega) < 1 - \frac{\sqrt{2}}{2}, \quad \forall k. \quad (\text{A.1})$$

## BIBLIOGRAPHY

- [1] Hans-Jurgen Butt, Brunero Cappella, and Michael Kappl. Force measurements with the atomic force microscope: Technique, interpretation and applications. *Surface Science Reports*, 59:1–152, 2005.
- [2] Kyongsoo Kim, Zhiqun Lin, Pranav Shriotrya, Sriram Sundararajan, and Qingze Zou. Iterative control approach to high-speed force-distance curve measurement using AFM: Time dependent response of PDMS example. *Ultramicroscopy*, 108(9):911–920, Aug. 2008.
- [3] A. E. Schmid J. P. Cleveland, B. Anczykowski and V. B. Elings. Energy dissipation in tapping-mode atomic force microscopy. *Applied Physics Letters*, 72(20):1–3, May 1998.
- [4] Asif S. A. Syed, K. J. Wahl, R. J. Colton, and O. L. Warren. Quantitative imaging of nanoscale mechanical properties using hybrid nanoindentation and force modulation. *Journal of Applied Physics*, 90(3):1192–1200, 2001.
- [5] Stephen Jesse, Sergei V Kalinin, Roger Proksch, A. P. Baddorf, and B. J. Rodriguez. The band excitation method in scanning probe microscopy for rapid mapping of energy dissipation on the nanoscale. *Nanotechnology*, 18(43):1–8, Oct. 2007.
- [6] Jose R. Lozano and Ricardo Garcia. Theory of multifrequency atomic force microscopy. *Physical Review Letters*, 100(07):1–4, Feb. 2008.

- [7] Roger Proksch. Multifrequency, repulsive-mode amplitude-modulated atomic force microscopy. *Applied Physics Letters*, 89(11):1–4, July 2006.
- [8] H. F. Brinson and L. C. Brinson, *Polymer Engineering Science and Viscoelasticity: An Introduction*. Springer, 2007.
- [9] Zhonghua Xu, Kyongsoo Kim, Qingze Zou, and Pranav Shrotriya. Broadband measurement of rate-dependent viscoelasticity at nanoscale using scanning probe microscope: Poly(dimethylsiloxane) example. *Applied Physics Letter*, 93:133103–133105, 2008.
- [10] Zhonghua Xu and Qingze Zou. A model-based approach to compensate for the dynamics convolution effect on nanomechanical property measurement. *Journal of Applied Physics*, 107(6):064315, 2010.
- [11] L. Mandelkern, “Crystallization kinetics in high polymers. ii. polymer-diluent mixtures,” *Journal of Applied Physics*, vol. 26, no. 4, pp. 443 – 451, 2009.
- [12] P. Xie, Z. Xu, and Q. Zou, “Compensation for the dynamics effect on nanoscale broadband viscoelasticity measurements using adaptive filtering approach,” *IEEE Transactions Instrumentation and Measurement*, vol. PP, no. 99, pp. 1–8, 2010.
- [13] S. Noselli, “Drosophila, actin and videotape new insights in wound healing,” *Nature Cell Biology*, vol. 4, pp. E251 – E253, 2002.
- [14] Kyong-Soo Kim and Qingze Zou. Model-less inversion-based iterative control for output tracking: Piezo actuator example. In *Proceedings of American Control Conference*, pp. 2710–2715, Seattle, WA, June 2008.

- [15] R. K. Mehra, “Frequency-domain synthesis of optimal inputs for linear system parameter estimation,” *Journal of Dynamic Systems, Measurement, and Control*, vol. 98, no. 2, pp. 130–138, 1976.
- [16] S. M. Kay, *Fundamentals of Statistical Signal Processing, Volume I: Estimation Theory*. Prentice Hall, 1993.
- [17] Van Vliet, K. J., G. Bao, and S. Suresh. The biomechanics toolbox: experimental approaches for living cells and biomolecules. *Acta Materialia*, 51(19):5881–5905, 2003.
- [18] J. Guck, R. Ananthakrishnan, H. Mahmood, T. J. Moon, and J. Cunningham, C. C.; Kas. The optical stretcher: A novel laser tool to micromanipulate cells. *Biophysical Journal*, 81(2):767–784, 2001.
- [19] E.M. Lupton, C. Nonnenberg, I. Frank, F. Achenbach, J. Weis, and C. Bräuchle. Stretching siloxanes: An ab initio molecular dynamics study. *Chemical Physics*, 414:132–137, 2005.
- [20] Guillaume T. Charras and Mike A. Horton. Determination of Cellular Strains by Combined Atomic Force Microscopy and Finite Element Modeling. *Biophys. J.*, 83(2):858–879, 2002.
- [21] S. A. Syed Asif, K. J. Wahl, and R. J. Colton. Nanoindentation and contact stiffness measurement using force modulation with a capacitive load-displacement transducer. *Review of Scientific Instruments*, 70(5):2408–2413, 1999.
- [22] Ying Wu and Qingze Zou. Iterative control approach to compensate for both the hysteresis and the dynamics effects of piezo actuators. *IEEE Trans. on Control Systems Technology*, 15:936–944, 2007.

- [23] D. Croft, G. Shedd, and S. Devasia. Creep, hysteresis, and vibration compensation for piezoactuators: Atomic force microscopy application. *ASME Journal of Dynamic Systems, Measurement and Control*, 123(1):35–43, March, 2001.
- [24] KyongSoo Kim, Qingze Zou, and Chanmin Su. A new approach to scan-trajectory design and track: AFM force measurement example. *ASME Journal of Dynamic Systems, Measurement and Control*, 130, September 2008.
- [25] S. Salapaka, A. Sebastian, J. P. Cleveland, and M. V. Salapaka. High bandwidth nanopositioner: A robust control approach. *Review of Scientific Instruments*, 73(9):3232–3241, Sept., 2002.
- [26] Ying Wu and Qingze Zou. Robust-inversion-based 2DOF-control design for output tracking: Piezoelectric actuator example. *IEEE Trans. on Control Systems Technology*, 2008. in press.
- [27] Lennart Ljung. *System Identification: Theory for the User*, chapter 2, 6. Prentice Hall PTR, 2<sup>nd</sup> edition, 1999.
- [28] Hajime Takano, Jeremy R. Kenseth, Sze-Shun Wong, Janses C. O’Brien, and Marc D. Porter. Chemical and biochemical analysis using scanning force microscopy. *Chemical Reviews*, 99:2845–2890, 1999.
- [29] G.W. Marshall, I.C. Wu-Magidi, L.G. Watanabe, N. Inai, M. Balooch, J.H. Kinney, and S.J. Marshall. Effect of citric acid concentration on dentin demineralization, dehydration, and rehydration: Atomic force microscopy study. *Journal of Biomedical Material Research*, 42:500–507, 1998.
- [30] F. El Feninat, T.H. Ellis, E. Sacher, and I. Stangel. A tapping mode AFM study of collapse and denaturation in dentinal collagen. *Dental Materials*, 17:284–288, 2001.

- [31] Paul L. McNeil and Richard A. Steinhardt. Plasmamembrane disruption: Repair, prevention, adaptation. *Annu. Rev. Cell Dev. Biol.*, 19:697–731, 2003.
- [32] Kyongsoo Kim and Qingze Zou. Iterative-based scan-trajectory design and control with output-oscillation minimization: Adhesion force measurement example. In *Proceedings of American Control Conference*. ASME Journal of Dynamic Systems, Measurement and Control (accepted).
- [33] Shuang Yang and Yong Wei Zhang. Analysis of nanoindentation creep for polymeric materials. *Journal of Applied Physics*, 95(7):3655–3666, April 2004.
- [34] J. L. Hutter and Bechhoefer J. Calibration of atomic-force microscope tips. *Review of Scientific Instruments*, 64(7):1868–1873, 1993.
- [35] K.J. Wahl and S.A.S. Asif and J.A. Greenwood and K.L. Johnson. Oscillating adhesive contacts between micron-scale tips and compliant polymers. *Journal of Colloid and Interface Science*, 296: 178–188, 2006.
- [36] J.A. Greenwood and K.L. Johnson. Oscillatory loading of a viscoelastic adhesive contact. *Journal of Colloid and Interface Science*, 296: 284–291, 2006.
- [37] E. Barthel. Adhesive elastic contacts: JKR and more. *Journal of Physics D: Applied Physics*, 41(16): 163001, 2008.
- [38] Nikhil S. Tambe and Bharat Bhushan. Micro/nanotribological characterization of PDMS and PMMA used for BioMEMS/NEMS applications. *Ultramicroscopy*, 105 (1-4): 238–247, 2005.
- [39] A. Mitchell and P. Shrotriya. Onset of nanoscale wear of metallic implant materials: Influence of surface residual stresses and contact loads. *Wear*, 263:1117–1123, 2007.

- [40] A. Mitchell and P. Shrotriya. Mechanical load assisted dissolution of metallic implant surfaces: Influence of contact loads and surface stress state. *Acta Biomaterialia*, 4(2):296–304, 2008.
- [41] Michelle L. Oyen. Spherical indentation creep following ramp loading. *Journal of Materials Research*, 20(8):2094, Aug. 2005.
- [42] Abraham Shtark, Hagay Grosbein, Guy Sameach and Harry H. Hilton. An Alternative Protocol for Determining Viscoelastic Material Properties Based on Tensile Tests Without the Use of Poisson’s Ratios. *Proceedings of IMECE2007*, Volume 10: Mechanics of Solids and Structures, Parts A and B :437–454, 2007.
- [43] Michael Michaeli, Abraham Shtark, Hagay Grossbein, and Harry H. Hilton. Computational Protocols for Viscoelastic Material Property Characterizations without the Use of Poisson’s Ratios. *AIP Conference Proceedings*, 1255: 37–39, 2010.
- [44] Daniel J. O’Brien, Patrick T. Mather, and Scott R. White. Viscoelastic Properties of an Epoxy Resin during Cure. *Journal of Composite Materials*, 35(10): 883–904 , 2001.
- [45] H. F. Brinson and L. C. Brinson. (2008). Polymer engineering science and viscoelasticity: An introduction. *Springer, New York*,
- [46] Daniel Maugis. Adhesion of spheres: The JKR-DMT transition using a dugdale model. *Journal of Colloid and Interface Science*, 150(1):243–269, 1992.

- [47] A. Hategan, R. Law, S. Kahn, and D. E. Discher, “Adhesively-tensed cell membranes: Lysis kinetics and atomic force microscopy probing,” *Biophysical Journal*, vol. 85, pp. 2746-2759, 2003.
- [48] R. Afrin, T. Yamada, and A. Ikai, “Analysis of force curves obtained on the live cell membrane using chemically modified AFM probes,” *Ultramicroscopy*, vol. 100, pp. 187-195, 2004.
- [49] C.A. Tweedie, K.J. Van Vliet, “Contact creep compliance of viscoelastic materials via nanoindentation,” *Journal of Materials Research*, vol. 21, No. 6, pp. 1576-1589, Jun., 2006.
- [50] A.E. Giannakopoulos, “Elastic and viscoelastic indentation of flat surfaces by pyramid indentors,” *Journal of Mechanics and Physics of Solids*, vol. 54, pp. 1305-1332, 2006.
- [51] N. Yang, K. K. HoWong, J. R. de Bruyn, and J. L. Hutter, “Frequency-dependent viscoelasticity measurement by atomic force microscopy,” *Measurement Science & Technology*, vol. 20 (2), pp. 1–9, 2009.
- [52] N. A. Burnham, G. Gremaud, A. J. Kulik, P.-J. Gallo, and F. Oulevey, “Materials properties measurements: Choosing the optimal scanning probe microscope configuration,” *Journal of Vacuum Science and Technology B*, vol. 14, no. 2, pp. 1308–1312, 1996.
- [53] G. Binnig and C. Quate, “Atomic force microscope,” *Physical Review Letters*, vol. 56, no. 9, pp. 930–933, 1986.
- [54] K. Wahl, S. Asif, J. Greenwoodc, and K. Johnson, “Oscillating adhesive contacts between micron-scale tips and compliant polymers,” *Journal of Colloid and Interface Science*, vol. 296, pp. 178-188, 2006.
- [55] B. Cappella and G. Dietler, “Force-distance curves by atomic force microscopy,” *Surface Science Reports*, vol. 34, no. 1-3, pp. 1–104, 1999.

- [56] R. Proksch, “Multifrequency, repulsive-mode amplitude-modulated atomic force microscopy,” *Applied Physics Letters*, vol. 89, pp. 113-121, 2006
- [57] U. Hubner, W. Morgenroth, H. Meyer, T. Sulzbach, B. Brendel, and W. Mirande, “Downwards to metrology in nanoscale: determination of the AFM tip shape with well-known sharp-edged calibration structures,” *Applied Physics A*, vol. 76, pp. 913–917, 2003.
- [58] M. Campoy-Quiles, T. Ferenczi, T. Agostinelli, P. G. Etchegoin, Y. Kim, T. D. Anthopoulos, P. N. Stavrinou, D. D. C. Bradley, and J. Nelson, “Morphology evolution via self-organization and lateral and vertical diffusion in polymer:fullerene solar cell blends,” *Nature Materials*, vol. 7, pp. 158 – 164, 2008.
- [59] M. Mossberg, “Optimal experimental design for identification of viscoelastic materials,” *IEEE TRANSACTIONS ON CONTROL SYSTEMS TECHNOLOGY*, vol. 12, no. 4, pp. 578–582, 2004.
- [60] A. Rensfelt, S. Mousavib, M. Mossberg, and T. Sderstrm, “Optimal sensor locations for nonparametric identification of viscoelastic materials,” *Automatic*, vol. 44, no. 1, pp. 28–38, 2008.
- [61] L. Gerencsr, H. Hjalmarsson, and J. Mrtensson, “Identification of arx systems with non-stationary inputs — asymptotic analysis with application to adaptive input design,” *Automatica*, vol. 45, no. 3, pp. 623 – 633, 2009.
- [62] L. Pronzato, “Optimal experimental design and some related control problems,” *Automatica*, vol. 44, no. 2, pp. 303 – 325, 2008.
- [63] R. K. Mehra, “Optimal input signals for parameter estimation in dynamic systems—survey and new results,” *IEEE Transactions on Automatic Control*, vol. 19, no. 6, pp. 753–768, 1974.

- [64] R. K. Mehra, "Frequency-domain synthesis of optimal inputs for linear system parameter estimation," *Div. Eng. Appl. Phys., Harvard Univ.*, vol. TR 645, 1973.
- [65] K. Kim, Q. Zou, and C. Su, "A new approach to scan trajectory design and track: AFM force measurement example," *Journal of Dynamic Systems, Measurement and Control*, vol. 130, pp. 1–10, Sep. 2008.
- [66] N. A. Burnham and R. J. Colton, "Measuring the nanomechanical properties and surface forces of materials using an atomic force microscope," *Journal of Vacuum Science & Technology A: Vacuum, Surfaces, and Films*, vol. 7, no. 4, pp. 2906 – 2913, 1989.
- [67] Y. Martin, C. C. Williams, and H. K. Wickramasinghe, "Atomic force microscope force mapping and profiling on a sub 100- scale," *Journal of Applied Physics*, vol. 61, no. 10, pp. 4723 – 4729, 1987.
- [68] A. Touhami, B. Nysten, and Y. F. Dufrene, "Nanoscale mapping of the elasticity of microbial cells by atomic force microscopy," *Langmuir*, vol. 19, no. 11, p. 45394543, 2003.
- [69] T. L. Vincent, C. Novara, K. Hsu, and K. Poolla, "Input design for structured nonlinear system identification," *Automatica*, vol. 46, no. 6, pp. 990 – 998, 2010.
- [70] G. Franceschini and S. Macchietto, "Model-based design of experiments for parameter precision: State of the art," *Chemical Engineering Science*, vol. 63, no. 19, p. 4846 4872, 2008.
- [71] G. M. Clayton, S. Tien, K. K. Leang, Q. Zou, and S. Devasia, "A review of feedforward control approaches in nanopositioning for high-speed spm," *Journal of Dynamic Systems, Measurement, and Control*, vol. 131, no. 6, p. 061101, 2009.
- [72] S. Devasia, E. Eleftheriou, and S. Moheimani, "A survey of control issues in nanopositioning," *IEEE TRANSACTIONS ON CONTROL SYSTEMS TECHNOLOGY*, vol. 15, no. 5, pp. 802–823, 2007.

- [73] D. Abramovitch, S. Andersson, L. Pao, and G. Schitter, "A tutorial on the mechanisms, dynamics, and control of atomic force microscopes," *American Control Conference*, pp. 3488 – 3502, 2007.
- [74] S. Salapaka and M. Salapaka, "Scanning probe microscopy," *IEEE Transaction on Control Systems Magazine*, vol. 28, no. 2, pp. 65 – 83, 2008.
- [75] G. Binnig, C. F. Quate, and C. Gerber, "Atomic force microscope," *Physical Review Letters*, vol. 56, no. 9, pp. 930–934, 1986.
- [76] R. Wiesendanger, *Scanning probe microscopy and spectroscopy: methods and applications*. Cambridge University Press, 1994.
- [77] F. J. Giessibl, "Advances in atomic force microscopy," *Reviews of Modern Physics*, vol. 75, no. 3, p. 949983, 2003.
- [78] J. R. Pratt, J. A. Kramar, D. B. Newell, and D. T. Smith, "Review of SI traceable force metrology for instrumented indentation and atomic force microscopy," *Measurement science and technology*, vol. 16, pp. 2129–2137, 2005.
- [79] T. Ting, "The contact stresses between a rigid indenter and a viscoelastic half-space," *Transactions of the ASME, Series E, Journal of Applied Mechanics*, vol. 33, p. 845, 1966.
- [80] H. Hertz, *Miscellaneous Papers; On the contact of elastic solids*. 1896.
- [81] M. Green and J. B. Moore, "Persistence of excitation in linear systems," *Acta Biomaterialia*, vol. 7, pp. 351–360, 1986.
- [82] C. R. Rao, *Linear Statistical Inference and its Applications*. Wiley, New York, 1965.
- [83] J. Kiefer, "Optimum experimental designs," *Journal of the Royal Statistical Society. Series B (Methodological)*, vol. 21, no. 2, pp. 272–319, 1959.

- [84] S. Karlin and W. J. Studden, “Optimal experimental designs,” *The Annals of Mathematical Statistics*, vol. 37, no. 4, pp. 783–815, 1973.
- [85] P. Whittle, “Some general points in the theory of optimal experimental design,” *Journal of the Royal Statistical Society. Series B (Methodological)*, vol. 35, no. 1, pp. 123–130, 1973.
- [86] R. A. DeVore and V. N. Temlyakov, “Some remarks on greedy algorithms,” *Advances in Computational Mathematics*, vol. 5, no. 1, pp. 173–187, 2003.
- [87] D. M. Chickering, “Optimal structure identification with greedy search,” *The Journal of Machine Learning Research*, vol. 3, pp. 507–554, March 2003.